

PRESSURE BAG MOLDING: MANUFACTURING, MECHANICAL TESTING,
NON-DESTRUCTIVE EVALUATION, AND ANALYSIS

by

Erik Barnholt Larsen

A thesis submitted in partial fulfillment
of the requirements for the degree

of

Master of Science

in

Mechanical Engineering

MONTANA STATE UNIVERSITY-BOZEMAN
Bozeman, Montana

January 2004

STATEMENT OF PERMISSION TO USE

In presenting this thesis in partial fulfillment of the requirements for a master's degree at Montana State University-Bozeman, I agree that the Library shall make it available to borrowers under rules of the Library.

If I have indicated my intention to copyright this thesis by including a copyright notice page, copying is allowable only for scholarly purposes, consistent with "fair use" as prescribed in the U.S. Copyright Law. Requests for permission for extended quotation from or reproduction of this thesis in whole or in parts may be granted only by the copyright holder.

Signature _____

Date _____

TABLE OF CONTENTS

LIST OF TABLES	vii
LIST OF FIGURES	viii
ABSTRACT	xiv
1. INTRODUCTION	1
Manufacturing Fiberglass Laminates.....	2
Motivation for Work.....	2
Research Approach.....	4
Pressure Bag Molding.....	4
Infrared Transmittance Testing.....	5
Numerical Progressive Damage Model	6
Organization of This Thesis.....	7
2. BACKGROUND	8
Composite Materials	8
E-Glass and Polyester Resin	11
Current Manufacturing Techniques	12
Hand Lay-up	13
Resin Transfer Molding.....	14
Vacuum Assisted Resin Transfer Molding.....	18
SCRIMP	20
FASTRAC.....	23
Resin Flow	25
Stokes Flow.....	25
Darcy Flow.....	27
Material Properties.....	28
Validation Methods.....	30
Determination of Fiber Volume Content	31
Tensile Test.....	32
Compression Test.....	33
Short Beam Shear Test.....	34
Fatigue.....	36
Delamination.....	36
Fiber Alignment.....	38
Porosity	39

3. DAMAGE ASSESSMENT USING INFRARED TRANSMITTANCE	42
Damage in Fiberglass.....	42
Infrared Transmittance Test.....	43
IR Transmittance to Quantify Matrix Cracking.....	45
4. VACUUM ASSISTED PRESSURE BAG MOLDING	60
The Pressure Bag Molding Process	60
Pressure Bag Molding.....	61
Comparison to Existing Processes.....	71
Injection Experiments.....	73
Injection Distance, Time, and resulting Fiber Volume Content for RTM and Pressure Bag Molding.....	76
5. VALIDATION OF RESULTANT PRODUCT.....	83
Mechanical Performance Verification	83
Fiber Volume Percent Comparison.....	84
Mechanical Testing.....	87
Quantifying Damage Accumulation Properties.....	96
Ansys Progressive Damage Model.....	98
Material Properties and Failure.....	102
Solution Algorithm.....	105
Mesh Sensitivity Analysis.....	109
50 Displacement Step Solution.....	113
Damage Mapping of Fiberglass.....	122
Damage Map Results.....	127
Comparing Numerical Solution and Damage Maps.....	132
Reasons for Discrepancies.....	133
Comparing Transmittance Properties of RTM and Pressure Bag Molded Samples.....	136
6. CONCLUSIONS AND FUTURE WORK.....	139
Pressure Bag Molding.....	139
Pressure Bag Molding Conclusions.....	140
Pressure Bag Molding Future Work.....	141
Progressive Damage Model.....	143
Progressive Damage Model Results.....	143
Progressive Damage Model Future Work.....	144
Infrared Transmittance.....	145
Infrared Transmittance Results.....	145
Infrared Transmittance Future Work.....	147

IR Transmittance as a Lab Tool.....	147
IR Transmittance for Lifetime Structural Health Monitoring.....	147
REFERENCES CITED.....	150
APPENDICES	152
Appendix A - Main Ansys fea macro file.....	153
Appendix B - Ansys fea macro file for “damage” subroutine	161
Appendix C - Matlab commands	164

LIST OF TABLES

Table		Page
1.	Summary of manufacturing process details.	29
2.	Summary of typical mechanical tests and information gained.....	41
3.	Components used in hand-held IR transmittance device.	50
4.	Materials used for zero degree direction plies in common lay-up.	66
5.	Summary of injection experiments conducted to compare performances of RTM to pressure bag molding.	74
6.	Various parameters used for pressure bag molding flat plate tests.	76
7.	Injected distance performance as mold gap was reduced for 244 cm mold.	80
8.	Maximum flow distances in the fiber direction after 5 minutes at 115 to 140 kPa injection pressure.	81
9.	Nominal material properties used in numerical model.....	102
10.	Order of damage progression used in Ansys damage model.	103
11.	Components used in IR mapping fixture.....	123
12.	Loading points where damage was mapped.....	126

LIST OF FIGURES

Figure		Page
1.	Typical wind turbine blade construction.....	7
2.	Common glass fabrics	12
3.	Tools used in hand lay-up.....	14
4.	RTM mold.....	15
5.	Resin Transfer Molding equipment.....	17
6.	Vacuum assisted RTM.....	20
7.	SCRIMP	22
8.	FASTRAC mold details.....	25
9.	Capillary rheometer.....	30
10.	Burn-off test showing combustion products.....	32
11.	Tension test with an extensometer to collect displacement data.....	33
12.	Compression test using short gage length to minimize buckling effects.....	34
13.	General schematic for short beam shear test.....	35
14.	Three delamination failure modes	38
15.	Woven A130 fabric showing poor wet-out characteristics at local areas near weft weaving strands	40
16.	Before and after ultimate tensile strength test of fiberglass.....	42
17.	Reflectance	44
18.	Refraction	45
19.	Reflected and refracted light	46

20.	Visible light spectrum.....	47
21.	Light scattering resulting from defects and damage.....	48
22.	Matrix cracking between fiber tows.	48
23.	Hand-held device for spot-testing of IR transmittance.....	49
24.	Wiring diagram for IR LEDs and phototransistors used.	50
25.	Infrared opto-interrupt sensor used in a tensile test.....	51
26.	Stress-strain and opto-interrupt voltage response for fiberglass sample.....	51
27.	Photograph of samples of differing void content.	52
28.	Stress-strain and IR transmittance for differing porosity samples of UC1018GV material in the zero degree direction in [0/45/-45/0]s laminate.....	54
29.	Stress-strain and IR transmittance for differing porosity samples of D155 fabric in the zero degree directions in [0/45/-45/0]s laminate.	55
30.	IR voltage output during multiple loading and unloading cycles.....	56
31.	Thick VARTM laminate used for thickness IR transmittance test.	58
32.	Infrared Transmittance response along a varying thickness VARTM sample.....	58
33.	Pressure bag mold parts.....	61
34.	Resin flow in the channel above the preform during injection.....	63
35.	Kinematic viscosity history of Interplastics Corporation’s orthophthalic polyester 63-AX-051 (Corezyn) used by the composites group at MSU.	65
36.	Mold gap definition	67

37.	Catastrophic fiber wash on top layer of injection port end of 244 cm plate.....	69
38.	Surface texture on non-molded surface created by bagging film with hydrostatic pressure applied.....	71
39.	Radius 2100 Injector System.....	75
40.	Alcatel Vacuum Pump used in this work	75
41.	RTM mold configuration for "Clamped" experiments.....	77
42.	RTM mold configuration for Shimmed experiment.....	78
43.	Fiber volume percents for RTM and pressure bag molded plates.	86
44.	Fiber volume percent distribution along 244 cm pressure bag molded plate.....	87
45.	Ultimate tensile strength of samples taken from plates manufactured for pressure bag molding and flow distance experiments.....	89
46.	Ultimate compressive strength of samples taken from plates manufactured for pressure bag molding and flow distance experiments.....	91
47.	Microscope view of a cross-section of a [0/45/-45/0] _s laminate with perturbed surface tows.	92
48.	Sketch implying reduced surface texture effect for thicker laminates.	93
49.	ASTM D2344 short beam shear test apparatus.	94
50.	Apparent shear strengths of samples tested as determined by ASTM 2344D short beam shear test.....	95
51.	Significant sample dimensions for damage accumulation tests.....	98
52.	Ansys solution showing stress distribution around a hole in a plate made of an isotropic material under uniaxial loading.....	99
53.	Ansys shell91 element.....	100

54.	Ansys mesh definition of a plate with a hole in it using quarter-symmetry.	101
55.	Ansys model showing layered elements of [0/45/-45/0] _s laminate used in progressive damage tests of plate with a hole under tension.	101
56.	Material property response to damage states for zero degree plies.	104
57.	Material property response to damage states for 45 degree plies.	105
58.	Flowchart of Ansys progressive damage model solution algorithm	108
59.	Ansys display of stress intensity showing stresses carried in each layer of [0/45/-45/0] _s laminate.	109
60.	Point of highest stress chosen for mesh sensitivity analysis.....	110
61.	Meshes from macro line division variables at "4-4" (left) and "8-10" (right).....	111
62.	Maximum stress in the zero degree and 45 degree layers after one displacement step for increasing mesh densities.	111
63.	Maximum stress in the zero degree and 45 degree layers after five displacement steps for increasing mesh densities.	112
64.	Legend for color “damage state” contours.	114
65.	Ansys images showing progression of damage state created during displacement step solution looping.	115
66.	Ansys images showing stress intensity in the zero degree layer during displacement step solution looping.	116
67.	Ansys images showing stress intensity in the 45 degree layer during displacement step solution looping.	117

68.	Ansys images showing x-direction strain in the zero degree layer during displacement step solution looping.	118
69.	Ansys images showing x-direction strain in the 45 degree layer during displacement step solution looping.	119
70.	Ansys images showing y-direction strain in the zero degree layer during displacement step solution looping.	120
71.	Ansys images showing y-direction strain in the 45 degree layer during displacement step solution looping.	121
72.	IR transmittance test fixture built for these tests.	123
73.	Sample mounting consistency test measurement area.	124
74.	Sample indexing consistency test results.	125
75.	Quarter-symmetry used for transmittance mapping.	126
76.	Excel surface plot of percent IR transmittance after 36.7kN load step.	127
77.	Baseline infrared transmittance map for fiberglass plate with a hole using quarter-symmetry.	128
78.	Infrared transmittance of plate with a hole after loading to 36.7 kN.	128
79.	Infrared transmittance of plate with a hole after loading to 40 kN.	129
80.	Infrared transmittance of plate with a hole after loading to 42.3 kN.	129
81.	Infrared transmittance of plate with a hole after loading to 46.7 kN.	130
82.	Ninety data point area used for local average IR transmittance study.	131

83.	Overall and local percent transmittances for data sets measured during incremental loading of fiberglass plate with a hole.	132
84.	Difference in percent transmittance for sample after 42.3 kN load step compared to undamaged transmittance.	133
85.	Resolution test results comparing the 1.27 mm resolution with .203 mm resolution.	135
86.	Resolution test results comparing 0.203 mm resolution with 0.102 mm resolution.	136
87.	Difference in transmittance for RTM plate with a hole after loading to 36.7kN compared to undamaged transmittance.	137

ABSTRACT

It is desirable in the wind turbine industry to use low-cost fiberglass composite materials. However, current manufacturing capabilities for these materials can not keep pace with the increases in size and demands of new wind turbine designs. Process limitations in Resin Transfer Molding (RTM) have been identified that make this otherwise popular process less attractive for wind turbine blades, especially as the size of new blades increases. Other factors such as reliability and maintenance costs also need to reduce to allow for the continued competitiveness of these low cost materials. There were three main areas of research addressed in this work which were intended to address these needs.

The first was “pressure bag molding”, a variation of RTM which was designed to remedy some of the limitations inherent with RTM. Critical manufacturing process parameters were identified and testing was conducted to compare these parameters for pressure bag molding to those of RTM. Mechanical testing was conducted to compare products of RTM to products of pressure bag molding.

The second area of research was a new non-destructive evaluation method for fiberglass materials. This method involves the transmittance of infrared light through a laminate. This optical evaluation method is described in detail. Several exploratory tests were conducted to gain an understanding of the behavior of this method of evaluation. Then, a damage accumulation test was designed to compare damage accumulation properties of products of RTM to those of pressure bag molding.

The third research focus was the development of a numerical progressive damage model. Ansys was used to model the complex damage behavior of the layered, angled laminates that were chosen for the damage behavior comparison discussed above.

The process parameter tests showed superior performance for pressure bag molding. Mechanical testing of the products showed similar performance for pressure bag molding products, except for slightly reduced performance in the compressive strength test, which was discussed. The progressive damage model seemed to provide reasonable results. However, it was found (and discussed) that the resolution in the mechanical damage accumulation measurement was not adequate to facilitate reasonable comparison to the Ansys model.

CHAPTER 1

INTRODUCTION

The use of modern composite materials in critical structural applications has seen significant increase in recent years. The ability to “engineer” a composite material to meet specific design requirements makes them attractive for many applications. One application that has experienced increased use of composite materials is wind turbine blades.

Wind is a potential source of clean domestic energy. Wind generation facilities that convert wind into electricity are increasing in number and generation capacity. Wind generators that are being developed are also increasing in size and capacity. Offshore wind turbines with generation capacities over three megawatts are currently installed in many locations around the world [1, 2]. As the demands on the turbine blades have increased, the use of composite materials for turbine blades has also increased. Typical wind turbine blade construction details are shown in Figure 1.

Composite materials are available in many variations ranging from low cost E-glass fibers combined with thermosetting polyester resins (typically referred to as “fiberglass”) to high quality aerospace materials such as metal matrix composites. For some wind turbine blade applications, fiber reinforced plastics have become the chosen materials [3].

Manufacturing Fiberglass Laminates

Currently, there are not many choices for the method of manufacture for structures such as these. Hand lay-up is used for the manufacture of some turbine blades [4, 5]. However, hand lay-up has been shown to have several critical drawbacks [5]. Resin Transfer Molding (RTM) is a relatively recent development for the manufacture of composite structures, and has shown abilities to produce higher quality products while alleviating some of the drawbacks of hand lay-up. Traditional RTM uses low cost glass fabric materials and a net-shape two-sided mold. Liquid resin is injected from one or more locations and flows in the plane of the fabrics until the mold is filled. RTM is considered the “standard” manufacturing method used for comparisons in this work.

Despite distinct advantages to using RTM, it also has been shown to have limitations in process capabilities, especially for larger structures. The in-plane flow mechanism described above is a limiting aspect of RTM. The in-plane flow requires high injection pressures, long injection times, and has limited injected distances and volumes. The limitations inherent to RTM prevent current manufacturing capabilities to keep pace with increasing demands from the turbine blade industry.

Motivation for Work

The cost of energy produced from wind has decreased in recent years. To continue this trend, which is necessary to allow this clean energy source compete well with traditional generation methods, the associated costs need to continue to decline. There are several opportunities to improve the cost-effectiveness of using low-cost fiberglass materials in wind turbine blades:

1. Improved manufacturing methods can result in potential cost reduction when using low cost fiberglass materials in the form of improved structure quality. Wind turbine blades experience widely varying loadings and environments. Failure of a wind turbine blade can be catastrophic to the entire turbine.
2. In the relative absence of an understanding of material behavior in the structural design process, structures are typically overbuilt. This approach is costly and still may not prevent the potential failures that may occur because of failures in local regions. Improved understanding of material behavior in extreme situations may allow for more economical designs.
3. A better understanding of the link between manufacturing process and mechanical performance is likely to improve the economics of wind energy. It has been shown that the manufacturing method affects the final properties of a fiberglass structure [5]. A more complete understanding of material properties resulting from the preferred manufacturing process will allow for more economical designs.
4. Maintenance costs are also a significant factor in the wind industry. Blades that are in service are periodically investigated for early indications of impending failure. Nondestructive evaluation methods are sometimes used to detect damage in structures. X-ray methods and Ultrasonic methods have been used to some success. However, the use of X-rays needs to be done in a controlled environment because of health risks, and ultrasonic techniques frequently result in

ambiguous results [5]. Improved non-destructive evaluation technologies are needed to determine sub-critical damage and will reduce maintenance costs.

It is crucial to the industry to reduce costs while improving product performance. Advancement in these areas will continue to improve wind energy's ability to compete with traditional energy sources.

Research Approach

This thesis approaches these needs in three ways. Although these three areas of research are presented under the single thesis topic, they address the main theme of manufacturing-related cost reduction separately, and could be considered to have intrinsic value individually.

Pressure Bag Molding

A variation of RTM that is designed to remedy some of the limitations of the RTM process when used to produce large structures is introduced. This manufacturing method, "pressure bag molding," is described in detail. Mold construction and process parameters are identified.

Some of the critical molding process parameters are identified and compared with those of RTM. The limiting processing aspect of RTM for increased structure sizes is the in-plane flow mechanism. The pressure bag molding process was designed to reduce the effects of in-plane resin flow. Two critical parameters affected by the flow mechanism were chosen to be compared, injection time and injection distance from the injection port.

Since previous work has revealed a link between manufacturing method and mechanical performance [5], mechanical properties of products of pressure bag molding were compared with those of RTM products. Several mechanical tests were conducted to quantify the resulting mechanical performance of the resulting products of pressure bag molding. Fiber volume content, tensile strength, compressive strength, and short beam shear strength were compared.

Infrared Transmittance Testing

A new nondestructive evaluation method was developed for this work. This method is used in this work to compare damage properties of RTM products and pressure bag molding products, as well as to serve as a laminate “quality” metric.

This method involves the transmittance of light through the fiberglass material. The transmitted light is quantified and output voltage is recorded. A brief discussion of the physics involved in this method followed by a series of exploratory tests is included in Chapter 3.

In addition to the typical mechanical testing described above, a damage accumulation test comparing RTM to pressure bag molding products is described and demonstrated. This test involves two-dimensionally mapping the damage imposed on a chosen geometry of samples from the candidate processes. An X-Y stage apparatus was constructed to facilitate this test. The apparatus and electronics are described, along with the test methodology and results.

Numerical Progressive Damage Model

A numerical progressive damage model was also developed for this work. It was designed to aid in development of the damage accumulation test to correlate with the infrared transmittance technique discussed above, but as mentioned previously, the development of this model may have merit in other applications as well. Ansys was used to model the geometry that was chosen for the damage mapping test described above. Layered shell elements were used. An incremental displacement approach was applied in the model. At each incremental loading step, strains were checked against previously established failure criteria to determine if damage was introduced. If damage was determined to have taken place, the properties were downgraded and the solution at that displacement was reacquired.

The solution algorithm and Ansys code is included along with discussion of assumptions made. Results are displayed in the form of series of images showing Ansys' prediction of the progression of damage along with several other images of selected stress and strain distribution responses as damage accumulated.

Results from this test are compared with the two-dimensional mapping of damage in manufactured samples. The results of this comparison are difficult to interpret due to several factors which are discussed. The damage mapping resolution was found to be inadequate to accurately display damage properties. A failure mode also occurred in the mechanical testing that the progressive damage model did not account for. These limitations are discussed in detail.

Organization of This Thesis

A discussion of background material is in Chapter 2. Fiberglass materials are discussed along with current manufacturing processes. Typical mechanical testing is discussed. A presentation of the exploratory infrared transmittance work is in Chapter 3. Presentation of the pressure bag molding process and critical process parameter comparisons are in Chapter 4. Mechanical testing to compare products of pressure bag molding with products of RTM follows in Chapter 5. Also in Chapter 5 is the damage mapping experiment and progressive damage model development. Finally, Chapter 6 includes a brief discussion of specific results and suggested future work for each research topic.

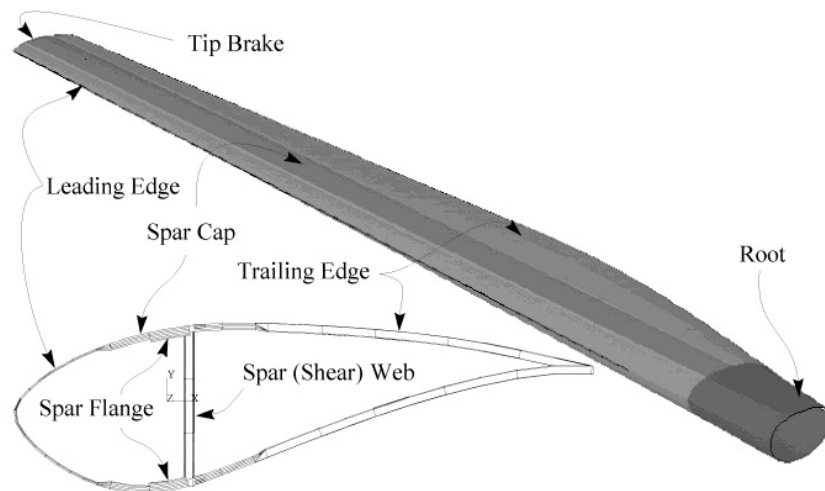


Figure 1: Typical wind turbine blade construction [5].

CHAPTER 2

BACKGROUND

Composite Materials

A composite material consists of a combination of two or more materials with differing properties. The resulting product has a combination of the constituent properties. Fiber reinforced plastics are common composite materials consisting of fibers, typically glass or carbon, and a polymer matrix material. The fibers exhibit high tensile strength and stiffness but alone have relatively poor compressive and shear properties [6-8]. When combined with a polymer matrix material, the fibers handle the majority of tensile loading, and the matrix offers support in compression and shear, creating a part with superior overall properties. Various combinations of fiber types and configurations at specific orientation angles are combined with different types of matrix materials at specified ratios to yield desired mechanical properties that match specific design requirements. These well-understood directional properties make fiber-reinforced plastics excellent engineering materials.

Composite materials have been utilized in construction for millennium. An early reference to the use of composite materials is found in the Bible, when Pharaoh Ramses II required that the slaves gather their own straw for making bricks [9]. Composites in the form of metal alloys were used in the bronze age which represented a significant technological advancement. The use of engineered composite materials has greatly

increased in recent times, and many different types of composites have been developed. Fiber reinforced plastics (FRPs) were first used toward the end of World War II in filament wound rocket motors and other critical structural applications [6]. These rocket motors used glass fibers as reinforcement in a polymer matrix. This combination of low cost glass fibers combined with a liquid polyester thermosetting resin became what is known as fiberglass. After the war, fiberglass materials were developed into low cost engineering materials and are still in use today.

Fiber reinforced plastics are thermosetting or thermoplastic materials that have a certain volume of fibers added to strengthen the matrix material. The ratio of fibers to matrix material in a composite is an important parameter and is commonly described by its fiber volume fraction or percent. The “Rule of Mixtures” [7], shown in Equation 1, can reasonably approximate some of the final properties of the composite.

$$P_c = P_f V_f + P_m V_m \quad 1)$$

Where P_c is a property of the composite

P_f is the property of the fibers used

V_f is the fiber volume fraction

P_m is the property of the matrix

V_m is the matrix volume fraction

Because of the axial direction of the fibers, the resulting properties of the composite are highly dependent on the orientations of the fibers used as reinforcement. The prescribed orientation and type of each layer that makes up a laminar composite is called its “lay-up”. The materials used, lay-up, and relative percentage of fibers and resin determine the final properties of a composite.

There are many different types of fibers used today ranging from low cost glass to high performance carbon and tungsten fibers [10]. The choice of which fiber to use in an application is made by typical engineering material selection: cost, availability, mechanical performance, environment, lifetime, etc. In some cases, glass fibers have been chosen for high performance applications such as large wind turbine blades even though some of their mechanical performance characteristics are poor compared to other fiber types such as carbon.

There are also many types of matrix materials currently used. Thermosetting resins are polymers that crosslink, which is an irreversible process. This chemical process takes place after the resin is combined with fibers. Thermoplastic resins are not cross-linked, and can be to some degree reheated and reformed. Thermosetting matrix materials typically have better mechanical properties than thermoplastics, especially thermal and creep properties. Ceramic matrix materials can be used in very high temperature applications, such as space vehicle re-entry heat shielding. Metal matrix materials are also used in space vehicles. One of their unique characteristics is the ability to have very low coefficients of thermal expansion, making them attractive for the extreme temperature ranges experienced outside of earth’s atmosphere [11]. By far, the

most common matrix material used with low cost glass fibers is the thermosetting polymer type.

E-Glass and Polyester Resin

The focus of this thesis is on manufacturing considerations of applications that utilize low cost E-glass fibers. The chemical composition of glass fibers is predominately silica (SiO_2), similar to ordinary window glass. The high tensile strength of glass fibers (in the range of 3.4 GPa [12]) is a result of their very small average flaw size.

Immediately after their production, fibers have a sizing applied to them. The sizing provides environmental protection for the fibers and also provides improved surface tension properties for the intended resin system. Therefore glass fibers are “sized” for a specific resin type, i.e. polyester or epoxy. E-glass fibers are manufactured in high volume facilities for a very wide range of applications, and are among the lowest cost reinforcements used in modern composites.

Glass fibers are made available for production in many general forms. Common products of E-glass fibers are chopped fibers, roving (constant strand spool) and fabrics. Typical ways to produce fabrics are to weave, stitch, or bond them into a fabric which is sold on a roll similar to products produced by the textile industry as shown in Figure 2. Some of the equipment used to produce glass fabrics is similar to equipment used in the clothing industry. It is these types of fabrics that are used in this thesis because of their potential use in larger, demanding components such as wind turbine blades.

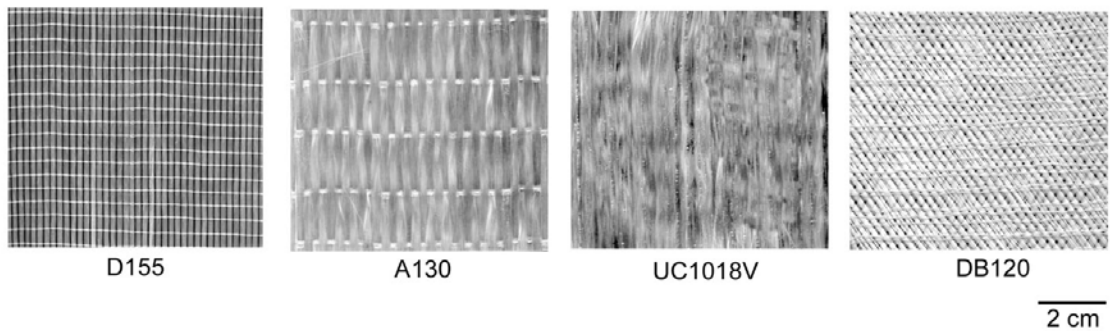


Figure 2: Common glass fabrics

The matrix material used in this work is a commonly used polyester resin for low cost applications. The formulation for polyester resins can be adjusted to result in different toughness and modulus properties. Polyester resins have a relatively low viscosity, low cost, and have relatively fast cure times, but generally inferior properties compared with epoxies. The greatest disadvantage of polyester is the relatively high volumetric shrink rate when curing. The specific product used in this thesis was Interplastics Corporation's orthophthalic polyester 63-AX-051. The resin was catalyzed using Methyl Ethyl Ketone Peroxide (MEKP) at 1.5% - 2% by volume. This resin system is commonly used for low cost fiberglass composites in typical manufacturing techniques.

Current Manufacturing Techniques

There are many methods currently employed in the manufacture of fiberglass parts using pre-manufactured fabrics and liquid resins. Several factors determine which method would be best to use for a particular application, such as the number of parts

required, rate per year, cost, dimensional and surface finish requirements, and mechanical performance requirements. A brief discussion of some of the major processes currently in use is in order.

Hand Lay-up

The least capitally-intensive manufacturing method used for fiberglass parts is to saturate the glass fabric lay-up with liquid resin by hand. A one-sided mold in the final shape of the part is constructed with the desired surface finish. The mold surface is treated with mold release compounds consisting of wax and/or other chemical compositions. Resin is worked into the fabrics using rollers, squeegees, or brushes either directly onto the mold surface or on a wet-out table. If a wet-out table is used, the saturated fabric is placed onto the mold surface. As much air as is practical is worked out of the laminate and it is allowed to cure.

Advantages of hand lay-up are the relatively lower mold costs and strength requirements, the tools required for production are readily available, the molds are easy to maintain and the part's lay-up can usually be changed without altering the mold. However, the disadvantages are many. Hand lay-up is a manual process, and therefore results are very subject to the user that is doing the work. Since the fibers have the superior mechanical properties, it is often desirable to control and typically maximize the fiber volume percent, which is relatively difficult with hand lay-up [5].



Figure 3: Tools used in hand lay-up.

Recently, the volatile emissions of this open mold process have created concern. Styrene diffuses out of the resin at room temperature and pressure and is a significant health concern [13]. The Occupational Safety and Health Administration (OSHA) and industry organizations have been focusing on the reduction of styrene levels in the workplace [14]. Replacing hand lay-up mold processes with closed mold processes can significantly reduce levels of styrene in the workplace.

Resin Transfer Molding

The introduction of Resin Transfer Molding (RTM) has dramatically changed the composites industry. It is a closed mold process that can produce higher fiber content, dimensionally repeatable parts with significantly reduced styrene emissions, avoiding some of the disadvantages of hand lay-up [5].

The resin transfer molding process is typified by the mold used. RTM typically uses a mold constructed in two halves that are clamped together creating a cavity in the shape of the desired final product. The inside mold surfaces are prepared with the desired surface finishes and treated with mold release compounds before the molding process. Dry fabric is placed into the “bottom” half of the mold in the prescribed lay-up and angular orientations. After clamping the mold halves together, injection equipment is used to inject resin into a port located at a strategic point on the part until the dry fabric is completely wet out. Vent ports are located at the extremities of the resin flow path for air to exit the mold cavity. The vent ports can be closed when a clean flow of resin (little or no air bubbles in the exiting resin) is observed from the port, conserving material. When injection is completed, the injection port is closed and injection equipment is removed for cleaning or subsequent use. The part is allowed to cure in the mold, and removed.

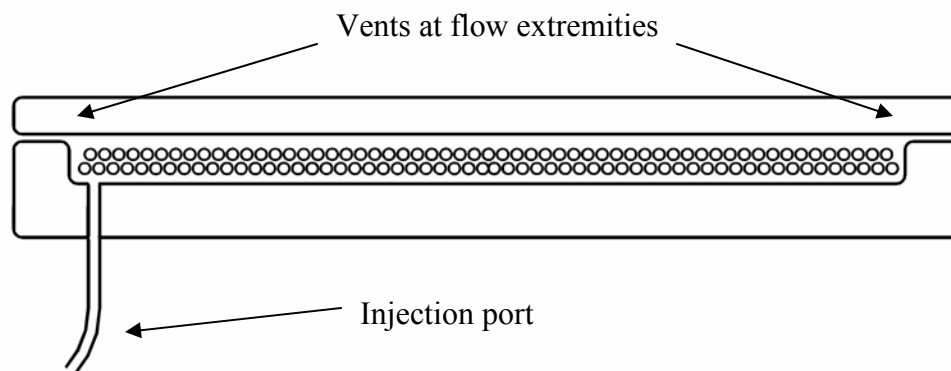


Figure 4: RTM mold.

A variation can be when the dry fabric first undergoes a “pre-form” operation, which is when the desired lay-up is temporarily bonded together in the mold shape and with the prescribed angular and laminar orientation. The preform is typically held together with a thermoplastic adhesive by heating and cooling the fabrics with a certain amount of thermoplastic binder applied in the desired shape [15]. This facilitates easier insertion into the mold cavity, and can help to hold the fabric in place during injection.

There are many advantages to RTM. The closed mold architecture drastically reduces the styrene emissions into the workplace. The clamped, 2 sided mold increases dimensional repeatability. It also allows for higher fiber volume percents compared with what can be achieved with hand lay-up [5]. Since there is much less “hand” work done during infusion, RTM introduces an ability to maintain greater process control during production. These advantages introduced with the RTM process allow low cost fiberglass materials to be used in a much greater number of demanding applications.

The RTM process also has its own set of drawbacks. The purchase and maintenance of injection equipment represents a substantial increase in startup and maintenance costs. Mold design is more complex, not only because of the two sided nature of RTM, but also because of the stress applied by the liquid resin being injected under pressure. Molds need to be not only strong enough to withstand the force of the resin under the hydrostatic pressures during injection, but the elastic deformation needs to be controlled such that the final fiber volume percent is not lower than desired because of elastic mold deflection. Parts with large, continuous surface areas need extremely rigid mold construction for spatially consistent fiber volumes. However, the additional costs

and design requirements of an RTM mold are not the greatest challenges when implementing an RTM process.

The flow characteristics during injection present a major design challenge to RTM [4, 16]. Since the fiber reinforcement has properties superior to the matrix material, it is usually desired to design for a high fiber volume percent. However, as the fiber volume percent increases, the micro-channel areas between fibers decrease, which makes filling the part more difficult. When higher injection pressures are applied to compensate for the smaller flow channels, a phenomenon called “fiber wash” may result. Fiber wash occurs when the pressure gradient is large enough to push the fabric out of its desired location and/or orientation angles, resulting in a defective part. To reduce the



Figure 5: Resin Transfer Molding equipment

need for high pressure gradients, fabric architectures have been developed that have channels between high fiber concentrations which improve flow properties [17]. However, the spatially uneven flow fronts that develop during injection between high and low fiber concentrations in these types of fabrics can lead to increased voids and porosity if the flow fronts “close” around dry areas as resin follows the path of least resistance. Reducing injection pressures to avoid fiber wash limits the maximum injection distance that can be achieved from a port. For larger parts, this results in a need for multiple injection ports. When injection is done from several ports, multiple flow fronts develop, introducing other opportunities to entrap air. Additionally, there may be undesirable mechanical property artifacts that occur in the finished part at the confluence of two or more flow fronts. Complex flow analysis software continues to be developed to aid in the design of RTM parts and tools [16]. Although RTM has allowed low cost fiberglass materials to be used in a wider variety of applications, the inherent resin flow in the plane of the fabric during injection remains a drawback of RTM.

Vacuum Assisted Resin Transfer Molding

A variation of RTM is Vacuum Assisted Resin Transfer Molding (VARTM). In this process, instead of venting the air at the extremities of the flow distance, a vacuum is applied at the vent ports. This vacuum serves several purposes. First, it increases the magnitude of the pressure gradient without increasing the injection pressure. Secondly, the reduced pressure in the mold cavity removes air mass that is available to become entrapped, leading to increased porosity and voids. Finally, the vacuum acts to hold the mold halves together, potentially reducing necessary clamping forces.

VARTM has its disadvantages also. Before using polyester resins in a vacuum assisted environment, the resin should be degassed to remove atmospheric gases and water in solution. This is done by applying a moderate vacuum for an extended period (in the range of 24 hours). The degree of vacuum applied to polyester resins during VARTM can not exceed the vapor pressure of styrene (2.4 mm Hg [18]), or boiling will occur. Another drawback to VARTM is the requirement that the mold halves be air-tight. In traditional RTM, if the mold halves are not perfectly sealed during injection, some resin may leak out of the cavity, but the resulting part does not usually suffer a decrease in quality. However, if the seal develops a leak in a VARTM operation after the flow front passes the leaking area, air is pulled into the resin to such a degree that it almost always causes the part to be scrapped, even for a very small leak. If a leak is detected during injection, the process is typically aborted, causing a substantial waste of time and material. Another drawback of VARTM is the additional cost of equipment. Purchasing and maintaining vacuum pump equipment that can withstand the gases that come out of polyester resin can be a significant investment. Even considering the drawbacks of VARTM, it still is preferred for the production of many fiberglass parts.

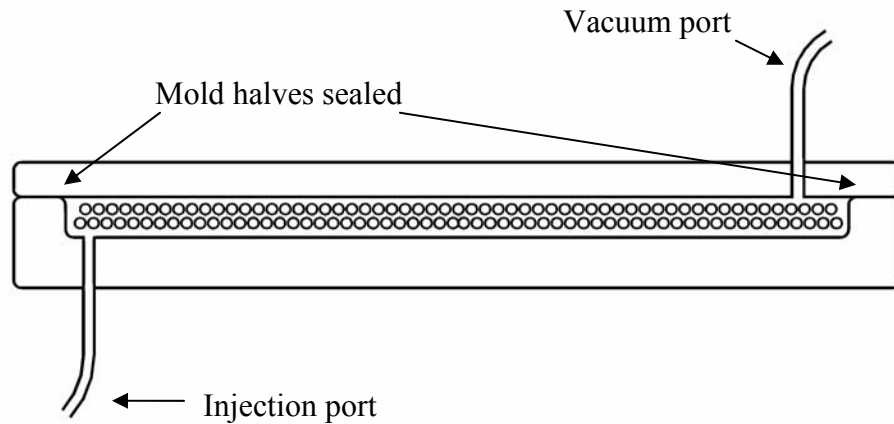


Figure 6: Vacuum assisted RTM.

SCRIMP

The Seemanns Composite Resin Infusion Molding Process (SCRIMP) was developed in the late 1980s as an alternative infusion process [19]. This is also a closed mold process, utilizing a one-sided mold. In its simplest form, the fabric lay-up is placed into the mold. A flexible film is placed over the fabric. The film is sealed against the mold outside of the edges of the part, creating an airtight cavity, and a vacuum is pulled in the fabric. An injection port is opened at the opposite end of the part from the vacuum port, and resin bleeds into the fabric. Typically, the resin reservoir is open to atmospheric pressure, which provides the pressure gradient during injection. After the part is filled, the injection port is closed, but the vacuum remains to hold the laminate in the desired shape against the mold surface. After curing is complete, the vacuum is removed, and the film can be removed (and sometimes re-used). The part is then removed from the mold.

There are some variations of the basic SCRIMP process that have been developed. Since resin is caused to flow in the plane of the fabric, its maximum injection distance is limited. Compounding this is the reduced permeability of the lay-up caused by fiber compaction from the atmospheric pressure on the film. To reduce the number of ports needed (and avoid the multi-port effects), a high permeability layer is sometimes added to the top of the lay-up. This is usually separated by a perforated release film so that this resin-rich layer can be removed from the final product. Another development is to install some form of inserts to the top of the lay-up that form channels for the resin to flow out of the plane of the lay-up. The channels can be tuned to divert resin directly to areas of the mold that are relatively difficult to fill. The channels usually stay with the part after curing. Both of these variations succeed at significantly improving the flow capabilities during SCRIMP, but both result in a less efficient use of material. The method of channeling the resin can also add unnecessary weight and volume to the final part if the channels are not removed.

There are several advantages to SCRIMP. The resulting fiber volume percents can be significantly higher than realized in hand lay-up and RTM, resulting in parts with superior mechanical properties. Lower mold costs are a result of the one-sided mold and application of hydrostatic atmospheric pressure (due to the vacuum inside the cavity). The atmospheric pressure on the film translating directly to the fabric (holding the fabric in place against the mold) also tends to reduce the possibility of fiber wash. The absence of costly injection equipment also reduces overall processing costs. The variations that include a method to improve flow properties allow for very large parts to be

manufactured with a limited number of ports. The ability to produce large parts with superior properties makes SCRIMP an attractive candidate for fiberglass production, even though there are some disadvantages.

The disadvantages to SCRIMP are relatively minor in light of the capabilities. SCRIMP is a proprietary process, requiring licensing for its use. Several domestic patents cover SCRIMP [19] and filings have been made in several other countries as well. Aside from the intellectual property rights to SCRIMP, the disadvantages are few. The use of a distribution layer (channels or high permeability material) to reduce the limitations of in-plane resin flow necessitates some waste of resin. Also, the use of the one-sided mold produces parts with only one finished side. The bag side of the part retains the surface texture of the fabric under vacuum. Aside from these limitations, SCRIMP has proven its ability to economically produce large parts with excellent mechanical properties with reasonable associated costs.

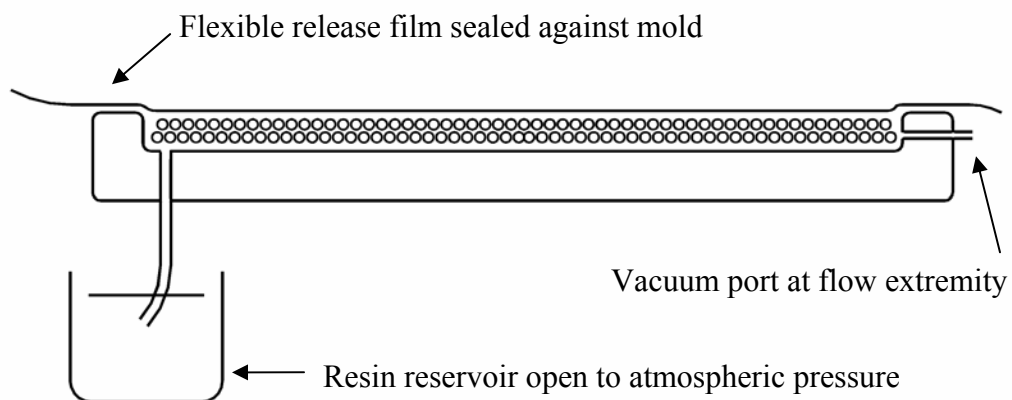


Figure 7: SCRIMP

FASTRAC

A recent development in the low cost composites processing industry is the Fast Remotely Actuated Channeling process (FASTRAC) [20, 21]. FASTRAC, another closed mold technique, attempts to implement the same resin channeling technique during injection as SCRIMP, but the channels are made to collapse before the resin cures. This is done by using a two-chamber architecture. A “lower” chamber contains the fabric pre-form adjacent to a one-sided mold surface. The “upper” chamber contains a “FASTRAC layer”, which is a semi-rigid support member with the channel profile that, under vacuum in the fabric chamber, will rest against the pre-form (between channels) separated from it by a release film.

The FASTRAC process requires more accurate control. A vacuum is first drawn in the upper chamber, deforming the bagging film into the channel geometry of the FASTRAC layer. This initial vacuum operation creates the channels for the resin to flow in during injection. After the channels are formed, the pressure in the lower chamber is reduced to evacuate air mass, similar to VARTM. Atmospheric pressure holds the FASTRAC layer against the fabric, but the semi-rigid material allows the channel structure to maintain its shape. Resin is then injected or pulled into the fabric chamber and it flows according to the channel geometry in the FASTRAC layer. After injecting a prescribed resin volume, the vacuum in the upper chamber is released, and atmospheric pressure causes the channel geometry to collapse, forcing resin into the fabric in the thickness direction. With properly sized flow channels and the proper injected volume, the channels will completely collapse, leaving little or no evidence of their use.

Advantages of FASTRAC include those of SCRIMP. High fiber volume percents are possible with large injection volumes per port, with relatively short injection times and little or no applied injection pressures. FASTRAC also eliminates the largest drawback of SCRIMP (and other RTM and VARTM methods) by eliminating the wasted resin and distribution media associated with those methods.

Disadvantages of FASTRAC are mainly related to the complexity of the process. Accurate control of the pressures in both chambers is critical. Timing is also a process parameter in injection rates and when to open the upper chamber to atmospheric pressure. The FASTRAC layer needs to be manufactured, and material choice and availability as well as manufacturing difficulties with “tuning” the channel design may be significant challenges. Similar to SCRIMP, FASTRAC products have one finished (mold finish) side. The opposite side will have the finish of the release film with the atmospheric pressure applied to the fabric. Also, artifacts of the collapsing channels may remain on the unfinished side as well. These artifacts may manifest as a wrinkle pattern, if the release film underwent significant plastic deformation during formation of the flow channels before injection. Considering all aspects, FASTRAC appears to be an excellent process that should increase in popularity as industry becomes familiar with it.

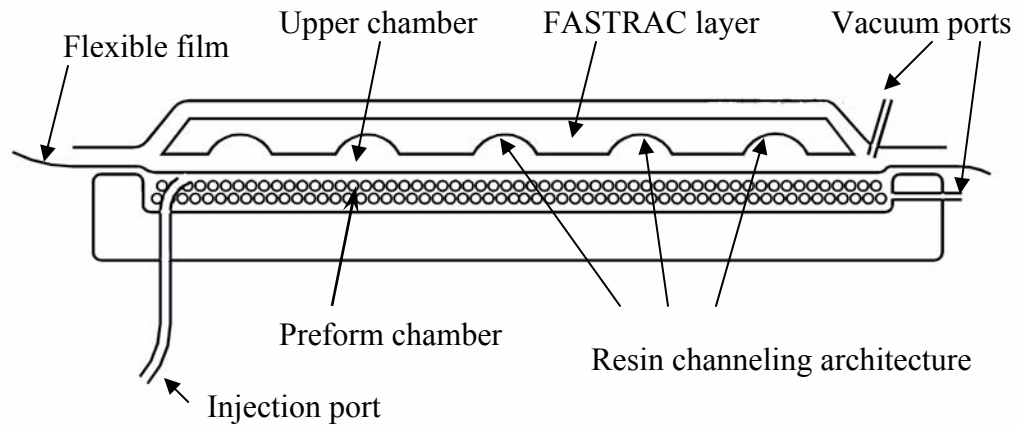


Figure 8: FASTRAC mold details.

Resin Flow

The manufacturing methods that are available for these types of materials (glass fabrics, polyester resins) are relatively few in number, but have distinct differences in mechanisms. Except for the hand lay-up process, all of the methods described above depend on liquid resin flowing from one or more injection ports. To further understand the differences in manufacturing methods, a discussion of resin flow is in order.

Stokes Flow

The Navier-Stokes equation (2) describes flow of a Newtonian fluid with constant density and viscosity [22].

$$\frac{\partial v_i}{\partial t} + v_j v_{i,j} = \frac{-p_{,i}}{\rho} + \nu v_{i,jj} + \frac{F}{\rho} \quad 2)$$

Where ρ is mass density,

v is velocity,

p is pressure,

ν is resin kinematic viscosity,

F is body force

For typical resin injection analyses, the dynamic term and the body force term (gravity) can be neglected. Also, if the flow is in a channel where the cross-sectional area is relatively constant, the material or substantial derivative term can be neglected, and the resulting equation describes “Stokes’ Flow” (Equation 3) [4].

$$0 = -p_{,i} + \mu v_{i,jj} \quad 3)$$

Where μ is resin dynamic viscosity

Stokes’ flow best describes channel flow, and is dominated by the viscosity of the fluid. The processes that cause resin to flow in this manner are SCRIMP (with resin channeling architecture), and FASTRAC, since channels are formed in the FASTRAC

layer. While it is theoretically possible to use the Navier-Stokes equations to model flow in the glass fabrics and high permeability distribution materials, evaluation of the boundary conditions and the 3-dimensional aspects make it prohibitively complex [4]. Another mathematical model describes fabric flow better.

Darcy Flow

Liquid flowing through a porous media is described by Darcy's law (Equation 4). This equation is frequently used as a more convenient method to describe resin flowing through glass fabrics [23]. Darcy's law simply states that flow is proportional to a pressure gradient. Resin flow in glass fabric described by Darcy's law is dominated by not only resin viscosity, but three-dimensional fabric permeability as well.

$$v_i = \frac{-K_{ij}}{\mu} p_{,j} \quad 4)$$

The permeability tensor, K , is a second order tensor and is a physical characteristic of the fabrics and lay-up in the case of polyester resin flow in a glass fabric infusion flow problem.

Normal RTM processes are commonly modeled using Darcy's law, since the flow is constrained the within the fabric (except for poorly designed mold/lay-up combinations where the mold gap is much greater that the fabric thickness, which would yield undesirable results due to the inhomogeneity of the resulting product). In this situation,

the flow is generally two-dimensional, in the plane of the fabric. Since the permeabilities of fabric lay-ups can be determined, Darcy's law is typically used to analyze resin flow [4].

In the FASTRAC process, when the distribution channels are collapsing (when the vacuum in the upper chamber is released), the flow type shifts from predominately channel flow to Darcy flow. This introduces a great complexity in analysis of this flow. Analyzing this flow would require accounting for the rapid filling of the distribution channels while there is x, y, and z flow in the fabric, followed by the collapsing channel stage with the three dimensional flow in the fabric, and finally a final stage, where Darcy flow would occur. During a search for research pertaining to the FASTRAC process, no flow analysis was found that accounted for the collapsing channels.

Table 1 is a summary of the basic manufacturing processes previously discussed, including the dominating flow mechanisms involved in each.

Material Properties

The ability to engineer a material with directional properties is one of the aspects of using fiber reinforced plastics that makes them desirable. The design of a composite material using glass fabrics and polyester resin would include specifying the fabric types, surface finishes, the number of layers of each type, layer order, and angular orientation of each layer, resin type, and fiber volume percent. Maximum void content and other quality metrics could also be specified.

Table 1: Summary of manufacturing process details.

Process	Basic Principles	Advantages	Disadvantages
Hand Lay-up	Open mold Manual infusion One sided mold	Low cost Fastest implementation	Volatile emissions Health risks Inconsistent results Less efficient material usage
RTM	Closed mold In-plane resin flow Two-sided mold	Higher dimensional consistency Less volatile emissions Both sides finished	Higher mold cost Resin flow pattern critical Costly equipment required Lowest volume per port
VARTM	Closed mold In-plane resin flow Two-sided mold Evacuated mold	Higher dimensional consistency Less volatile emissions Both sides finished Higher quality products than RTM	Higher mold cost Resin flow behavior critical Costly equipment required Complexity of vacuum porting
SCRIMP	Closed mold In-plane resin flow One-sided mold Evacuated mold	Higher dimensional consistency Less volatile emissions Higher quality products than RTM	Proprietary process One side finished
FASTRAC	Closed mold Channel flow One-sided mold Evacuated mold	High quality High dimensional consistency Less volatile emissions Largest injection volume per port	Added cost of FASTRAC layer Highest complexity Possible artifacts from bag Costly equipment required

The final properties of the composite are sensitive to the actual angles of the fibers in the individual plies [8]. Several factors can affect the final fiber orientation angles of a composite part. Fabrics that are stitched together at a prescribed angle (such as DB120) can have some angular variation on the roll as purchased. This error can be significant, and should be checked if the fabric is intended for use in a critical application. Second, the pre-form stage can introduce error in orientation angles. Hand installation of fabrics into a mold is an inexact process. Third, injection of resin during any of the major injection processes discussed can cause fiber wash. Fiber wash can be catastrophic, causing huge deviations from the desired lay-up or can cause slight fiber

misalignment in one or more layers. The possibilities of fiber wash occurring need to be considered when specifying manufacturing processes. Since composites are sensitive to slight angular variations, angular tolerances should be studied and specified for critical parts.

Resin viscosity is a critical parameter of all injection processes. In this thesis, the resin viscosity was not varied as a process parameter, but was monitored to support valid results. The determination of resin viscosity was done using the method described in [4]. Viscosities were determined experimentally using a capillary rheometer designed to ASTM Standard D3835-79 and shown in Figure 9.

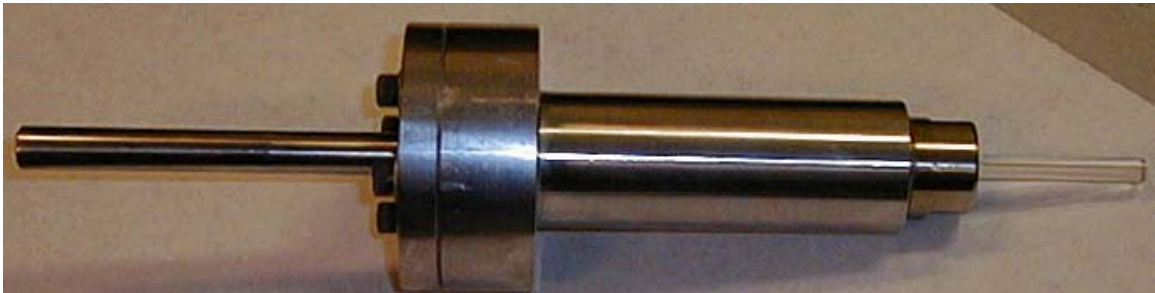


Figure 9: Capillary rheometer [4].

Validation Methods

One of the goals of this work is to show that the parts produced by this manufacturing method (pressure bag molding) are mechanically comparable to parts produced by other common techniques. Therefore, a brief discussion of methods of testing mechanical properties follows. The mechanical tests generally address the

different failure modes that composite materials may experience in service. Evaluating the performance of a composite to its mechanical limits is intended to validate its manufacturing method.

Determination of Fiber Volume Content

The amount of fibers relative to the amount of matrix in a composite is commonly described as the composite's fiber volume percent. For this thesis, fiber volume percents were determined using an ASTM standard "burn-off test" [24]. Since the melt temperature of glass fibers is much greater than the combustion temperatures of polyester matrix materials and common stitching or weaving materials, a fiberglass sample can be heated until all matrix and binding materials combust out of the sample leaving only the glass fibers. Before heating the sample in the oven, the volume of the sample is measured. After combustion is complete, and after the sample is cool enough to handle safely, the glass fibers are weighed, and the density of glass is used to determine the volume of glass remaining. Dividing this glass volume by the original composite volume yields the fiber volume fraction.



Figure 10: Burn-off test showing combustion products.

It has been shown that after a single burn-off test has been conducted for a specific lay-up, the fiber volume percent can be determined by simply measuring the thickness of a sample of the same fabrics and lay-up [25]. This was the approach used in this work.

Tensile Test

A very common test is the tensile test. Flat plate products are cut into coupons for destructive testing. Coupon width should be wide enough to negate the variation that can be introduced if the coupon is cut through a fiber tow or between fiber tows [8]. The gage length, or the distance between grips needs to be large enough to account for statistical variations in the material being tested. The sample is gripped in a test apparatus and loaded axially (typically by displacement controlled loading) until complete failure. The maximum load is divided by the cross-sectional area of the sample

to determine the ultimate tensile strength. Displacements associated with specific load are sometimes collected to construct a stress-strain diagram which could provide valuable details of the failure behavior.

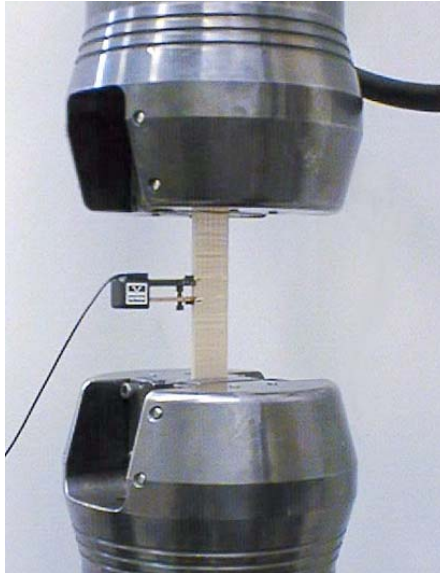


Figure 11: Tension test with an extensometer to collect displacement data.

Compression Test

Compression properties of composite materials are at least as important as tensile properties because compressive strengths are typically lower than tensile strengths. If a part is going to experience tensile and compressive loading of equal magnitude (such as a turbine blade with a bending load applied), it is likely to fail in compression. There are at least three ASTM standard compression tests that have been developed for composites [8]. Compressive properties are difficult to obtain because of the tendency for a coupon to fail by buckling during testing. Therefore, the test equipment and methods used to

determine compressive strengths are as important as the values obtained themselves. In this thesis, ultimate compressive strengths were obtained by using 25 mm wide coupons and a 12 mm gage length to minimize the possibility of buckling.

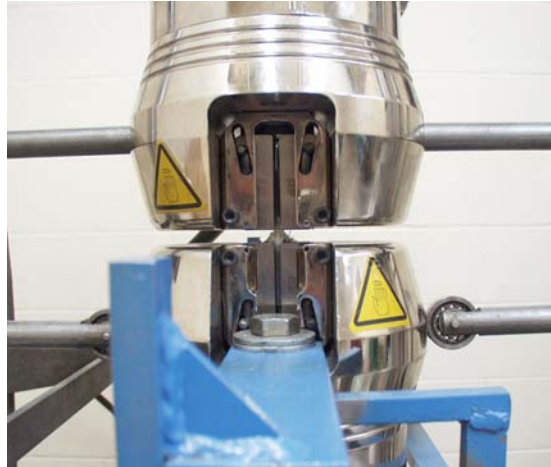


Figure 12: Compression test using short gage length to minimize buckling effects

Short Beam Shear Test

An ASTM standard short beam shear test [26] has been developed to address the unique shear strength considerations of laminar materials. In this test, a short beam is tested in 3-point bending to failure. Since the interlaminar shear strength of these types of laminar materials is inferior to the in-plane properties, samples in this test tend to fail in shear, delaminating between layers. This interlaminar shear behavior is sometimes used to qualify manufacturing processes for composite materials such as the materials used in this study.

The standard specifies the support span given the thickness of the samples. For glass-reinforced composites, the span/thickness ratio is specified as 5, and the sample thickness/thickness ratio is 7.

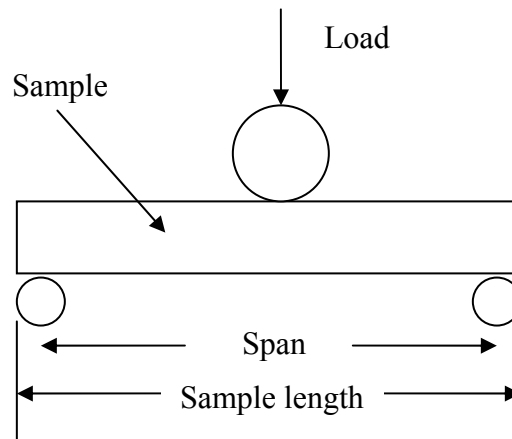


Figure 13: General schematic for short beam shear test.

To perform this test, the 6.35 mm diameter loading nose loads the sample at a rate of 1.3 mm/minute until the sample fails. At least 10 samples are averaged together and the short beam shear strength is obtained from Equation 5 [26]:

$$S_H = 0.75 * \frac{P_B}{b * d} \quad 5)$$

Where S_H is the apparent shear strength

P_B is the maximum load at failure

b and d are the width and thickness of the sample

Fatigue

Since fatigue is a design consideration when using composites, testing is done to determine fatigue strengths. There is an infinite combination of loading situations that can be used in fatigue testing. Fatigue testing should be designed to represent the specific design requirements of the application. Loading is commonly applied with a sinusoidal waveform. A specific loading combination is typically described by its “R Value”, which is defined as:

$$R \text{ Value} = \frac{\text{Minimum Cycle Stress}}{\text{Maximum Cycle Stress}} \quad 6)$$

Fatigue testing to high cycles can take a considerable amount of time [8]. Because of the extensive time requirements and limited equipment availability, fatigue testing was not performed as a part of the manufacturing process validation.

Delamination

The differing properties of discrete layers of fabrics separated by a thin resin layer introduce failure mechanisms unique to laminar materials. Delamination can occur between fabric layers in a composite. Three loading situations that can cause delamination are shown in Figure 14.

Mode I and mode II failure are the most common because they occur due to typical loading situations. Mode I failure can occur in bonded joints, stiffeners, etc. A “Double Cantilever Beam” (DCB) test is used to quantify the performance of a laminate in a Mode I loading situation [27]. Mode II failure can occur anywhere that a composite

has a bending load applied to it. In bending, transverse shear stresses can result in delamination failure before normal stresses reach their ultimate. Transverse shear results from bending loads as described by Equation 7 [28].

$$\tau = \frac{VQ}{Ib} \quad 7)$$

Where τ = Transverse shear stress

V = Internal shear force (from equilibrium)

Q = First moment of the area about the neutral axis

I = Moment of Inertia

b = thickness

Since shear stresses are greatest at the neutral axis (where Q is maximum), delamination tends to occur between fiber layers nearest the center of a laminate. An “End Notch Flexure” (ENF) test is commonly used to quantify the performance of a composite in a Mode II loading situation.

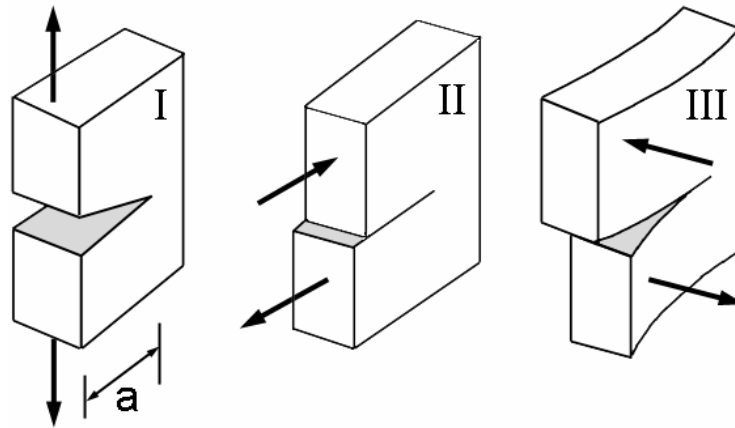


Figure 14: Three delamination failure modes

Fiber Alignment

Since the mechanical properties of composite materials that use fabrics made with oriented fibers are highly directional, the performance of a finished part is dependent on the exact orientation angles of the individual layers. Unbalanced or non-symmetric lay-ups experience warpage when removed from the mold because of uneven contraction and residual stresses about the neutral axis. Twisting and other behavior can result under mechanical deformation when a lay-up is not symmetric with respect to the ply angles. The need for tight control of fiber angles is one of the reasons that fiber wash is not desirable during manufacturing.

Methods for measuring fiber alignment are few. Tracers can be added to a fabric, which visually indicate the orientation of a layer in a finished part. This method, however, doesn't work well if the matrix material is not suitably translucent, or if there is a colored finish coat applied, such as a gel-coat applied to the mold surfaces before

injection. A method that has been used at Montana State University to measure fiber orientation for lab experiments uses the burn-off test procedure, similar to the test used to determine fiber volume percent. In this version of the burn-off test, the combustion is done carefully as to not dislocate fibers. After burning is complete, the layers are carefully removed and the angles are measured.

Porosity

Porosity is the presence of voids and gas pockets in the matrix of a laminate on a microscopic level. Porosity occurs to varying degrees in all of the common manufacturing processes discussed above. It can occur in vacuum assisted processes if the applied vacuum is enough to boil the styrene. If the resin used has saturated gases in solution or has absorbed water from the atmosphere, these impurities can boil off under even a modest vacuum, resulting in porosity in the final product.

Some fabric architectures are more prone to porosity than others. Porosity tends to occur at locally high glass concentrations in stitched and woven fabrics [8]. This is likely a result of the locally restricted flow resulting from the smaller channel area between fibers. Since resin can flow quickly around these local areas, flow fronts tend to close around them, entrapping gases near the locations of the stitching or weaving materials. Surface properties of the weft weaving strand materials used in A130 fabrics has been found to be incompatible with some resin materials, further encouraging this phenomenon (Figure 15) [8].

Measuring porosity is difficult [29]. The preferred method of porosity measurement for laboratory samples that has been employed at MSU has been

microscope viewing. Small samples are cut and mounted in transoptic viewing material and polished. Pores are viewed and measured under magnification, and pore area summed and averaged over several iterations on different layers of the same sample. Other methods have been investigated such as computed tomography (CT) [5]. While CT technology shows promise, equipment is expensive, involves the use of transmission frequencies that represent significant health risk, and the process is somewhat subjective for consistent results [5].

This thesis introduces a technique that could be developed to provide porosity data in a research or manufacturing environment. It involves the measuring of the transmission of infrared light through a sample. This process and equipment will be discussed in detail in subsequent sections. However, the development of a method to acquire porosity data is beyond the scope of this thesis and is discussed in the “Future Work” section.

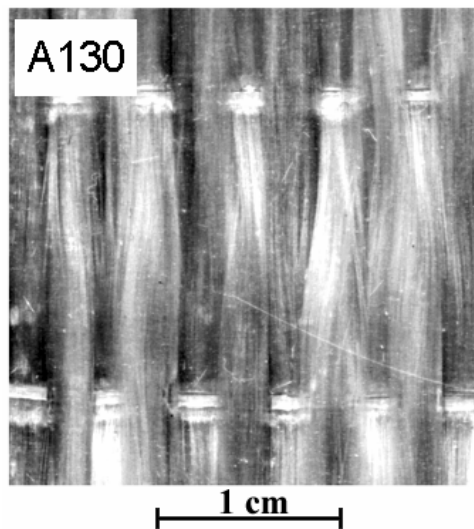


Figure 15: Woven A130 fabric showing poor wet-out characteristics at local areas near weft weaving strands [8].

Table 2: Summary of typical mechanical tests and information gained.

Procedure	Motivation	Information gained
Burn-off test	Ratio of fibers to matrix provides information about laminate design and product quality	Fiber volume content
Tensile test	Shows if materials are performing up to their abilities	Ultimate tensile strength
Compression test	Can determine if fiber alignment and other factors are affecting mechanical properties	Ultimate compressive strength
Short beam shear test	Assists in how manufacturing process affects shear strength	Short beam shear strength
Fatigue test	Provides insight into product lifetime mechanical performance	Fatigue strength
Delamination testing	Provides insight into product delamination performance	Mode I, II, III shear strength
Fiber alignment measurement	Injection processes can affect product properties by displacing fibers	Injection process performance metric
Porosity measurement	Voids and porosity are considered manufacturing defects	Percent porosity

CHAPTER 3

DAMAGE ASSESSMENT USING INFRARED TRANSMITTANCE

Damage in Fiberglass

One of the qualities of fiberglass composites that make them attractive for engineering applications is their ability to tolerate damage. A relatively large amount of work needs to be done to a fiberglass part to break it. This is evidenced by the large amount of damage that is present after a destructive laboratory tensile test (Figure 16). Toughened resin systems continue to be developed which offer improved damage tolerance [30].

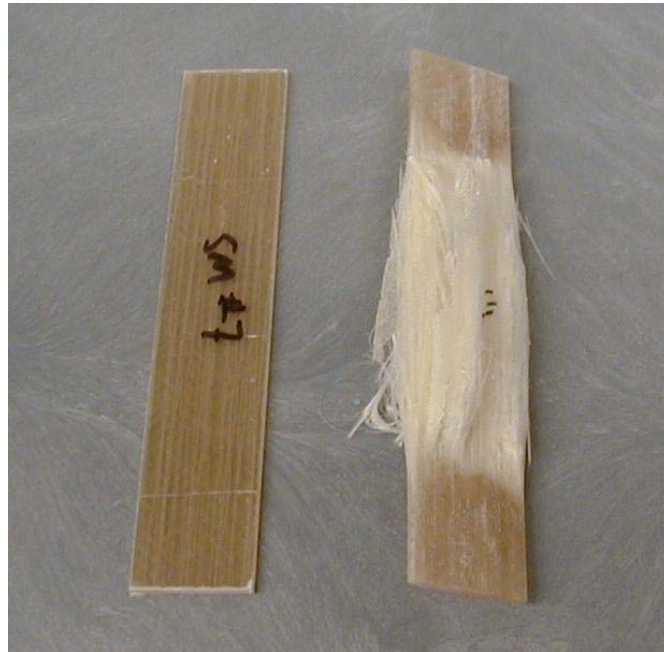


Figure 16: Before and after ultimate tensile strength test of fiberglass.

Damage in a laminar fiberglass composite occurs in stages. Since the ultimate strain of the matrix material is typically much lower than that of the fibers, the first noticeable damage that occurs is matrix cracking. As the strain increases from the onset of matrix cracking to the ultimate strain of the fiber, the density of matrix cracks increases. If a composite is unloaded after sustaining matrix cracking, there is some measurable difference in the stiffness of the sample in subsequent load applications as a result of the compromised matrix. However, since the stiffness contribution of the matrix material is typically an order of magnitude less than that of the fiber, the composite still performs nearly as well in common loading situations as it did before the damage was introduced. When a composite is strained to the point where fibers begin breaking, the damage is typically extreme and the performance of the part is significantly compromised. If damage is being introduced in a load-controlled manner, fiber breakage is usually catastrophic.

Infrared Transmittance Test.

A new non-destructive test is discussed in this thesis which was developed and used in this work to quantify the relative level of damage in a fiberglass composite. Most common matrix materials for low-cost fiberglass laminates are (to a varying degree) transparent. Glass fibers are transparent. When light passes through a fiberglass composite material, any boundaries that are encountered will either reflect or refract the light (Figure 19). Reflection occurs when the angle of incidence is greater than the critical angle for the given materials. The Law of Reflection (Equation 8) states that light reflects away from a boundary at the same angle as the angle of incidence [22].

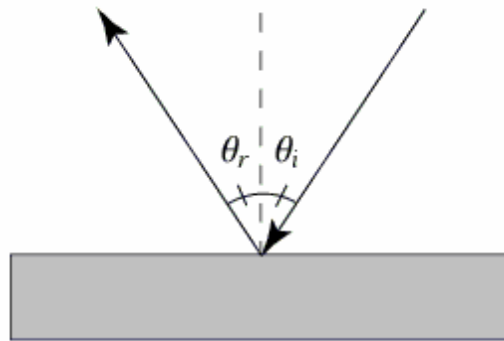


Figure 17: Reflectance

$$\theta_r = \theta_i \quad 8)$$

Refraction occurs when the angle of incidence is less than the critical angle. Refraction is predicted by Snell's Law (Equation 9) [22]. In both cases, there is less light transmitted in the incident direction than if there was no surface to pass through. For the same materials, lay-up, etc., higher quality composites can be differentiated from lower quality parts by visually observing the relative translucence of the parts. The lower quality part likely has more porosity. The voids and pores in a composite part have randomly oriented surfaces which scatter light as it travels through the material. Parts with less porosity will transmit more light than parts with higher porosity.

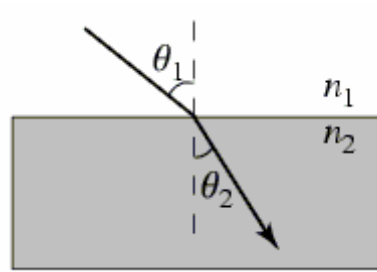


Figure 18: Refraction

$$n_1 \sin\theta_1 = n_2 \sin\theta_2 \quad 9)$$

Where n_1 and n_2 are material refractive indices

IR Transmittance to Quantify Matrix Cracking.

As mentioned above, the first damage that occurs as strain increases in a fiberglass composite is matrix cracking. As the strain continues to increase, matrix crack density increases until fiber failure causes catastrophic part failure. These matrix cracks create boundaries which scatter light in a similar manner as voids do (Figure 21). During a laboratory tensile test, the light scattering as a result of matrix cracking can be visually detected as the sample takes on a “milky” appearance at higher strains. It is this light scattering that a nondestructive test device was designed to measure for this work.

Infrared (IR) light transmission is used in many common devices. IR signals are used for data transfer for television remote controls, computer peripherals, etc. Fax machines and printers use IR interrupt devices to sense paper location while printing.

The infrared light wavelength is just off of the visible range of light on the long wavelength side. Infrared is used because of the low or consistent level of ambient noise. For this work, an opto-interrupt sensor that is commonly used in printers was adapted to investigate the light transmittance behavior of fiberglass composites as manufactured and as they sustained damage.

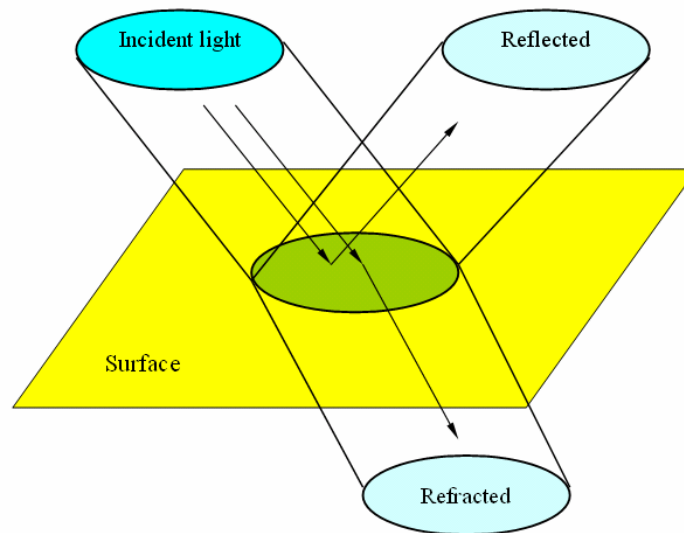


Figure 19: Reflected and refracted light

An Aleph OJ 1000 class infrared opto-interrupt sensor was used to study the transmittance properties of fiberglass samples. A hand-held device (Figure 23) was constructed according to the diagram shown in Figure 24 to test the ability of these electronic components to provide transmittance data. Table 3 lists the components used for this device. It should be noted that the output voltage is measured across the resistor

that is in series with the phototransistor. This means that a drop in output voltage corresponds to an increase in resistance across the transistor. This increase in resistance is a result of decreased light saturation. Although these components are typically used to provide “on” or “off” signals (light hitting the transistor or no light hitting the transistor), they proved to be capable of providing suitably accurate relative transmittance data also. Positioning a fiberglass sample between the sensor’s infrared LED and phototransistor with the sensor “on” caused a change (drop) in output voltage. Samples with the same lay-up but of differing quality showed different output voltage changes.

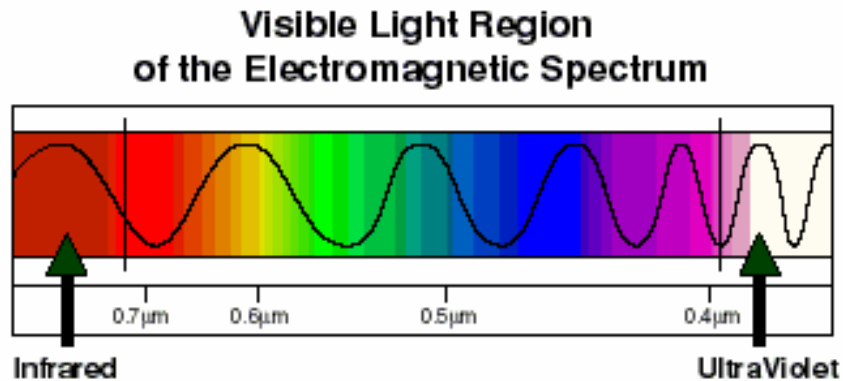


Figure 20: Visible light spectrum.

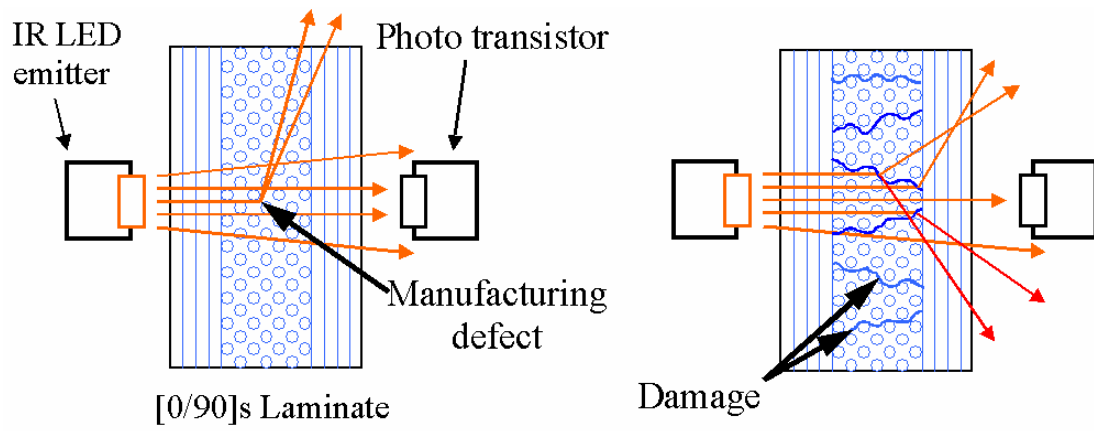


Figure 21: Light scattering resulting from defects and damage.

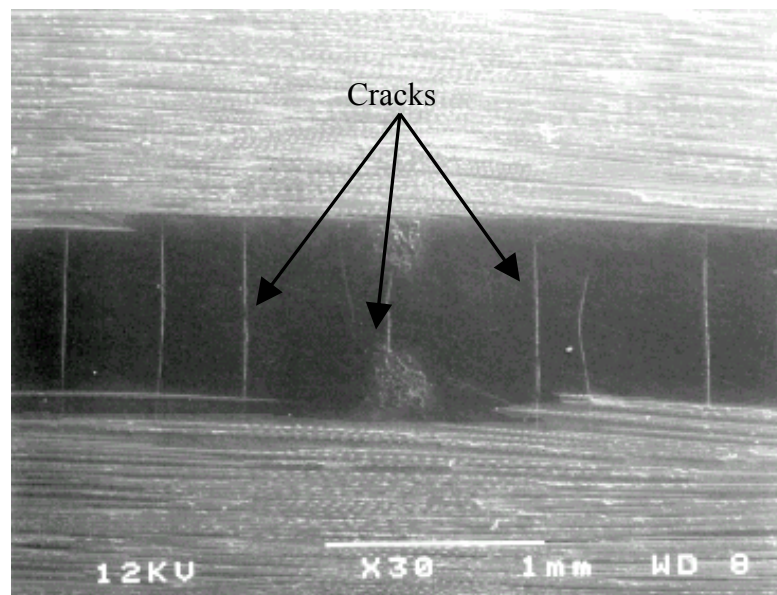


Figure 22: Matrix cracking between fiber tows.

To study this behavior further, the hand-held opto-interrupt device was altered such that the electronics were mounted on a small circuit board designed to attach to a composite sample as it underwent a tensile test (Figure 25). The IR sensor and an extensometer were attached to a [0/45/-45/0]_s E-glass/polyester resin sample and loaded uniaxially using an Instron 8562. Load, strain, and phototransistor voltage response was collected until the sample failed. The results are shown in Figure 26.

The ultimate strain of the matrix material in this composite is about 0.3%. From the load-strain curve, careful analysis will reveal a decreased slope after this strain, but it is difficult to see by inspection. The infrared response, however, shows a distinct difference as the strain exceeds the ultimate strain of the matrix. Before 0.3% strain, the voltage response was constant and linear. Beyond this strain, the voltage decreases nearly linearly until failure. This is a result of the matrix crack density (and light scattering) increasing with strain.

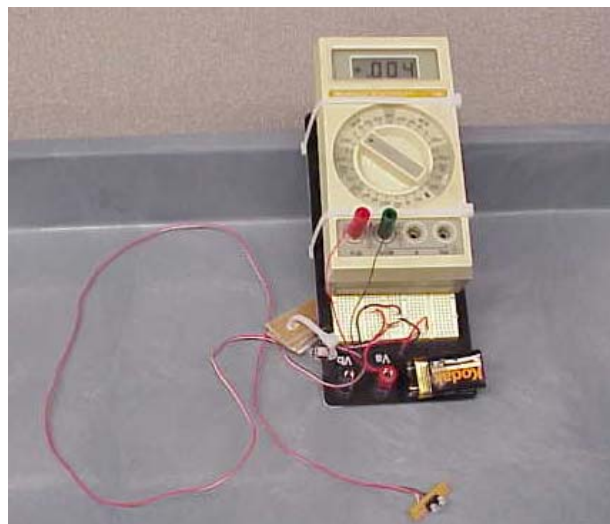


Figure 23: Hand-held device for spot-testing of IR transmittance.

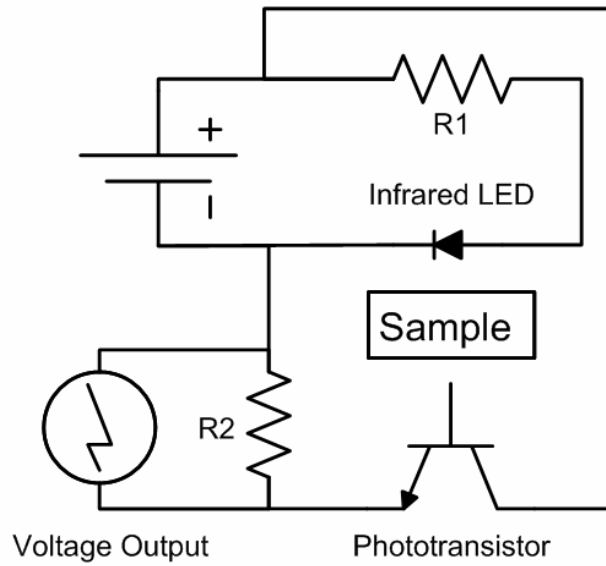


Figure 24: Wiring diagram for IR LEDs and phototransistors used.

Table 3: Components used in hand-held IR transmittance device.

DC power source	9 Volt battery	Kodak 6LR61
Voltage Output	Digital Multi-Meter	Beckman Industrial 310
R1	Standard resistor	680 Ω
R2	Standard resistor	100 Ω
IR LED and Phototransistor	Opto-interrupt sensor	Aleph OJ-1000

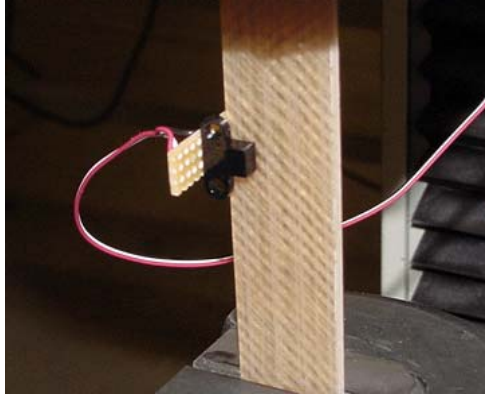


Figure 25: Infrared opto-interrupt sensor used in a tensile test.

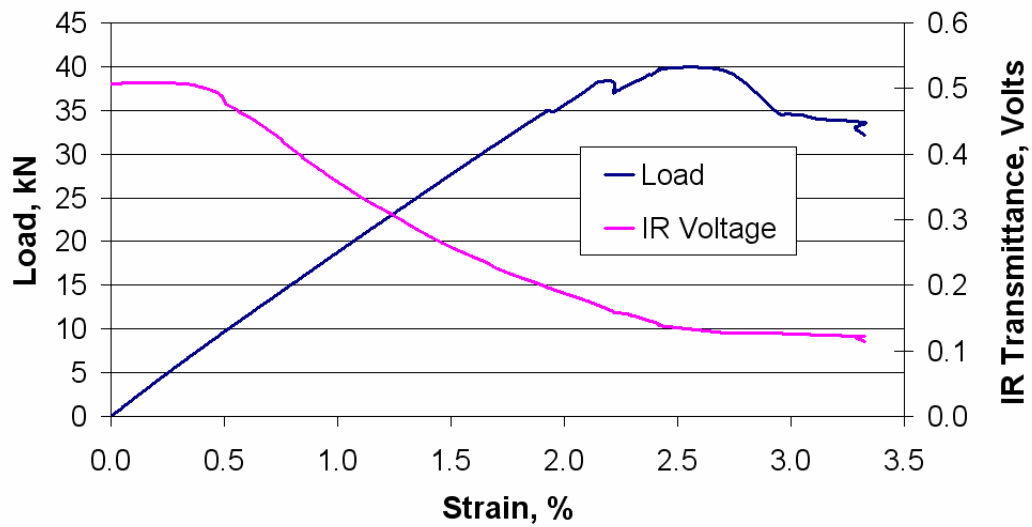


Figure 26: Stress-strain and opto-interrupt voltage response for fiberglass sample

To investigate the IR transmittance performance under loading of samples of differing qualities, this test was repeated for several samples of the same materials and

lay-up, but with distinctly different qualities with respect to void content. Three examples of the samples examined in this test are shown in Figure 27. The sample to the left in this figure was manufactured by a vacuum assisted molding method, and its void content is much lower than the void content of the other two. The middle and right samples in the figure were manufactured by RTM and are the same materials and lay-up. The rightmost sample was cut from an area near the flow front and contains much more entrapped gases. The photograph was taken against a background that had lines running across the samples. The lines can be easily seen through the highest quality sample. The lines can be seen faintly through the medium sample. The highest porosity sample hides the background lines completely. Different quality samples like these were tested in tension tests to failure as the transmittance, load, and strain data were collected. The results are shown in Figure 28.

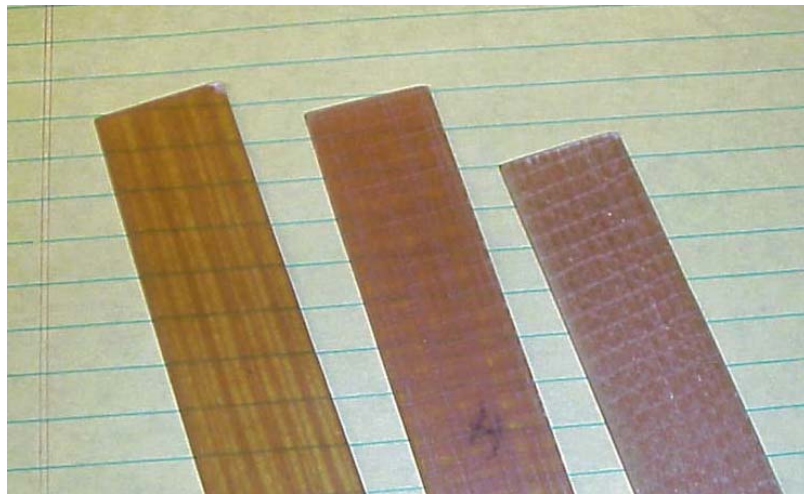


Figure 27: Photograph of samples of differing void content.

As can be seen from the results, the IR voltage response curves started at distinctly different levels which represent their differing porosities as manufactured, then at about the ultimate strain of the matrix material, they started to decrease in transmittance (at different slopes) until catastrophic failure.

A similar experiment was conducted for samples that were constructed with a different material for the zero degree plies. In this test, D155 fabric was used for the zero degree plies. Results, shown in Figure 29, were similar to those obtained in the test of materials using the UC1018GV material.

It should be noted for these tests that they were intended to be exploratory only. The strain data was collected using the internal LVDT on the Instron, which does not account for grip movement, grip slippage or crosshead deformation. As can be seen in the plots, the materials purported to be of higher qualities show a lower elastic modulus (the slope of the stress-strain curve). This is intuitively not correct. It is easily understandable if the higher quality samples coincidentally experienced more grip slippage during loading. Using the Instron's LVDT for data collection was convenient, but the strain data collected is not accurate due to the inability to account for these displacements during tensile testing. Additionally, there is an anomaly in the 0.1 – 0.2% strain range (as can be seen in Figure 28 and Figure 29) that is attributable to errors in the data collection functionality on the Instron. This anomaly is not due to matrix cracking and should be ignored. Since these tests were done as early exploratory work, these inaccuracies were deemed to be acceptable.

The results of these preliminary tests are noteworthy. The obvious knees in the transmittance curves followed by subsequent reductions in transmittance show that transmittance testing can be very sensitive to matrix cracking. This result implies promise for the ability to detect sub-critical damage in a fiberglass composite. It is this sub-critical damage that is quantified and mapped in the form of a damage progression test later in this work.

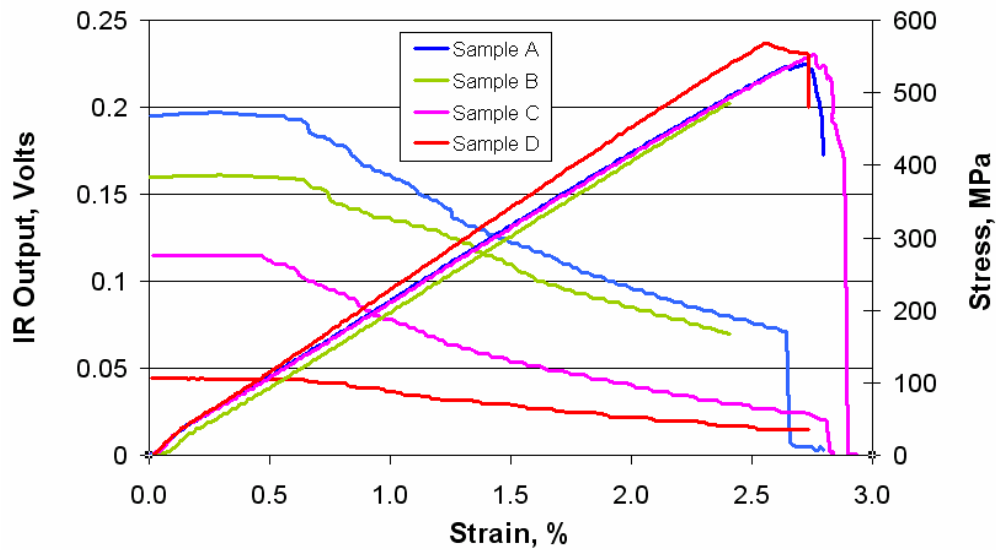


Figure 28: Stress-strain and IR transmittance for differing porosity samples of UC1018GV material in the zero degree direction in [0/45/-45/0]_s laminate.

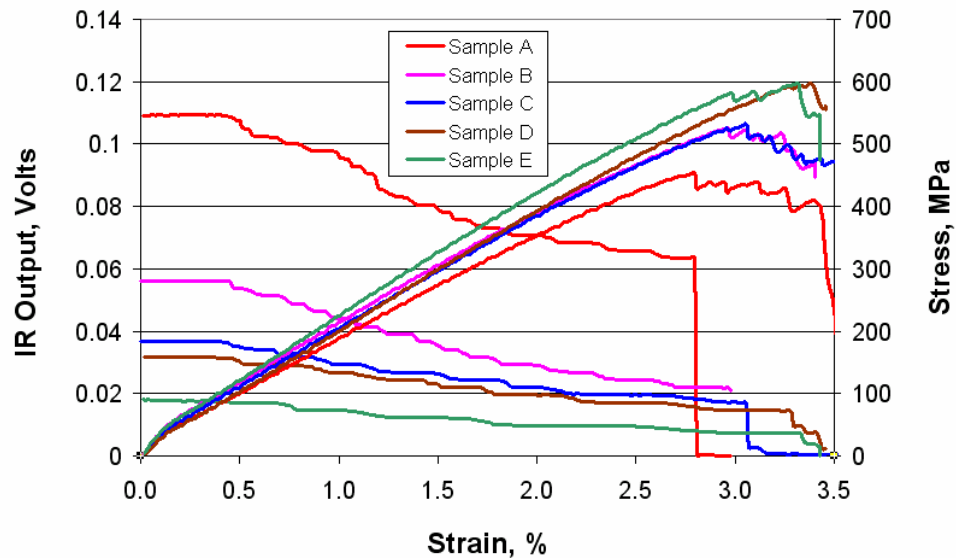


Figure 29: Stress-strain and IR transmittance for differing porosity samples of D155 fabric in the zero degree directions in $[0/45/-45/0]_s$ laminate.

Another experiment was performed to study IR transmittance during a series of loading and unloading. A sample was prepared of $[0/45/-45/0]_s$ using UC1018GV for the zero degree directions and DB120s for the 45 degree directions. The sample was loaded in tension such that the maximum strain was well into the matrix cracking region, but less than the ultimate strain of the fibers. The sample was unloaded and this cycle repeated ten times. The IR transmittance voltage output was recorded manually before each loading cycle and at each maximum strain. Results are presented in Figure 30. As can be seen, when the load was removed from the sample, the IR transmittance increased (a result of matrix cracks mechanically closing), but not back to the original transmittance. With each successive load cycle, transmittance decreased from the previous point at maximum strain and at no strain. This behavior trend continued asymptotically until it

appears there would be no change with continued cycling. This preliminary work implies that infrared transmittance measurements can detect a relative degree of matrix cracks not only as they are forming during a tensile test, but also after the composite is unloaded, and can possibly detect when a certain limited number of “overstrain” events has occurred.

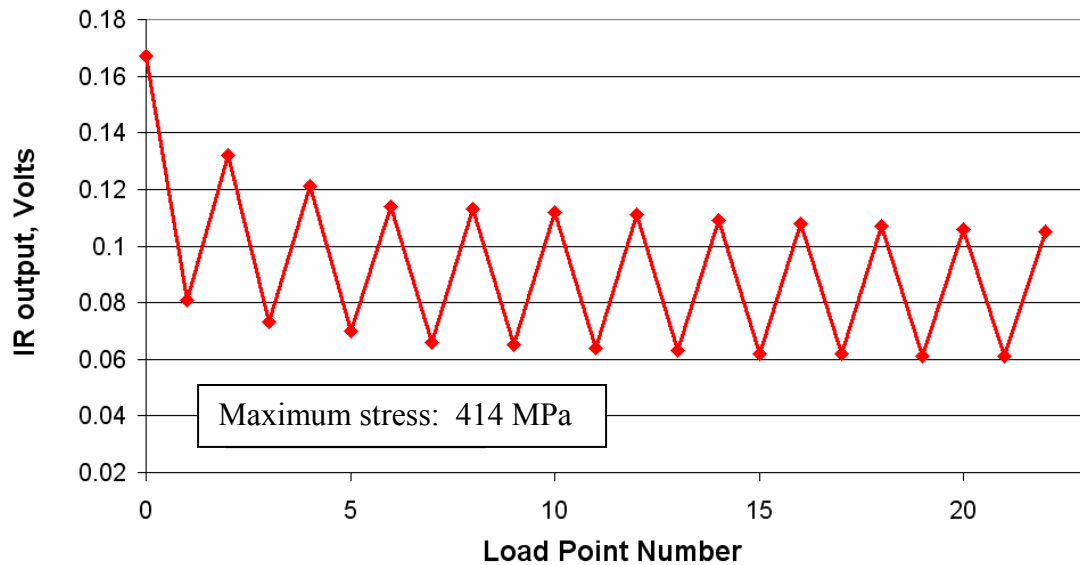


Figure 30: IR voltage output during multiple loading and unloading cycles.

Some limitations were also discovered in this preliminary investigation. Some of these limitations may be alleviated with further research while others are apparently intrinsic to the materials and electrical components used. First, the stitching and weaving materials used in some fabrics do not transmit light. If a sensor beam would happen to be positioned to intersect one of these materials, the transmittance would show to be very low, independent of the material damage or quality state. Also, thick laminates transmit

little light. For the material samples used for this work to this point, the average specimen thickness was about 3 mm. At this sample thickness, and with these components, voltages, light frequency, etc., the output voltage for a good quality sample is cut approximately by half compared to the “open window” voltage.

Another test was conducted to investigate the IR transmittance properties of a fiberglass composite of varying thickness. This test was conducted to gain an understanding of the behavior of the transmittance as the sample thickness (and distance between LED and phototransistor) increases. One of the potential applications of this technology may be to laminate the components into a structure and monitor transmittance periodically during the lifetime. Since likely applications of this technology may be in very thick laminates (for large wind turbine blades), an understanding of the behavior at different laminate thicknesses is in order.

A relatively thick, high quality laminate which was produced by VARTM was cut at an angle such that the thickness tapered from its original thickness to zero over a distance of 115 mm. The material used in this sample was D155 (uniaxial stitched fabric). The lay-up was $[0_2/90]_{4s}$. The surface which was exposed after cutting was polished to a FEPA P#1200 finish to minimize light scattering resulting from the cutting operation. This sample is shown in Figure 31. This sample was mounted in an x-y stage instrumented with transmittance electronics (this apparatus is discussed in next section). The Infrared transmittance was measured along three lines in the direction of varying thickness. Infrared transmittance voltage response measurements were recorded every

0.635 mm. The three sets of measurements were recorded and averaged, and the resulting average transmittance response is shown in Figure 32.

Results from this experiment were as expected. The transmittance decreases with increasing material thickness. The variations in transmittance that are apparent in Figure 32 are likely due to light scattering by the stitching materials used in the D155 fabrics.

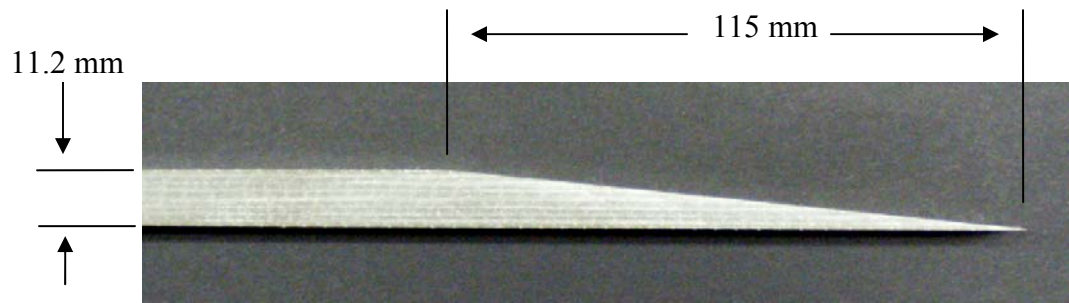


Figure 31: Thick VARTM laminate used for thickness IR transmittance test.

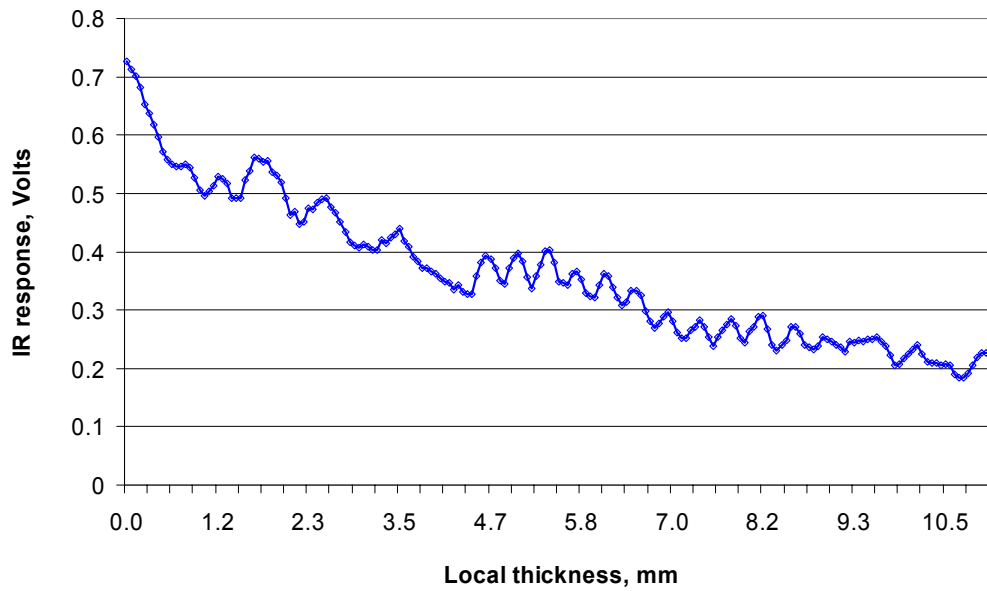


Figure 32: Infrared Transmittance response along a varying thickness VARTM sample.

In discussions about this investigation with professors, other researchers, etc., the question frequently is asked whether this measurement technique can be extended to carbon fiber laminates. Carbon fibers do not transmit visible light. However, x-ray techniques are used to evaluate carbon fiber composites. X-ray (a much higher frequency than visible light) use is not desirable because of its danger to humans. However, there may be a light frequency somewhere between visible light and x-ray that carbon fiber will transmit and is safer for human exposure. A thorough spectrum response study is in order to investigate the transmittance behavior of these materials. That study was beyond the scope of this work, and is mentioned in the “Future Work” section.

CHAPTER 4

VACUUM ASSISTED PRESSURE BAG MOLDING

The Pressure Bag Molding Process

Consideration of the flow requirements in the major closed-mold processes reveals two general types of resin infusion: in-plane flow and through-thickness flow. Laboratory experience and previous work have revealed limitations when using in-plane flow in an infusion process [5]. These limitations manifest as low injection volume from a port and high total injection time. Work has been done to develop infusion processes that encourage through-thickness flow [20, 21]. This thesis discusses an alternative vacuum assisted pressure bag molding infusion process (usually referred to in this thesis as just “pressure bag molding”) that also reduces dependence on in-plane resin flow. It is most similar in mechanisms to the FASTRAC process, with some distinct differences. Experimentation for this work had begun before most of the publications discussing FASTRAC were made available. Therefore, this work could be considered an independent verification of FASTRAC principles, or the principles of two-stage processes in general. In any case, the results of this work are intended to reveal greater potential for two-stage processes that employ through-thickness flow mechanisms as compared to processes that depend on in-plane flow such as standard RTM. Immediately following is a description of the general mold design and process used. Specific molds constructed and experiments performed will follow this general discussion.

Pressure Bag Molding

The pressure bag molding process investigated at MSU uses a two-sided mold. However, only one side of this mold has requirements for surface finish and critical finished part tolerances. A bagging film is used to separate the mold cavity into two chambers, a lower chamber for the preform and an upper chamber that will collapse after resin flow is accomplished. The major parts of the pressure bag mold are shown in Figure 33.

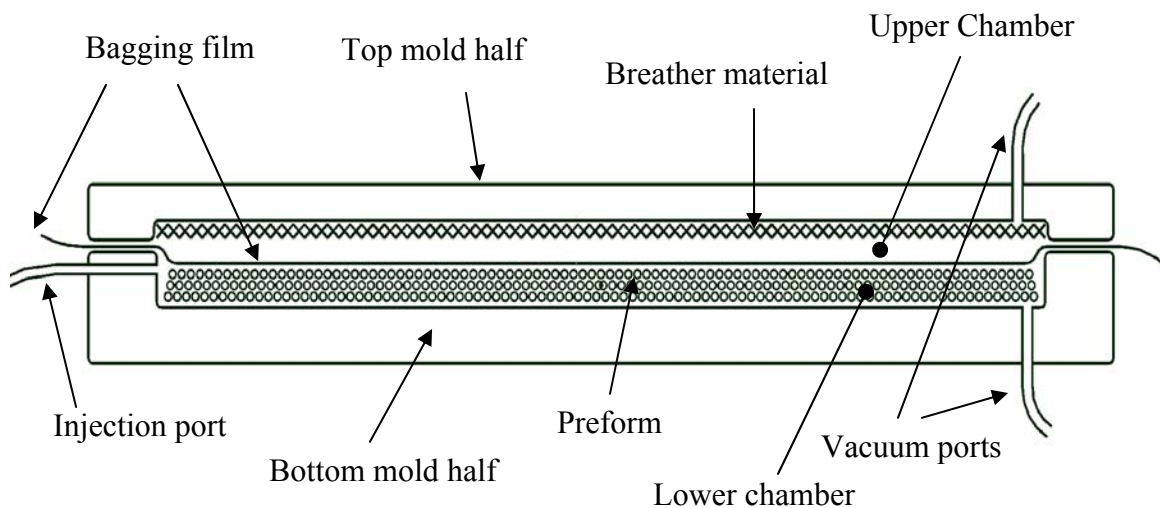


Figure 33: Pressure bag mold parts.

The finished mold surfaces of the bottom mold half are prepared by cleaning and applying suitable mold release agents. The preform or fabric is placed into the cavity in the bottom mold half. Bagging film is placed over the preform such that it would be sealed against the bottom mold half, creating the lower chamber. This seal was accomplished in the following experiments using a combination of tacky-tape and rubber

gaskets. The top mold half is then clamped to the bottom, creating the upper chamber. The upper chamber is also sealed to facilitate pressure control. After setting up the mold for an injection “shoot”, it was found to be a good time investment to test the seals by pulling a test vacuum and letting it remain for several minutes with vacuum gages monitoring pressure in both chambers. If no audible leaks are detected, and if the gages show that the mold is holding the vacuum in both chambers, it is ready for the injection of the resin.

At the beginning of the infusion process, the injection port is closed. Equal vacuum is pulled in both chambers. The vacuum typically used in this work was 200hPa (about a fifth of an atmosphere). This level of vacuum was used because it is above the vapor pressure of styrene, and it was a comfortable vacuum to maintain and repeat for different molds for the equipment used. After evacuating the chambers to this degree, resin is injected into the lower chamber. It was found to be critical to inject the resin between the bag and the fabric to prevent the lay-up from being displaced. Resin injection is accomplished while the vacuum is held in both chambers. With equal pressure above and below the bagging film, the resin is allowed to flow freely in the lower chamber. Resin pools in the area near the injection port. Since there is no net pressure on the bagging film as a result of equal pressure (or vacuum) in the chambers above and below, the resin flow front can displace the film and flow in the channel it forms between the fabric and the film.

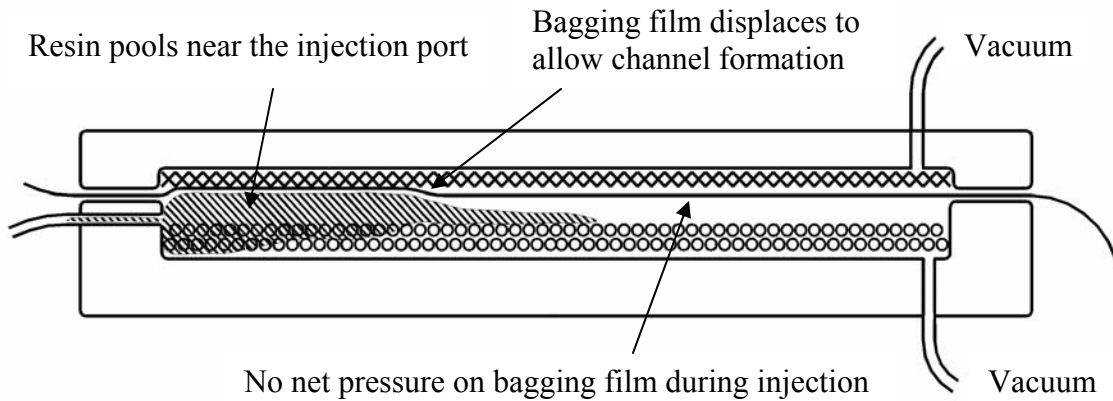


Figure 34: Resin flow in the channel above the preform during injection.

After injecting a pre-determined volume of resin, the injection port is typically closed. The vacuum port to the upper chamber is then opened to atmospheric pressure, while the vacuum in the lower chamber is maintained. When this net pressure is applied to the bagging film, the resin's ability to flow out of the plane of the fabric is significantly reduced. The flow mechanism then transitions from channel flow to Darcy flow. Unlike in-plane flow (RTM, etc.), the Darcy flow here has a significant component in the thickness direction. With the solid top mold half used in this geometry (as opposed to SCRIMP and FASTRAC), upper chamber pressures above atmospheric pressure can be applied to the bagging film, and have proven during initial experimentation to result in relatively higher fiber volume products. This state of increased pressure in the upper chamber will be referred to in this thesis as the second stage of the injection process.

Breather Material. During preliminary investigations with this infusion process and mold architecture, when a vacuum was applied to the upper chamber without the

“breather material” lining the surface of the top mold half, the bagging film was pulled against the top mold half surface around the vacuum port area, effectively closing the vacuum port in the top chamber before large pockets of air were evacuated from areas further away from the port. This caused the bagging film to be forced against the surface of the fabric by the remaining air mass (lack of vacuum) in these areas of the upper chamber, preventing the formation of the resin distribution area. The absence of the distribution channel then kept resin from distributing across the surface of the fabric resulting in dry (unsaturated) areas in the final part. Application of the breather material on the top mold half surface prevented this condition from developing.

Resin Viscosity. As mentioned previously, resin type was not altered as a parameter for this work. Resin viscosity was monitored to support valid results not only for this work, but also to maintain overall research integrity for the composites group at MSU. The resin used was Interplastics Corporation’s orthophthalic polyester 63-AX-051 (Corezyn). Resin was catalyzed using Methyl Ethyl Ketone Peroxide at 1.5% to 2%. Resin viscosity was measured occasionally over the course of this work using excess catalyzed resin after the injection of a mold was completed. As mentioned previously, viscosity was determined using the method described in [4]. A history of the viscosity of this resin type used at MSU is shown in Figure 35.

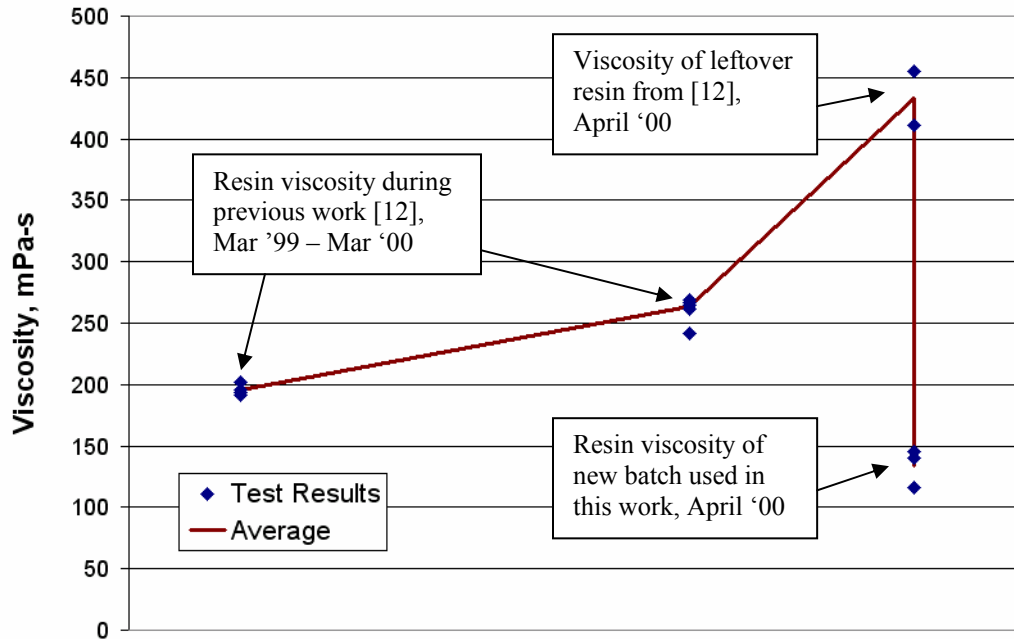


Figure 35: Kinematic viscosity history of Interplastics Corporation's orthophthalic polyester 63-AX-051 (Corezyn) used by the composites group at MSU.

The viscosity of this resin increased with time, and as the remaining volume in the bucket that was being used became relatively small, the viscosity increased drastically. When attempting hand lay-up work with this resin, it was immediately apparent by the poor wet-out properties that the viscosity (and surface properties) had become significantly compromised. A fresh bucket of resin was obtained and used for this work, represented in Figure 35 by the final, lowest measured viscosity reading.

Fabrics and Lay-up. To facilitate reasonable comparisons between tests, the lay-up used in this study was held constant with respect to layers and orientation angles. This lay-up used was $[0/45/-45/0]_s$. The material used for the 45 degree plies was also consistent throughout this work. DB120 material [8] was used for the 45 degree ply

pairs. The materials used for the zero degree direction were varied as a parameter to study their unique responses to infusion process, resulting fiber volumes and resulting mechanical properties. These materials used for the zero degree direction are shown in Table 4.

Table 4: Materials used for zero degree direction plies in common lay-up.

Material Identifier	Supplier	Architecture	Weight [31]
UC1015GV	CollinsCraft	Fiber bonded to glass veil	509 g/m ²
D155	Owens-Corning	Stitched fiber tows	527g/m ²
A130	Owens-Corning	Woven fiber tows	444 g/m ²

The UC1015GV material was chosen specifically because of its architecture. It was identified by [5] as being difficult to RTM. The difficulties are probably from two sources: first, the absence of distinct regions between tows where resin channels in other fabrics cause decreased permeability. Second, the binder typically used to hold the fibers together in these types of materials dissolves in the presence of styrene. This effectively limits the magnitude of pressure that can be applied while injecting in RTM and reduces the amount of time that the pressure can be maintained before fiber wash becomes critical.

Mold Geometry. Several aspects of the basic mold architecture were identified as being critical to the final product. The mold gap, defined here as the distance between the inside solid surfaces of the top and bottom mold halves (Figure 36), was found to be the most critical parameter. During experimentation, as the mold gap was increased, the

injected volume of resin would distribute over less of the surface area of fabric during the first stage of injection. Then, when the pressure was applied to the bag during the second stage, the resin was not able to completely fill the part, leaving dry fabric at the extremities of the part and a large mass of cured resin near the injection port. Conversely, as the mold gap was progressively reduced, the mold configuration approached that of a typical RTM process during the first stage of injection.

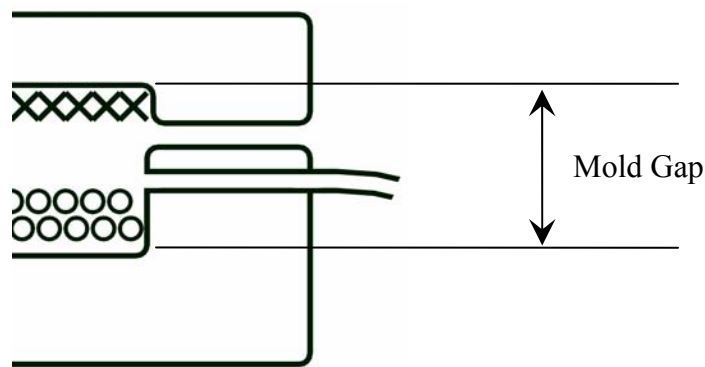


Figure 36: Mold gap definition

Other mold design aspects that are critical to process performance are the locations of the various ports used. Similar to VARTM processes, the injection port(s) need to be located at the opposite ends of the flow path from the vacuum ports to avoid the possibility of the formation of large void pockets. For the relatively simple molds used for this work, that was easy to achieve, but extending these principles to more complex geometries may require more attention to the location of ports.

Since resin is being injected into a three-dimensional cavity of varying thickness (the z-direction dimension is reduced during the second stage), there is some ambiguity in

the z-direction location of the preform during injection. For this work, the z-direction location of the preform during injection was controlled by the situation of the injection port. Resin was injected directly between the preform and the bagging film (see Figure 34). This constrained the fabric into its desired final location (against the solid mold surface) during the first stage of the process. However, there may be some advantages to injecting resin between the bottom mold surface and the preform (the other side of the fabric). This variation was not investigated for this work due to the likely drawback of this design that the fabric would be temporarily displaced from its intended final location against the bottom mold surface during injection.

Injection Rate. Since there is little flow resistance in the mold during injection, injection pressure would indicate more about the injection equipment than the dynamics of the flow in the mold. Therefore, for the pressure bag molding tests, the injection rate was not considered a critical parameter. Nevertheless, the injection time was collected, indicating the flow rate during injection.

During initial testing of the 244 cm mold, a rough process window study was established to become familiar with the mold, and to determine which parameters were critical. In these tests, one of the parameters varied was the injection rate. The rate was increased to about 1 liter/minute for one shoot. The result was catastrophic fiber wash (Figure 37), probably not because of the pressure gradient within the fabric (there is little pressure gradient during stage 1), but more likely because of the momentum of the resin. The waviness apparent in Figure 37 is the crumpled tows from the top layer of UC1015GV fabric that were apparently sheared off of their desired placement by the

resin momentum during injection. Since the resin velocity is a function of the port design, it was deemed a non-critical parameter for this study. Resin injection rates were reduced in subsequent tests to avoid repeated occurrence of this phenomenon.



Figure 37: Catastrophic fiber wash on top layer of injection port end of 244 cm plate.

Pressure, Vacuum, and Time as Parameters. Aside from mold design details and injection rate, several other process-specific parameters became evident. The vacuum applied in the first and second stages, any additional pressure applied to the upper

chamber in the second stage (above atmospheric pressure), and the timing of closing vacuum ports in the lower chamber during the second stage, were all process parameters that were found to affect the final product. However, determination of the extent of the effects of varying each parameter was left as qualitative for this work.

Surface Texture. As mentioned previously, only one side of the pressure bag mold needs to be finished according to the desired surface texture of the parts it creates. The surface on the opposite side of the part is created by the flexible bagging film that has the hydrostatic pressure applied by the pressure in the upper chamber during stage 2 of the injection process. The exact texture that results is a product of the lay-up, bagging film properties, and pressure applied during curing. For reference, the thickness variation seen as a result of this surface texture for the UC1018GV material in the [0/45/-45/0]_s laminate with an average thickness of 2.5 mm (manufactured by pressure bag molding) was around 0.2 mm. The resulting textured surface created by the pressure bag molding experiments done in this work is shown in Figure 38.

This resulting surface texture is probably not unique to pressure bag molding. Any one-sided mold manufacturing process that utilizes hydrostatic pressure on a bagging film will result in this surface effect. This may be a significant aspect of one-sided molding because of the perturbed (wavy) fibers on or near the surface of the laminate. This effect will be discussed in detail in the results of the compressive strength test results in the next chapter.

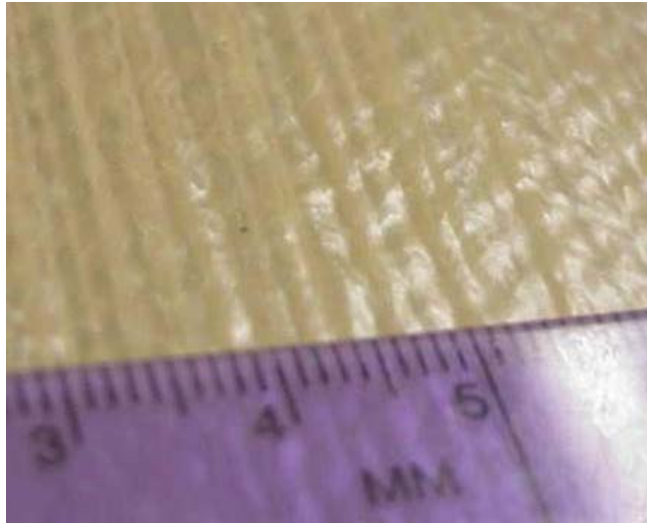


Figure 38: Surface texture on non-molded surface created by bagging film with hydrostatic pressure applied.

Comparison to Existing Processes

To better clarify this process, it may be beneficial to consider similarities to the major existing manufacturing processes that are currently being used for these materials. The closed mold architecture is similar to RTM, VARTM, SCRIMP, and FASTRAC. The benefits of this configuration include greatly reduced emissions.

Injecting resin into an evacuated cavity is similar to VARTM, SCRIMP, and FASTRAC. A major advantage of this is the reduction of air mass in the fabric that would otherwise need to be displaced to avoid porosity and voids. Another advantage of the reduced pressure is that the injection pressures can be reduced (for VARTM and SCRIMP), as the flow front is maintained at a negative (gage) pressure. However, for pressure bag molding described in this work (and FASTRAC), this particular advantage

is not realized because the resin is not injected into the fabric, but into a cavity adjacent to the surface of the preform.

The second stage of the pressure bag molding process involves applying a net positive pressure to the outside of the bagging material. This is similar to SCRIMP, where the entire injection is essentially done with the mold in the second stage (of the pressure bag molding process) configuration. FASTRAC employs the same second stage process, with the exception that the mold design used in this work is more amenable to applying net positive gage pressures to the film. The advantages of the applied hydrostatic pressure are many. The resulting fiber volume percents are more spatially consistent for parts with relatively larger surface areas. This reduces the dimensional requirements on the mold surfaces (for highly controlled fiber volume requirements), as the thickness (and therefore fiber volume percent) are not determined by the mechanical assembly of two mold halves, mold pressure, mold stiffness, fabric thickness consistency, ply drop locations, etc.

The textured surface finish resulting from the use of the bagging material during pressure bag molding is also present when using the SCRIMP and FASTRAC processes.

As discussed previously, the process described in this work is most similar in principle to the FASTRAC process, and can be considered a verification of the FASTRAC principles. The out-of-plane resin flow (without permanent flow channels) is what sets this process and FASTRAC apart from the rest. A possible variation from FASTRAC is the ability to apply a net positive gage pressure to the bagging film during the second stage of the pressure bag molding process due to the rigid upper plate.

Injection Experiments

Several flat plate mold experiments were conducted to investigate aspects of the pressure bag molding process. A mold was constructed to produce flat plates measuring 84 cm x 23 cm using the typical materials and lay-ups used in this study to facilitate a proof of concept for this process. Using the same materials and lay-up, standard RTM was also conducted to compare some of the injection limitations associated with RTM to the pressure bag molding process described in this work. Specifically, two experiments were conducted to investigate injection performance of traditional RTM, one with the plates shimmed apart, which would represent processing designed for higher flow distances, and one with the mold plates clamped directly against the material, which would represent the highest fiber volume percents that could be available using RTM. The goal of these experiments was to expose the limitations of traditional molding, and to show that these basic limitations are not present with pressure bag molding.

After finding in the previous experiment that greatly increased injection distances were likely to be possible with pressure bag molding, another mold was constructed to attempt to determine the maximum injection distance that could be realized with pressure bag molding. A 244 cm x 13 cm mold was constructed to investigate the injection distance capabilities for these materials and lay-up. The mold gap was varied as a parameter to show how it affected the maximum injection distance for this experiment. The injection equipment used was a Radius 2100 injector (shown in Figure 39). The vacuum pump used was an Alcatel 25 hp (shown in Figure 40).

A summary of the injection experiments and the desired results is shown in Table 5. It is also noteworthy that mechanical testing was conducted on the products of the “clamped” and “shimmed” RTM plates as well as the pressure bag molded plates produced from the 84 cm x 23 cm molds. This testing will be discussed in subsequent sections. Discussion of the injection performance tests follows Table 5.

Table 5: Summary of injection experiments conducted to compare performances of RTM to pressure bag molding.

Mold Used	Process type	Configuration	Zero degree material	Information Gathered
84 cm x 23 cm plate	RTM	Shimmed to 2.54 mm	A130, D155, UC1018GV	Injection time/distance for relatively higher injection distance design, Fiber volume, Mechanical testing
84 cm x 23 cm plate	RTM	Clamped against fabric	A130, D155, UC1018GV	Injection time/distance for relatively lower injection distance design, Fiber volume, Mechanical testing
84 cm x 23 cm plate	pressure bag molding	8 mm mold gap	UC1018GV	Injection time/distance for pressure bag molding process, Fiber volume, Mechanical testing
244 cm x 13 cm plate	pressure bag molding	various mold gap	UC1018GV	Injection distance limitations as mold gap varies, Fiber volume



Figure 39: Radius 2100 Injector System

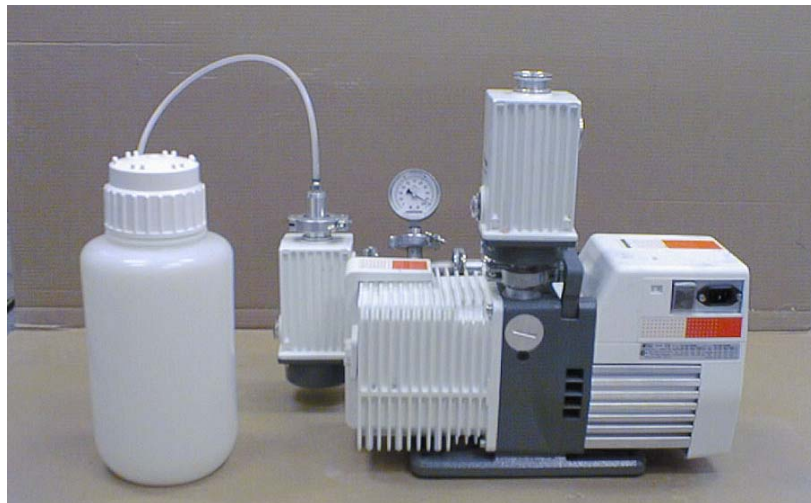


Figure 40: Alcatel Vacuum Pump used in this work

Injection Distance, Time, and resulting Fiber Volume Content for RTM and Pressure Bag Molding.

The maximum injection distance attainable using the traditional RTM processes depends on the fabrics used, specific lay-up, resin properties, mold wall spacing (fiber volume percent), injection pressure, and injection time. This experiment was set up to compare injection distance performances of the pressure bag process to traditional RTM. The zero degree ply fabrics were varied in several plates produced in this experiment to consider performance responses due to fabric architecture differences.

Pressure Bag Molded Plates. An 84 cm x 23 cm mold was constructed to produce flat plates by the pressure bag molding process. A series of plates were molded with the parameters held constant to verify process consistency. The process parameters and materials used for these plates are shown in Table 6.

Table 6: Various parameters used for pressure bag molding flat plate tests.

Parameter Name:	Used in flat plate tests:
Breather Material	Airtech Airweave N4
Bagging film	Airtech Wrightlon 5200
Vacuum during stage 1	200 hPa
Vacuum during stage 2	200 hPa
Gage pressure during stage 2	83 kPa
Average injection time	5 minutes
Mold Gap	8mm
Zero degree fabric	Collins Craft UC1015GV

RTM Plates. To facilitate a reasonable comparison of results obtained from the pressure bag molded plates, plates of the same materials and lay-up were produced using traditional RTM. The first RTM experiment was to produce a set of plates by clamping the mold surfaces directly onto the preform (Figure 41). This situation represented an injection process that would yield the highest fiber volume percents, but would also result in the lowest maximum injection volume per port (and highest injection times) because of the decreased permeability of the compressed fabrics. This experiment represented one end of the RTM process trade-off, where large injection volume per port is sacrificed for a higher resulting fiber volume for a given lay-up, resin system, injection pressure, etc. This clamped mold RTM experiment was conducted for three different common fabrics used for the zero direction plies: A130, D155, and UC1015GV. The purpose for incorporating the different zero-degree materials was to better understand general flow sensitivity to fabric architecture differences.

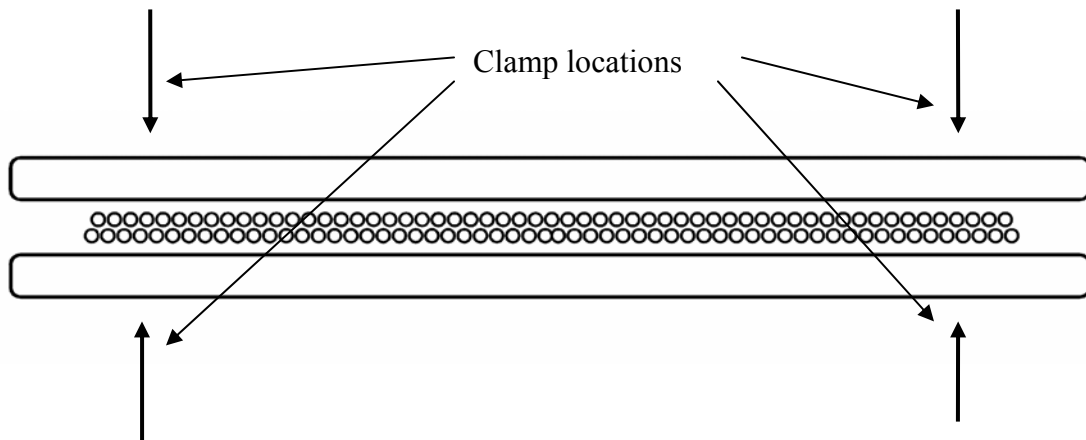


Figure 41: RTM mold configuration for "Clamped" experiments.

Another RTM experiment was conducted where the mold halves were shimmed apart outside of the fabric areas (Figure 42). The spacing used was 2.5 mm for all plates produced in this manner. The mold halves were clamped together at the shim locations to minimize mold deformation due to clamping forces. This configuration was intended to represent a process that would yield lower fiber volume percents, but higher injection distances and injected volumes per port. The same material variations were applied in this experiment as the clamped RTM plates.

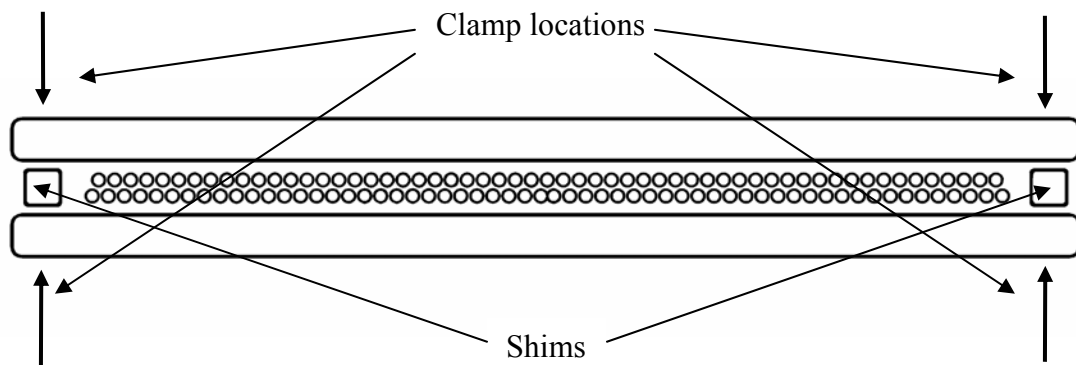


Figure 42: RTM mold configuration for Shimmed experiment

244 cm Mold Experiments. One of the desired results of the flat plate experiments was to reveal an increased injection distance potential for the pressure bag molding process. However, for successfully injected plates (no vacuum leaks, pressure leaks, etc.), the resin seemed to easily fill the part. It was clear that a different

experiment was needed to find the limits of injection distance and volume per port for the pressure bag molding process.

A mold was constructed to produce plates measuring 244 cm x 13 cm by the pressure bag molding process to further investigate these aspects. The small width of the mold was to conserve material, and to allow the same injection press (Radius 2100) to be used, as its injection cylinder volume is limited. The mold was designed to inject from one end of the 244 cm length, necessitating resin to flow the entire length of the plate for a successful shoot. The same materials, lay-up ([0/45/-45/0]_s), and general processing parameters were used to produce several plates using this mold. The material used for the zero degree plies was UC1015GV (Collins Craft unidirectional bonded tows). The mold was designed with an intentionally large mold gap of 1.05 cm, knowing that the mold gap would be reduced as a parameter by adding shim material between the mold top half and the breather film (see Figure 33).

Several attempts were made to successfully shoot the 244 cm distance of this plate with the original mold gap. However, even the best results obtained were plates where the resin did not flow to the end of the plate, and there was an extremely resin-rich area near the injection port. The mold gap was subsequently reduced, and further attempts were made to fill the length of this part. After the second reduction of the mold gap, the entire 244 cm length was repeatedly filled successfully.

Table 7: Injected distance performance as mold gap was reduced for 244 cm mold.

	No shim	One shim	Two shims
hard side spacing, mm	10.5	10.5	10.5
Part thickness, mm	2.54	2.54	2.54
Breather thickness, mm	1.9	1.9	1.9
Film thickness, mm	0.104	0.104	0.104
Shim thickness, mm	0	0.889	1.778
mold gap, mm	10.5	9.7	8.8
Successful Distance, cm	127	178	244+

Injected Distance Comparison. Another set of RTM flat plate injections were set up similar to the plates produced for the fiber volume experiments. Clamped and shimmed plates were set up for lay-ups similar to the previous experiments (using A130, D155, and UC1015GV for the zero degree plies). In this experiment, however, the injection pressure was removed after 5 minutes. The injection time of 5 minutes was chosen because that was the maximum injection time that was used for any of the pressure bag molded parts. The injected distances after 5 minutes under similar injection pressures were tabulated for the clamped and shimmed RTM and the pressure bag molding experiments and are shown in Table 8.

Table 8: Maximum flow distances in the fiber direction after 5 minutes at 115 to 140 kPa injection pressure.

Unidirectional Fabric	Flow Distances after 5 minutes	
	Clamped Mold	Shimmed 2.5 mm
A130 RTM	12.7 cm	20.5 cm
D155 RTM	15.9 cm	17.7 cm
UC1015GV RTM	15 cm	15 cm
UC1015GV Pressure Bag Molded	244+ cm	

The lay-up with A130 materials for zero degree plies proved to be the poorest material for resin flow in the clamped mold experiment. The greatly improved flow performance for A130s in the shimmed experiment is likely a result of the fact that this material contains less glass per unit area than the other materials (Table 4). For the same shimmed distance, the A130 fabric will allow more room for resin flow, but will result in lower fiber volume percent parts. This agrees with the results from the fiber volume results from Figure 43, where the shimmed A130 RTM plate yielded the lowest fiber volume of around 35%. Fiber volume content this low would likely disqualify this laminate from use in most demanding applications.

The pressure bag molding distance experiments using the 244 cm mold did not yield an absolute maximum distance, but the difficulties encountered filling the length until the mold gap was significantly reduced suggest that for this mold, materials, etc., 244 cm was likely close to the maximum that could be achieved. It is significant,

however, that the injection distance is more than 10 times what was observed in the RTM experiments for any of the materials used.

CHAPTER 5

VALIDATION OF RESULTANT PRODUCT

Mechanical Performance Verification

When considering the implementation of a new manufacturing process, or altering a process that has been previously qualified, certain tests are typically required to validate the resulting product. Specific qualification procedures are subjective and vary with different organizations, and are typically tailored to address the specific design requirements of the application. For the purposes of this thesis, a modest qualification test regime was conducted. This procedure consisted of several standard tests followed by a unique test developed for this work. The first was a comparison of the fiber volume percents of plates manufactured by traditional RTM with plates of similar lay-up and materials which were manufactured by pressure bag molding. Ultimate tensile and compressive strengths were determined for the products of both manufacturing processes. Then, an ASTM standard short beam shear strength test was conducted for the products of RTM and pressure bag molding. Finally, the infrared transmittance concept described previously was used to develop a method of quantifying progressive damage behavior in samples manufactured by the pressure bag molding process. The progressive damage performance of a pressure bag molded sample was compared to a numerical progressive damage model that was developed using Ansys.

Fiber Volume Percent Comparison

The plates produced by pressure bag molding and RTM (with mold plates shimmed apart and with mold plates clamped tight against the preform as discussed in the previous section) were cut into samples along the long dimension of the plate approximately in the middle of the width for testing. The fiber volumes were measured at the middle of the samples. Results are shown in Figure 43.

Several things are noteworthy from the fiber volumes chart. First, the pressure bag molded plates clearly yielded the highest fiber volumes. Secondly, the fiber volumes were much less consistent along the plate for the RTM processes. This is likely due to mold deformation from the clamping centered near the edges of the part, possibly compounded by the injection pressure applied at the center of the plate during injection. This spatial inconsistency is a typical challenge for traditional two-sided molding. Many factors can affect mold deformation, increasing the complexity of controlling the part thickness, especially for parts with large surface areas. Extremely rigid RTM molds are built to minimize this deformation.

Two of the data sets represented in Figure 43 have one less data point. This was due to the fact that the resulting injected distance was much less for these two plates, which were the “clamped” RTM plates for the lay-ups which used A130 and UC1015GV fabrics for the zero degree plies. This demonstrates the injection distance (or volume per part) limitation inherent with RTM when attempting higher fiber volumes. These two fabrics have relatively poorer longitudinal flow characteristics compared to the D155 material, the third fabric used. The data sets with one extra point were the unremarkable

result of the coupon length being reduced to allow one more coupon for testing, although it deserves explanation.

The fiber volumes for the shimmed and clamped RTM plates of UC1015GV zero degree materials were very similar. This resulted from the fact that the 2.5 mm shim spacing that was used for the shimmed plates was very close to the “natural” thickness of the “clamped” plates. Therefore there was actually little difference in these two experiments. However, it is noteworthy that the injected distance was sufficiently less to result in one less coupon being available from the clamped experiment plate, suggesting that the injection performance of lay-ups using this material architecture is very sensitive to mold plate spacing.

It is noteworthy to consider the injection times shown in Figure 43. The drastic difference in the time required to inject resin in the two different infusion processes is attributable to their differing governing flow mechanisms. As previously discussed, RTM relies on in-plane resin flow described by Darcy’s law. Pressure bag molding injection is done outside of the fabric, which is described by Stokes’ equation. This is one of the critical differences that could make two-stage molding processes (such as FASTRAC and pressure bag molding) attractive for larger structures such as wind turbine blades.

It is also noteworthy that the hydrostatic pressure applied to the bagging film during the pressure bag process resulted in considerably higher fiber volume percents than even the clamped RTM experiment, which could be considered the highest fiber volumes attainable using RTM processes.

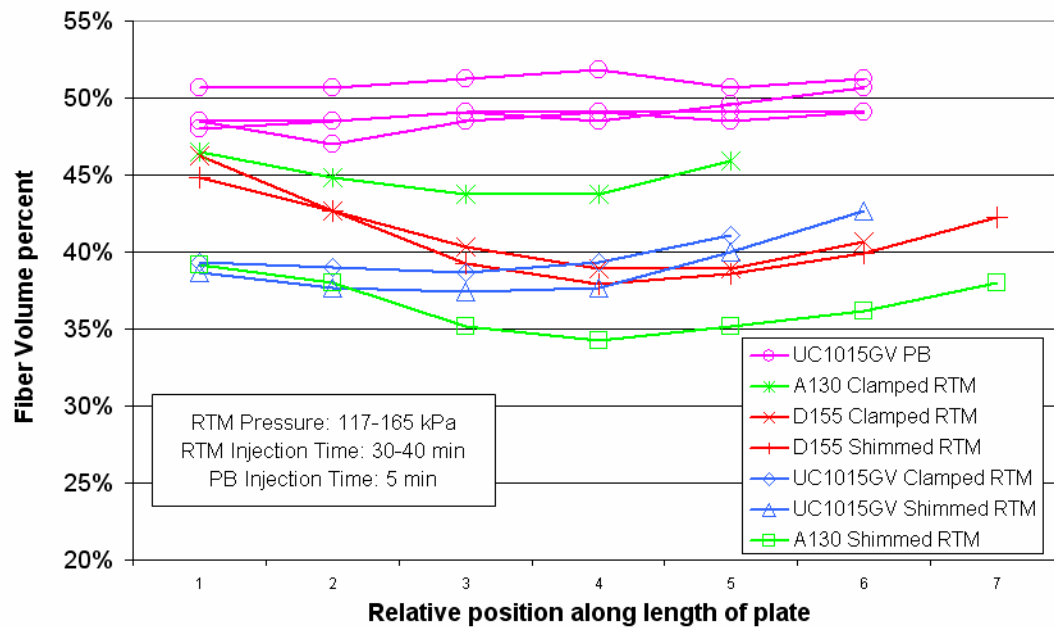


Figure 43: Fiber volume percents for RTM and pressure bag molded plates.

244 cm Plate Fiber Volume. Using a successful plate produced from the 244 cm mold, the fiber volume percent was obtained at several points along the length. This fiber volume profile is shown in Figure 44. This shows that the fiber volume along the 244 cm of this plate is relatively high and consistent. Considering that this injection was from one port at one end of the mold, this is a significant result.

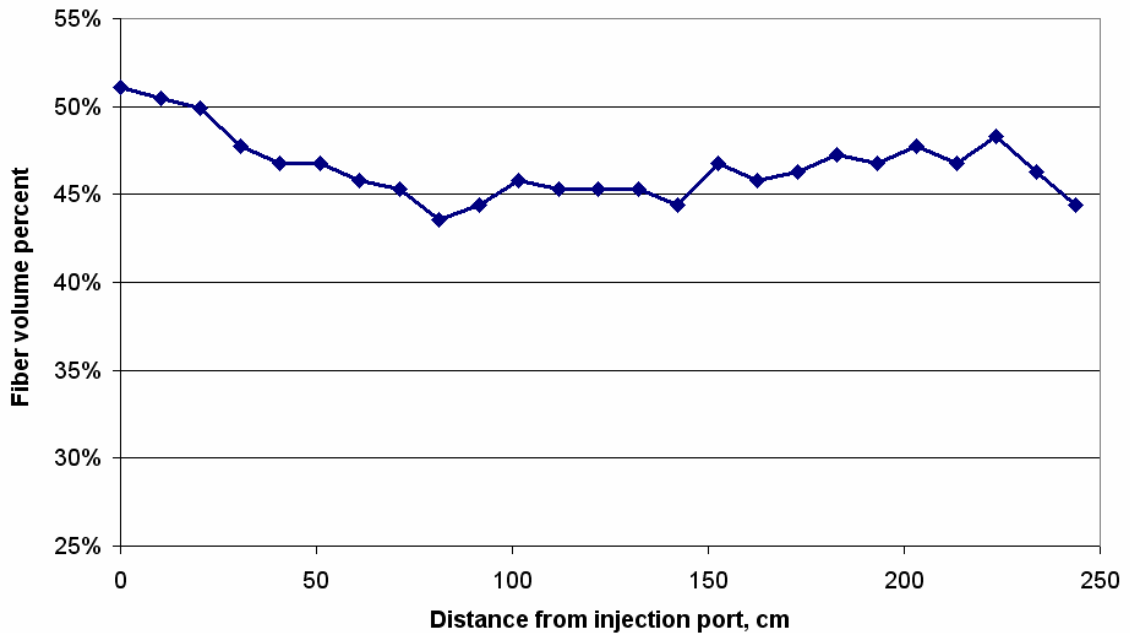


Figure 44: Fiber volume percent distribution along 244 cm pressure bag molded plate.

Mechanical Testing

Destructive testing was conducted to determine the ultimate tensile and compressive strengths. ASTM D2344 short beam shear tests were also performed on the same materials and manufacturing methods. For these three tests, an Instron 8562 was used to load and gather the ultimate load at failure.

Ultimate Tensile Strength. Ultimate tensile strength tests were performed on samples of the plates manufactured for the injection distance experiments. 25 mm wide samples were cut and loaded to failure. A 100 mm gage length was used in these tests to account for material variations that may cause locally weaker areas along the fiber direction. The samples were clamped directly into the jaws of the Instron. No tabs or “dog-bone” sample geometry was used to reduce the effects of the grips.

It is notable that the pressure bag molded products have a slightly different gripping situation due to the surface contour on the bag side of the part. There were no attempts to account for this difference in surface texture, but neither was there evidence that suggested that the differences affected test results significantly.

There was no normalization made for differing fiber volume percents of the samples. Differences in fiber volume content will manifest as thickness variation for laminates using fabrics such as those used in this study. Since the tensile stress is determined by dividing the load by the cross-sectional area, this thickness directly affects the determination of ultimate tensile strength. However, a thicker part (with the same lay-up) is only a result of additional matrix material, which contributes relatively little to the load carrying ability of the part. Therefore, normalization is sometimes done to adjust for fiber volume differences [8]. That was not done for these tests since fiber volume percents did not vary greatly, and since the differing fiber volumes were a direct result of the different manufacturing processes employed, which was what was being compared.

Results from the tension tests are shown in Figure 45. The error bars on the chart show the maximum plus and minus variation in the data set. Generally, all of the laminates with different materials used for zero degree plies performed similarly. The differences in tensile strength among the three different processes using the UC1015GV material are possibly a result of the differing fiber volumes, as the fiber volumes and tensile strengths were highest for the pressure bag molded samples.

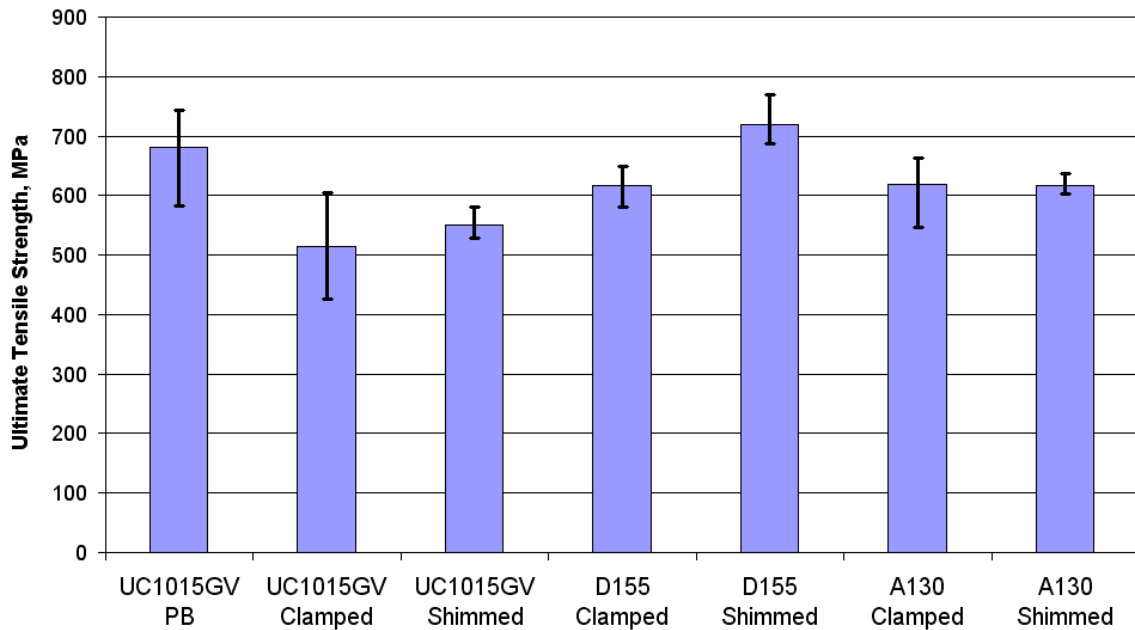


Figure 45: Ultimate tensile strength of samples taken from plates manufactured for pressure bag molding and flow distance experiments.

Ultimate Compressive Strength. Compressive strengths of these laminates were also determined as a part of this manufacturing process qualification. As mentioned previously, for many applications, compressive properties are at least as important as tensile properties. Compressive properties can also be more complicated to determine and design for because of the potential for a buckling situation to develop in testing or in an application.

Samples of the plates manufactured for the flow experiments were cut into 25 mm wide specimens. These specimens were loaded in compression using an Instron 8562 until failure occurred. The gage length used was 50 mm, and the loading rate was 50 mm per minute.

As can be seen in Figure 46, the compressive strengths of most materials were similar. The materials using the A130 fabrics, however, showed significantly reduced compressive performance. This was probably a result of the woven architecture of this fabric. The weaving causes a perturbed, wavy condition, significantly reducing the composite's ability to support compressive loads.

Another detail that stands out in Figure 46 is the apparent increase in scatter of the pressure bag molded samples. This, however, is at least partially a result of an increased sample size used for this material. There were 20 samples used for the pressure bag molded data, but only 5 samples for each the other manufacturing types represented.

The samples that were manufactured by the pressure bag molding process did show a decreased average compressive strength. One possible explanation for this result involves the application of the hydrostatic pressure during the second stage of the molding process. When the pressure is applied to the bagging film, the adjacent layer of zero-degree fabric is pressed against the next layer, which is the DB120 fabric (+/- 45 degree). Since this fabric is stitched together into discrete regions of fiber bundles separated by gaps, the zero-degree materials are forced to slightly conform to the pattern of the adjacent DB120 material. This pattern can be seen in Figure 38. This not only contributes to the unique surface texture, but it also introduces a perturbed situation mostly in the layer immediately adjacent to the bagging material (remotely similar to the A130 based samples), which can affect compressive performance. However, testing was not conducted to verify that the surface texture had affected the compressive performance.

If the wavy surface layer does detrimentally affect compressive strength, it would likely manifest in FASTRAC and SCRIMP products also, as they also employ a hydrostatic pressure through a bagging material to one side of their products. A microscope photograph showing the cross-section along the fiber direction (of the zero degree layers) of a pressure bag molded sample is shown in Figure 47.

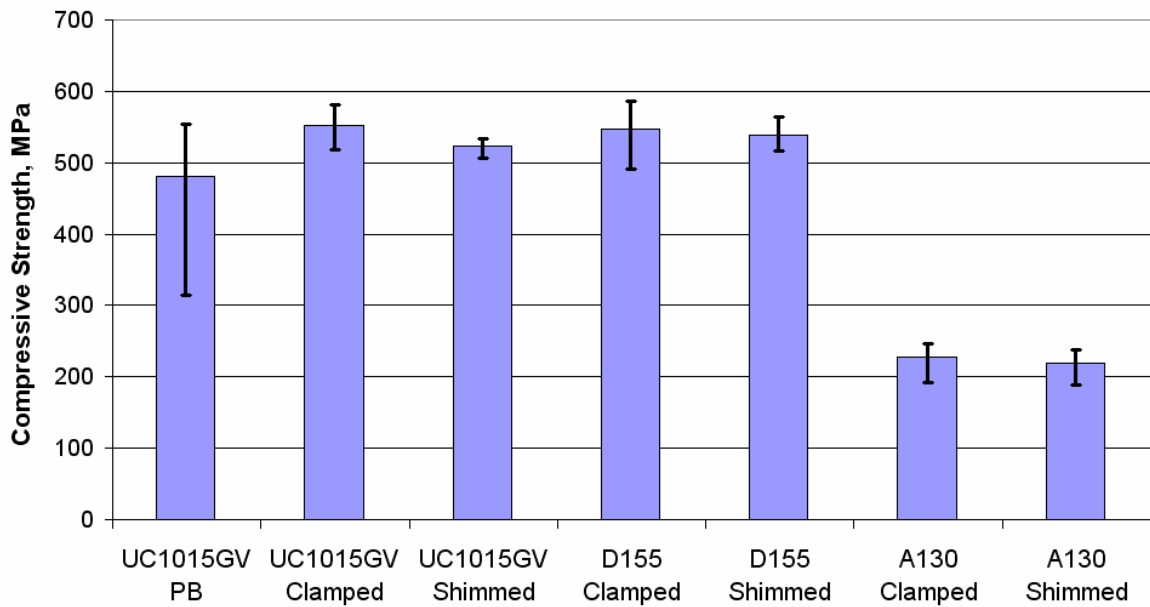


Figure 46: Ultimate compressive strength of samples taken from plates manufactured for pressure bag molding and flow distance experiments.

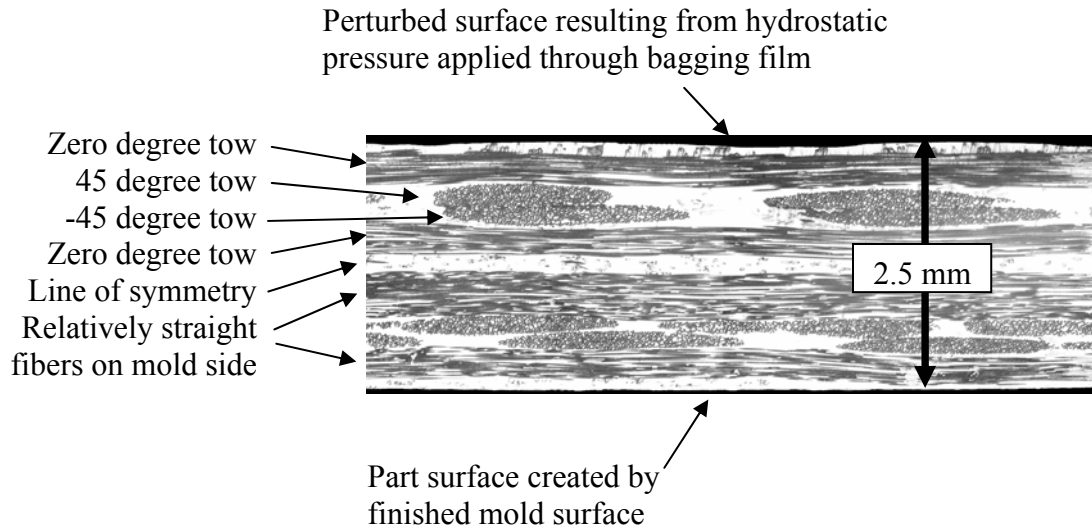


Figure 47: Microscope view of a cross-section of a $[0/45/-45/0]_s$ laminate with perturbed surface tows.

It is speculated that the reduction in compressive strength is likely to be less pronounced for thicker laminates (using greater numbers of layers of fabric) than thinner laminates (fewer layers). If this is the case, it is likely a result of the perturbed layers being a surface effect. For laminates with increased numbers of layers, the surface layers account for lower percentages of the laminate, decreasing the effect of the surface waviness. An illustration of the cause of this behavior is shown in Figure 48. Laminate “A” in Figure 48 has fewer layers than laminate “B”, and therefore the waviness of the surface layer will affect the performance of the laminate to a greater degree than in laminate “B”. Further investigation into this phenomenon was considered beyond the scope of this work and is suggested and discussed in the Future Work section.

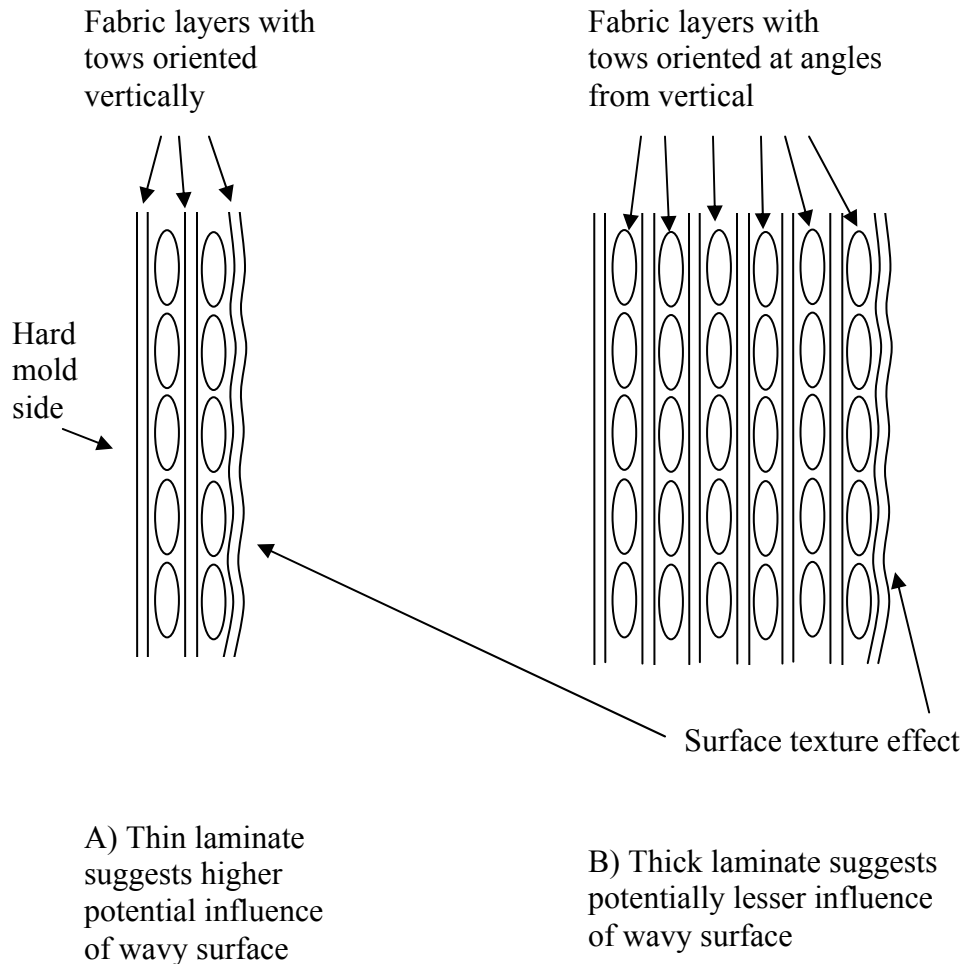


Figure 48: Sketch implying reduced surface texture effect for thicker laminates.

Short Beam Shear Test. The same group of materials was compared in an ASTM D2344 Short Beam Shear Test [26]. The specified span-to-thickness ratio of 5 was used along with the average sample thickness of 2.5mm to design a test fixture for the short beam shear test (Figure 49). The specified length-to-thickness ratio was 7, therefore samples were cut to 9mm x 17mm. The thickness is left as arbitrary in the ASTM specification. A thickness of 9mm was chosen for this study. The only concern about the

thickness was whether cutting a sample through a tow or next to the tow would make a difference in observed performance for fiber architectures with discrete fiber regions. However, no tests were done to determine if the cut location affected the performance. Five samples representing each type of material were loaded in bending using the Instron with the constant displacement rate of 1.3mm per minute. The current load was observed during each test, and when it was observed to drop, the load was removed. Maximum load was retrieved from the Instron data collection system, and recorded.

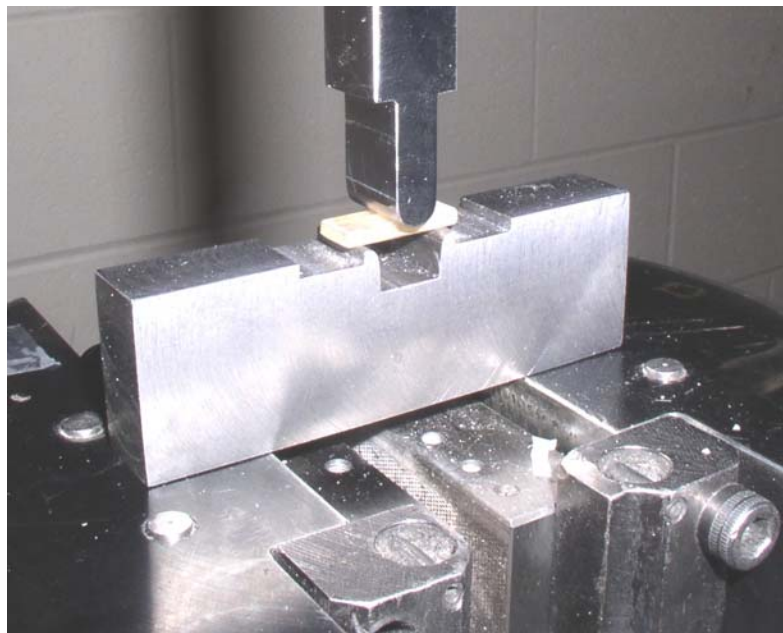


Figure 49: ASTM D2344 short beam shear test apparatus.

All of the samples tested failed in shear as expected. Some of the samples (mostly from the pressure bag molded plates) were observed after testing to have two or more sheared surfaces.

The apparent shear strength for each manufacturing method represented was determined using Equation 5, applying the maximum loads and sample dimensions. Figure 50 shows the resulting apparent shear strengths. The pressure bag molding specimens showed the highest apparent shear strengths in this test, but also showed the most scatter. Unlike the compression tests, the sample sizes were all the same (5 tests for each material type) for the short beam shear test. The samples with A130 materials showed the worst shear strength, probably because of the dry zones near the weaving materials. These voids would tend to cause stress concentrations, leading to failure at relatively lower loads.

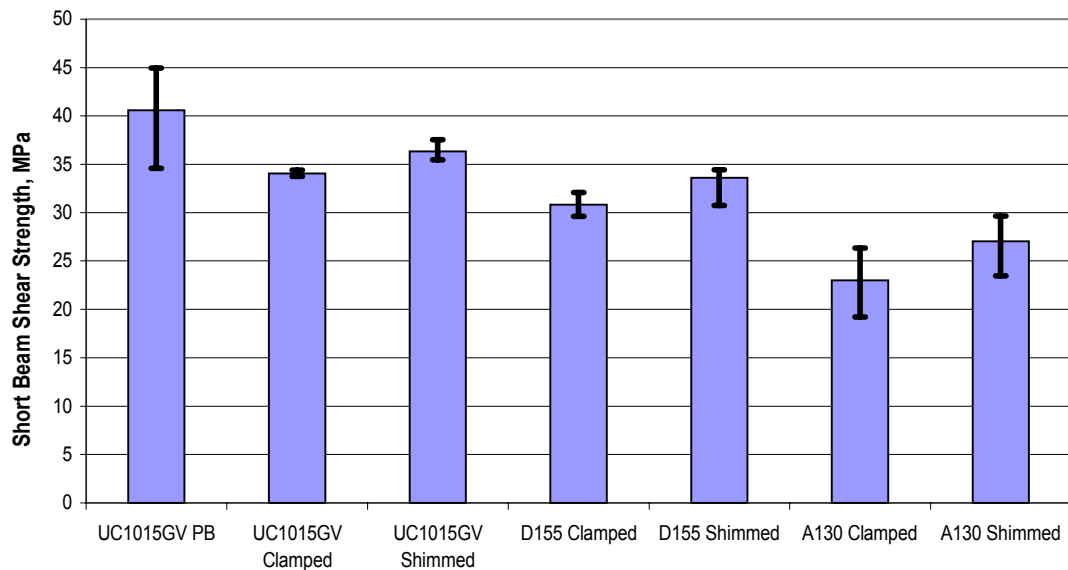


Figure 50: Apparent shear strengths of samples tested as determined by ASTM 2344D short beam shear test.

Quantifying Damage Accumulation Properties

As mentioned previously, one of the qualities of fiber reinforced composites that make them attractive for use in many applications is their ability to sustain damage without immediate catastrophic failure. When considering a manufacturing process qualification regime, it may be desirable to assess the damage accumulation properties of products of the intended process. In a sense, that is what the previous qualification tests have addressed, except that the previous tests isolated particular material properties. It could be perfectly valid and preferred to test many properties at once, and at a macro-level, which could also account for complex interactions of geometry, loading, and failure that the individual tests could not. After all, a manufacturer is more concerned about how the finished part performed in actual duty than how material samples performed in a lab. A damage accumulation test could be designed to more closely simulate extreme duty, and therefore provide better insight to material and process performance than material property testing on a micro-level.

This section introduces a test developed for this work to quantify and map damage in a fiberglass composite, and a numeric progressive damage model to compare experimental results with. The results of the test conducted were not particularly good for reasons that will be discussed, but since it involves an innovative approach to damage detection and quantification, and since the potential of this technology remains high, it was included in this thesis. This test consisted of incrementally loading a relatively complex fiberglass part such that damage was progressively introduced. At each loading step, the damage pattern was mapped using the infrared transmittance method described

previously. The infrared transmittance map was then compared to a numeric solution that was developed for this work using Ansys.

The damage accumulation test that is demonstrated in this work was designed according to a few principles. The criteria used for selecting geometry and loading was that it should generally represent a common design situation, and that it should also be relatively simple enough to increase the likelihood of arriving at good numerical results. A rectangular plate with a hole in it loaded in uniaxial tension was chosen. Examples of design scenarios that could have this combination are joints where a composite structure is bolted to another structure, or an access hole where wire harnesses need to pass through a fiberglass member that is loaded.

The material chosen was the laminate used previously in this study consisting of the Collins Craft UC1018GV fabric. This material was chosen because of the reduced amount of materials that would interfere with IR transmittance. The DB120 fabric (used for the 45 degree plies) has some stitching threads, but the UC1018GV material has no stitching or weaving materials. The important dimensions of the chosen geometry are shown in Figure 51. The samples used for mechanical testing were cut to longer lengths so that gripping could be done outside of the area that damage was to be measured in.

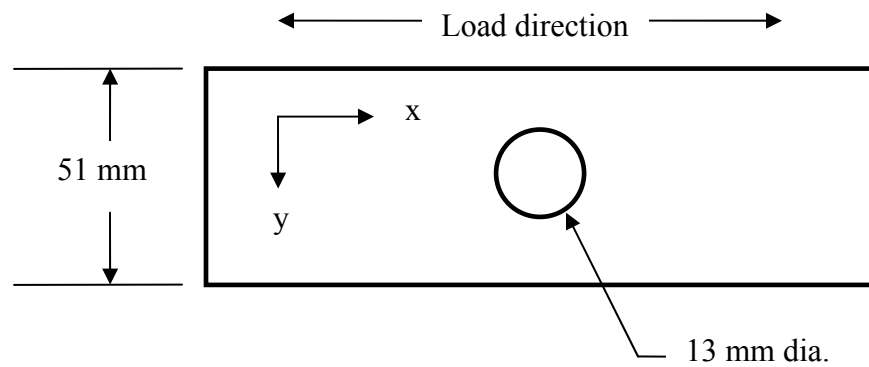


Figure 51: Significant sample dimensions for damage accumulation tests.

Ansys Progressive Damage Model.

If an isotropic plate with a hole was loaded in tension, the stress distribution would look similar to what is shown in Figure 52. For a laminar material with orthotropic layers oriented at differing angles, even with the relatively simple geometry chosen for this test, the stress distributions and damage properties (geometric damage zone shapes) are far too complex for traditional elasticity solutions to approximate. A numerical solution is needed to solve a problem such as this.

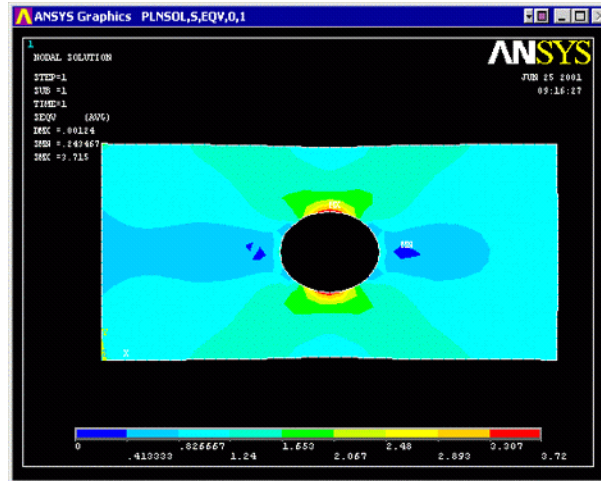


Figure 52: Ansys solution showing stress distribution around a hole in a plate made of an isotropic material under uniaxial loading.

Ansys [32] has a layered shell element (Shell91) in its element library built for angled laminar materials like fiber reinforced composites. Using this element can yield good results for typical loading situations up to the point where damage begins to occur. After the onset of damage in an angled laminar material, there is no clearly defined solution process available that can model composite behavior. For this work, however, the macro language in Ansys was used to build a solution that could model the progressive damage behavior of a composite.

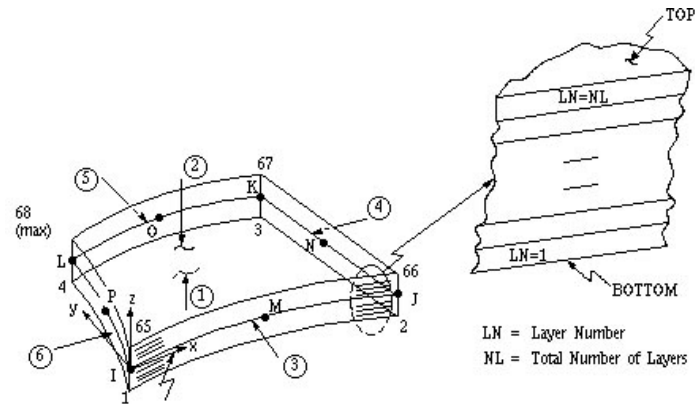


Figure 53: Ansys shell91 element.

Ansys can be used in two general modes, interactive and batch. Interactive mode allows for extensive use of on-screen mouse clicking for selecting items in various contexts. This makes for difficult reproduction and presentation of solutions. Batch mode takes text commands from an input line or from a file, and is therefore better suited for presenting this type of work.

The geometry was constructed in batch mode using various “Keypoint” and “Line” functions. Quarter-symmetry was used to reduce processing time and increase accuracy. The lines were divided to control mesh density. The line divisions were done using variables to facilitate easy density manipulation during a mesh sensitivity study to assess the model’s performance. The geometry was meshed according to the line divisions previously defined. The mesh near the hole was defined with a much smaller element size to better handle the anticipated complex and steep stress gradients in this area. Zero displacement boundary conditions were applied to the planes of symmetry

(top edge and right edge in Figure 54). The layered elements after meshing are shown in Figure 55.

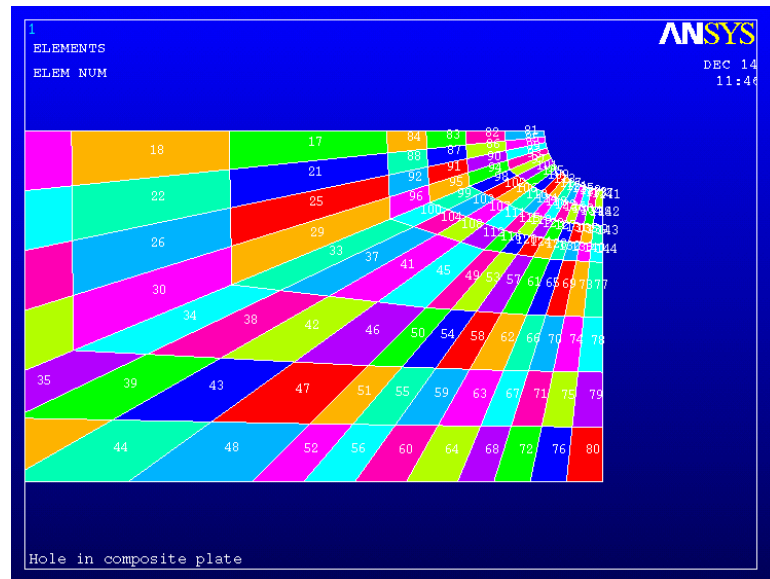


Figure 54: Ansys mesh definition of a plate with a hole in it using quarter-symmetry.

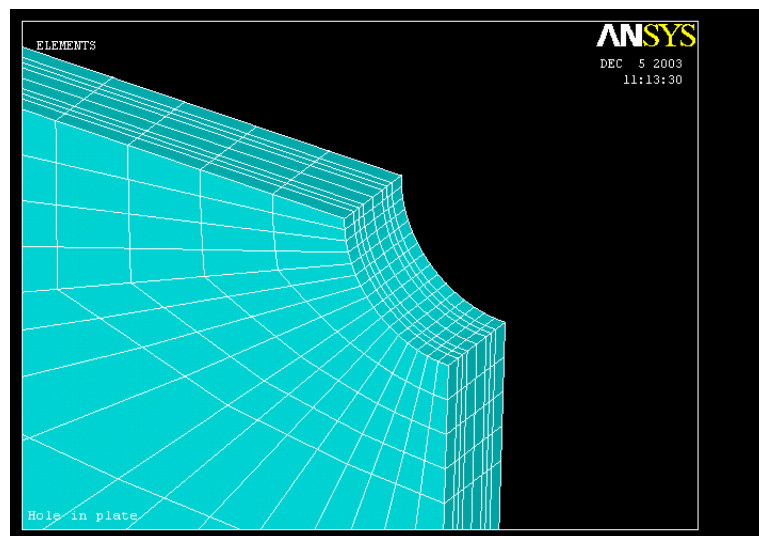


Figure 55: Ansys model showing layered elements of $[0/45/-45/0]_s$ laminate used in progressive damage tests of plate with a hole under tension.

Up to this point, this analysis is the same as any other linear elastic model. The next step was to define material properties. Since the material properties drastically change as damage occurs, Ansys needed to keep track of the damage state of the material and apply the appropriate properties when solving. This was done using the “Temperature” state in Ansys. This is an unfortunate misnomer, because this functionality can be used to vary material properties resulting from essentially any parametric data, including but not limited to the temperature. In this case, the ultimate strain was used as criteria to determine when to change material properties. The material properties were then manipulated element-by-element via the element’s “temperature”.

Material Properties and Failure. The material properties that were used in this analysis were from the MSU composite material database. Since the properties for the zero degree materials used were not immediately available, properties for the D155 fabric was used instead. This was deemed acceptable since no direct comparison of loads was made, and since the laminates with the Collins Craft UC1015GV materials performed very similarly to the lay-ups with D155 fabrics for all of the previous tests.

Table 9: Nominal material properties used in numerical model.

Material Property:	Value:
Longitudinal modulus, GPa	38.36
Transverse modulus, GPa	9.97
Shear modulus, GPa	4.23
Poisson's ratio	0.3

When defining material behavior during progressive damage, many assumptions were made. Most importantly, the order in which damage occurred was assumed prior to material property definition. The assumptions made were according to laboratory experience and previous work [8]. For this damage model, the states of progressive damage were assumed to be as shown in Table 10.

Table 10: Order of damage progression used in Ansys damage model.

Damage State	Description
1	Undamaged
2	Matrix cracking in the zero degree plies
3	Matrix cracking in the 45 degree plies
4	Fiber failure in the zero degree plies
5	Fiber failure in the 45 degree plies

Other assumptions made were the reduction behaviors in load carrying abilities after damage occurred. For instance, when matrix cracking occurred in the 45 degree plies, how much did the shear modulus decline? Did it occur as a single event or over a range of strains? For this model, the assumption was that the reductions were a one-time event. For example, the onset of matrix cracking was made to result in an abrupt 80% reduction in transverse and shear modulus. The assumptions used for property behavior are based on [8]. The applied property behaviors during the steps of progressive damage

for the elastic modulus in the longitudinal and transverse directions, the shear modulus, and poisson's ratio are shown in Figure 56 and Figure 57.

Strain was used to determine failure. For the transverse directions, the strain where matrix cracking occurred was assumed to be 0.2%. For longitudinal directions, 3% strain was used to signify fiber failure.

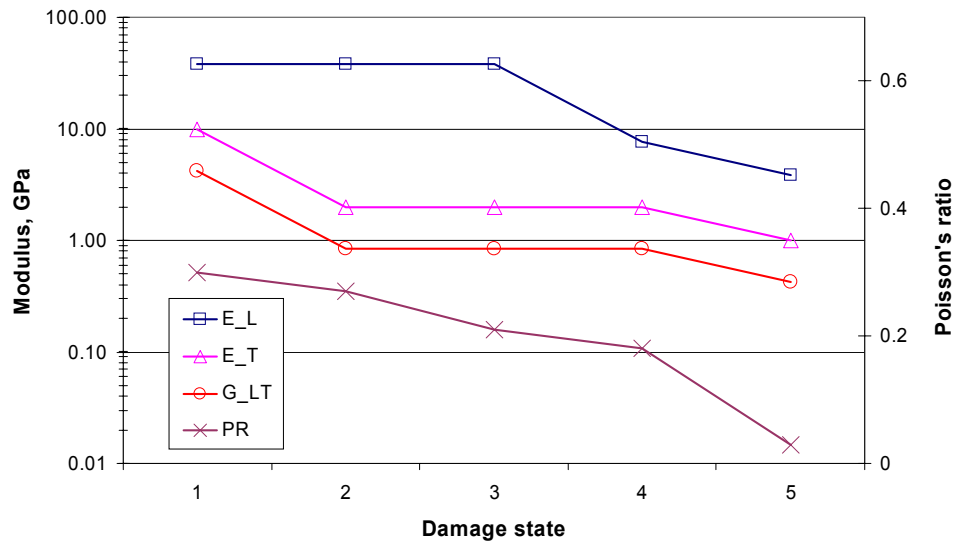


Figure 56: Material property response to damage states for zero degree plies.

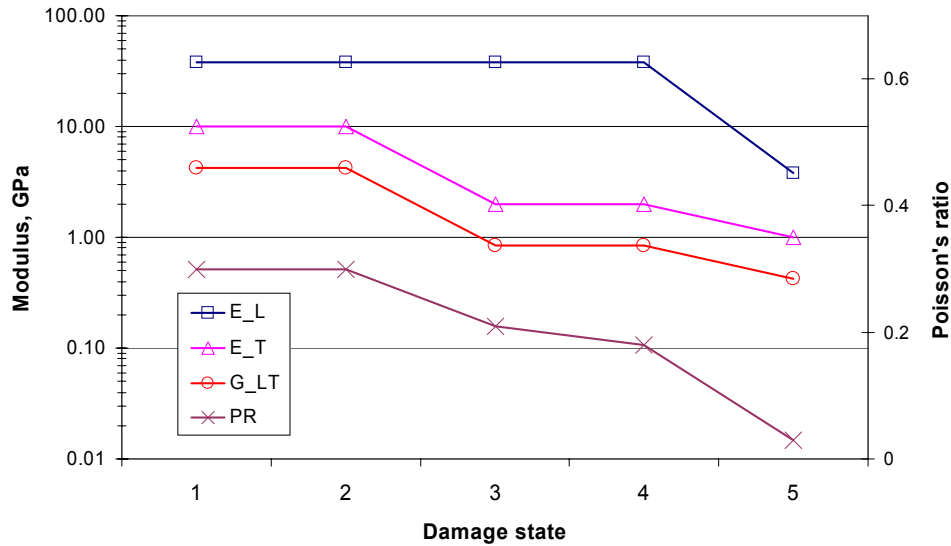


Figure 57: Material property response to damage states for 45 degree plies.

In these material behavior definition plots, it should be noted that the damage progression follows the failure description given previously. Moving from damage state 1 (undamaged) to damage state 2 results in reduced transverse and shear modulus in the zero degree plies as a result of matrix cracking. Moving from state 2 to state 3 results in reduced shear and transverse modulus in the 45 degree plies, and so forth.

Solution Algorithm. After building the geometry and defining material property behavior in Ansys, the model is ready for the solution process. A graphical representation of the steps in the solution algorithm is shown in Figure 58. Detailed descriptions of the steps used for solving for the damage behavior in this approach are as follows:

1. Displace the left boundary. This is the strain-inducing method that was chosen for this model. Attempting to apply a load would cause the model to become unstable at final failure. The same principle applies in an actual load controlled tensile test. As soon as the part fails, it is completely unconstrained, and wants to accelerate infinitely. In this model, a load controlled progression would probably lead to unstable behavior.
2. Solve for the resulting strains. The solution process until now is identical to that of a linear elastic solution.
3. Check for damage inducing strains. If any strains in any layer of any element have exceeded the failure criteria, the properties of that layer need to be changed to reflect the compromised ability to carry load. In the macro language in Ansys, this is done with extensive use of the “etable” functionality. All of the strains in each layer of each element are stored during the solution process for later comparison. As the macros loop through the etable, if any layer of any element is found to have exceeded a failure strain (for the first time), a flag is set which will re-start the solution process after all elements have their properties checked against their strain level. This is to account for the “cascading failure” phenomenon. When one area of a composite fails, its load carrying ability is compromised. However, equilibrium still needs to be satisfied, so the load it was carrying is transferred to neighboring elements. This additional load on adjacent elements may cause an over-strain condition in one of the layers of this element. Therefore, after the solution looping finds new damage, it solves for loads and

strains again to check for more new damage. This looping continues until there is no more new damage found. This load transfer phenomenon is reduced significantly by the displacement controlled nature of the analysis, but the potential for cascading damage still needs to be accounted for in the solution.

When checking each layer of each element for damaging strains, the coordinate system used for reporting results needed to be aligned with the fiber direction in each layer.

4. Update the damage state of elements that exceeded failure strain. The macro language keeps track of each element's damage state ("temperature" in Ansys). If an element has just exceeded an ultimate strain, its damage state is incremented. This causes the compromised properties to be applied during successive solutions.
5. Solve again or increment displacement. The solution is found again if new damage had occurred in the previous displacement step. If no new damage was found, the displacement is incremented and the whole process is started again.

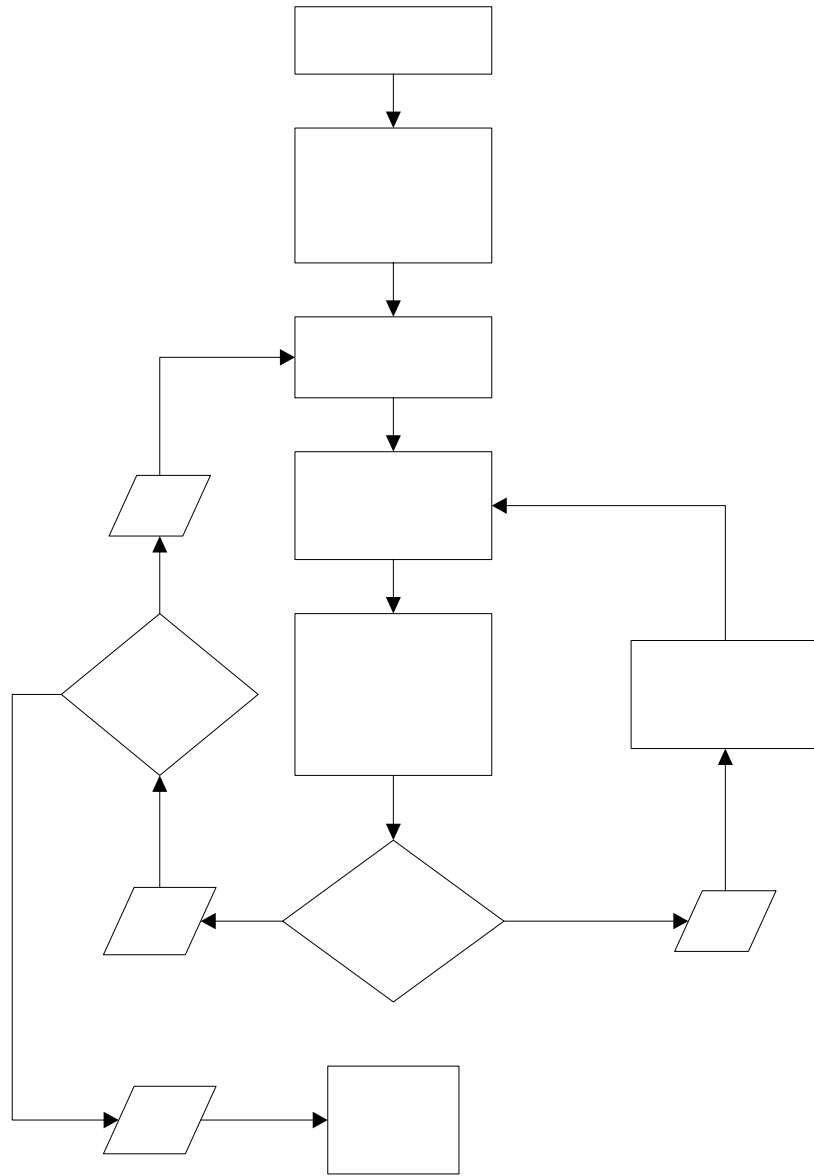


Figure 58: Flowchart of Ansys progressive damage model solution algorithm

This approach seemed to work well during this work. It seemed very stable, always behaved as expected (when coded properly), and showed results that seemed as if they

closely paralleled the intuitive failure progression for this geometry. A sample display of stresses solved for by Ansys is shown in Figure 59. The “stress intensity” is a value used by Ansys and is defined as the largest difference in the three principle stresses as shown in Equation 10 [32].

$$\text{Ansys Stress Intensity} = \max(|\sigma_1 - \sigma_3|, |\sigma_2 - \sigma_3|, |\sigma_1 - \sigma_2|) \quad (10)$$

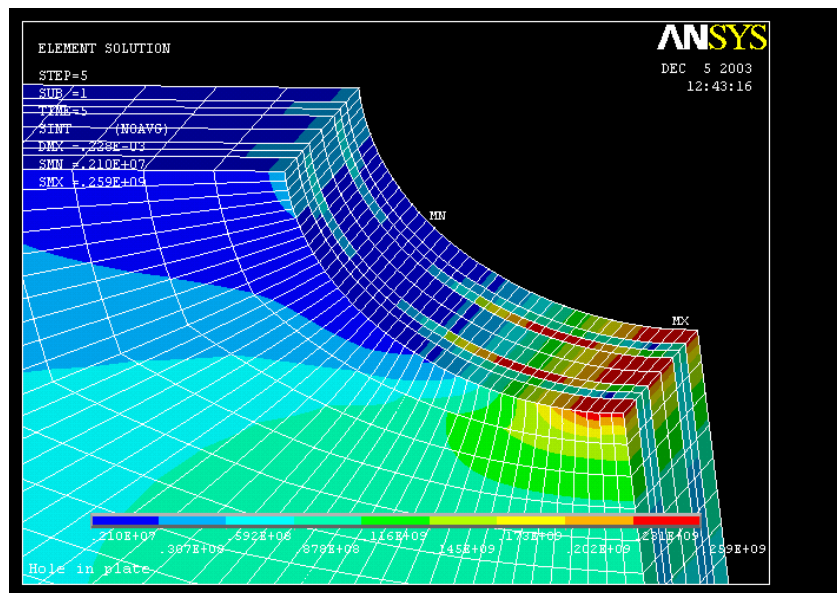


Figure 59: Ansys display of stress intensity showing stresses carried in each layer of $[0/45/-45/0]_s$ laminate.

Mesh Sensitivity Analysis. A study was done to test the stability of the solutions with varying mesh densities. An Ansys keypoint which was located at the point of highest stress (for the zero degree plies) was chosen to compare resulting stresses from

solutions obtained with different mesh densities (element size). This is a common check to determine a subjective level of confidence with a finite element solution. In this case, two different mesh sensitivity tests were conducted.

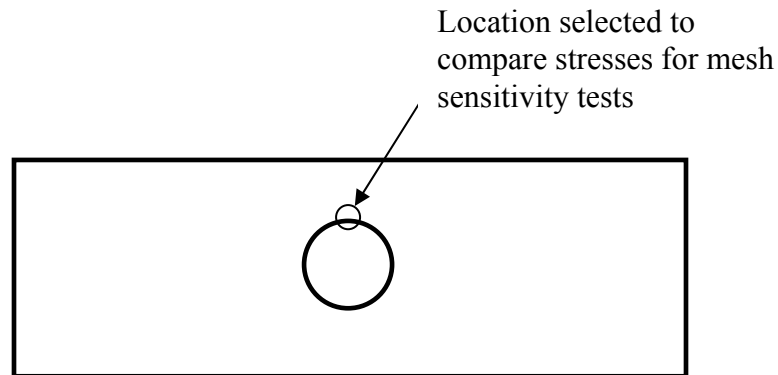


Figure 60: Point of highest stress chosen for mesh sensitivity analysis.

The first mesh sensitivity test was done after one displacement step. This solution was generated such that there was no resulting strains that would cause damage. In this scenario, the solution is only linear-elastic. This was done to perform a “traditional” mesh sensitivity test. The boundary displacement after one step was .128 mm.

Results of this test are shown in Figure 62. The x-axis on this plot shows the line division settings used in the Ansys macro code which determines the mesh density. For reference, the meshes that were generated with the macro line division settings at “4-4” and “8-10” are shown in Figure 61. The higher mesh densities were starting to take significant amounts of processing time to solve. The asymptotic behavior is typical of a mesh that is converging, and is a good indicator of a stable solution.

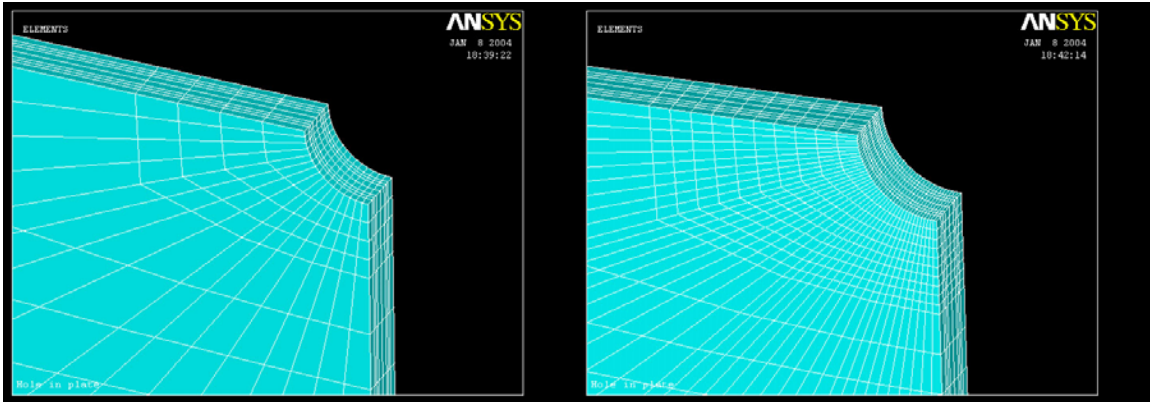


Figure 61: Meshes from macro line division variables at "4-4" (left) and "8-10" (right).

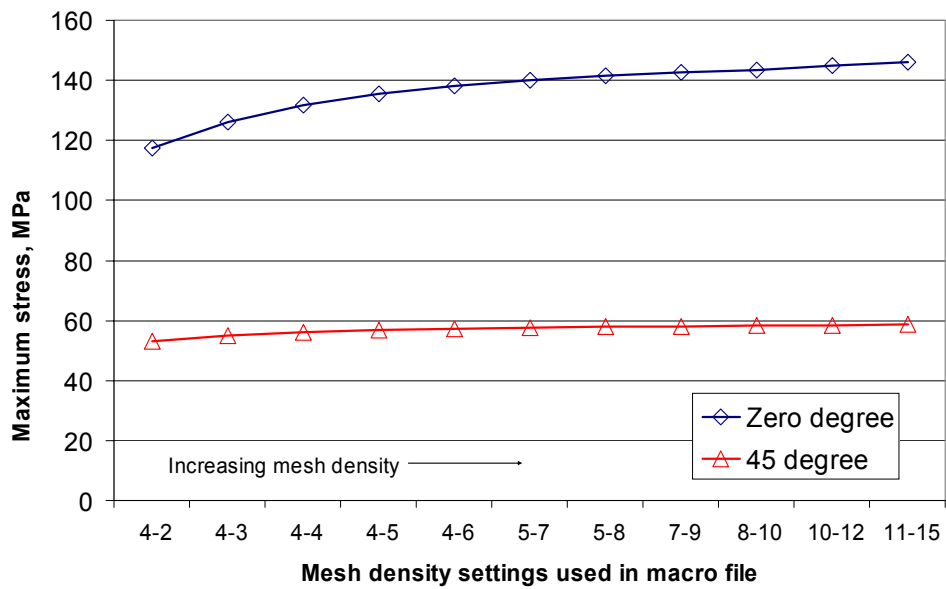


Figure 62: Maximum stress in the zero degree and 45 degree layers after one displacement step for increasing mesh densities.

The second test was done after five displacement steps. In this test, damage was present in several elements after the fifth displacement step. The damage included matrix cracking in the zero degree layers and in the 45 degree layers in a few elements near the

area of maximum stress. This test was added to investigate how the material degradation is affected by the mesh definition. The boundary displacement at the fifth step was .328 mm.

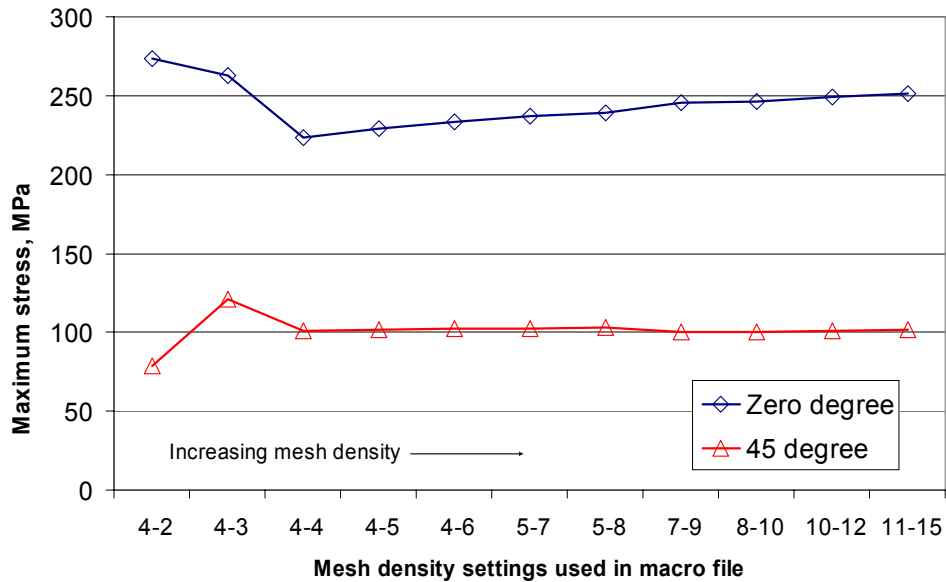


Figure 63: Maximum stress in the zero degree and 45 degree layers after five displacement steps for increasing mesh densities.

The mesh sensitivity tests suggest that the numerical model is performing well. The instability in the lower mesh densities of the five-step test indicates that there may be some difficulties with using a relatively large element size that normally would provide good results for a linear-elastic model. Since the slight instability was not evident in the one-step test, the conclusion could be drawn that the finite availability of element borders that define where the properties can change (recall that the properties are changed at the element level) cause the progressive damage model to be more sensitive to element size

than a normal linear-elastic solution. For the extensive displacement analysis that will be discussed next, the mesh density settings used in the code were “5-7”.

50 Displacement Step Solution. The input macro file was edited to cause Ansys to loop through 50 displacement steps. As with the previous runs, the first step was large, to advance the loading to just before damage initiated. The Ansys code that was written to accomplish this solution is included in the Appendix. After each stable solution for a displacement step (no new damage), Ansys was made to create bitmap contour plots of the longitudinal and transverse strains and the stress intensity in each layer. The stress intensity was chosen somewhat arbitrarily and is defined in Ansys documentation as the absolute value of the largest difference in principle stresses. The damage state was also plotted at each displacement step by instructing Ansys to create a contour plot of the temperature.

Following are compilations of select images created during the solution displacement steps. The displacement step order as they are arranged is left to right, then top to bottom. The first set of images, Figure 65, shows the progression of the damage state in the sample. It should be noted that this set of images (Figure 65 only) was created with an absolute color contour scale. It is the same scale for all of the images in this set. The legend associating colors to the possible damage states (described in Table 10) is shown in Figure 64.

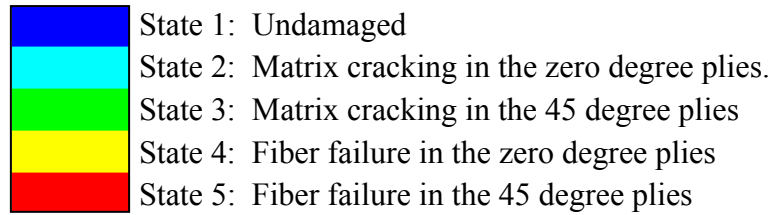


Figure 64: Legend for color “damage state” contours.

All of the other sets of images shown have a relative color contour scale. The contours are assigned automatically during Ansys’ image generation. It is notable in the stress plots that the highest stresses are shown to move away from the hole. This is the expected behavior as the material nearest the hole is compromised. For these images, the darkest red represents the areas of highest value at that particular displacement step. The strain images show values relative to the individual layer’s fiber direction. In other words, Figure 69 is showing strain at 45 degrees to the load direction, or in the fiber direction.

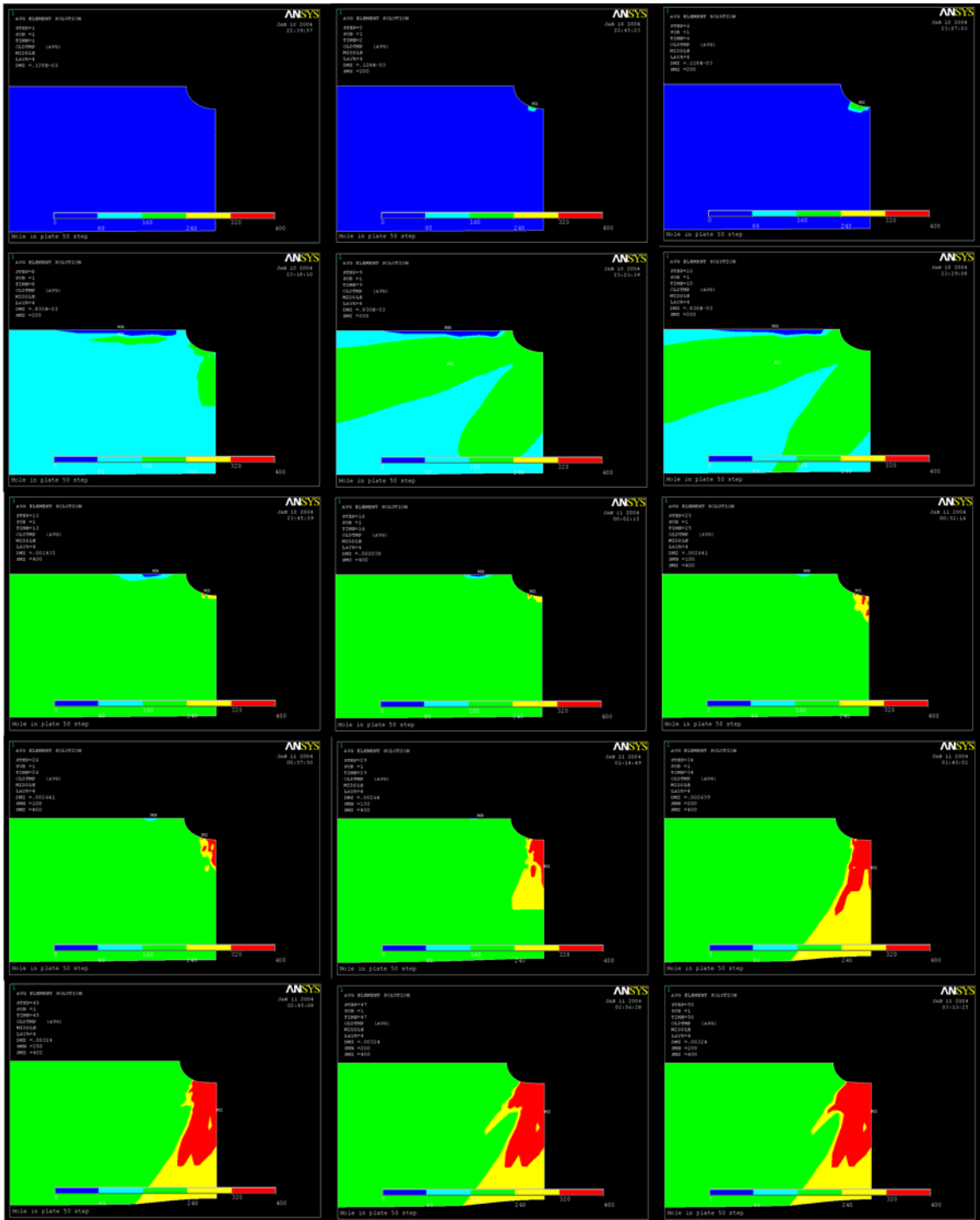


Figure 65: Ansys images showing progression of damage state created during displacement step solution looping.

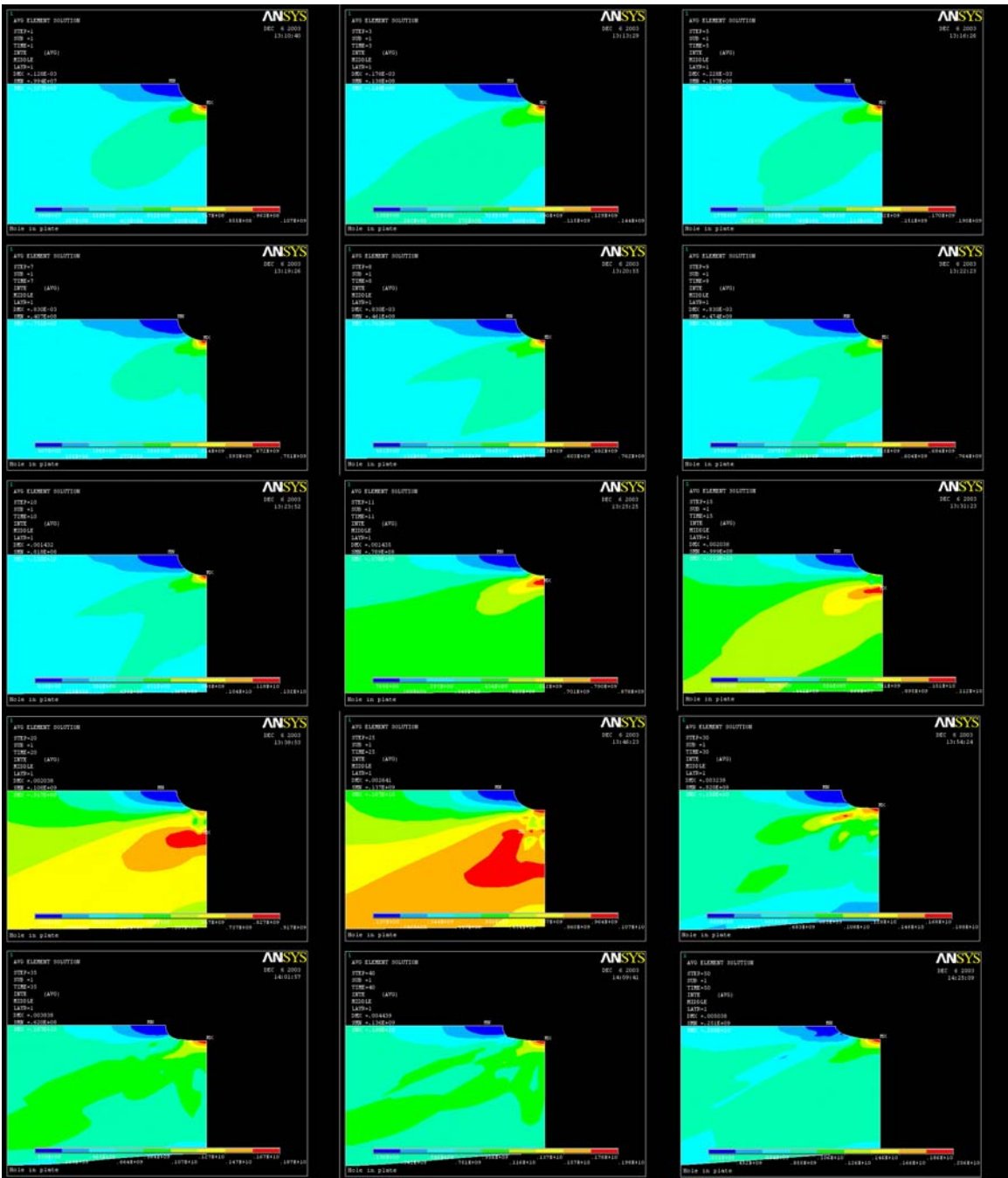


Figure 66: Ansys images showing stress intensity in the zero degree layer during displacement step solution looping.

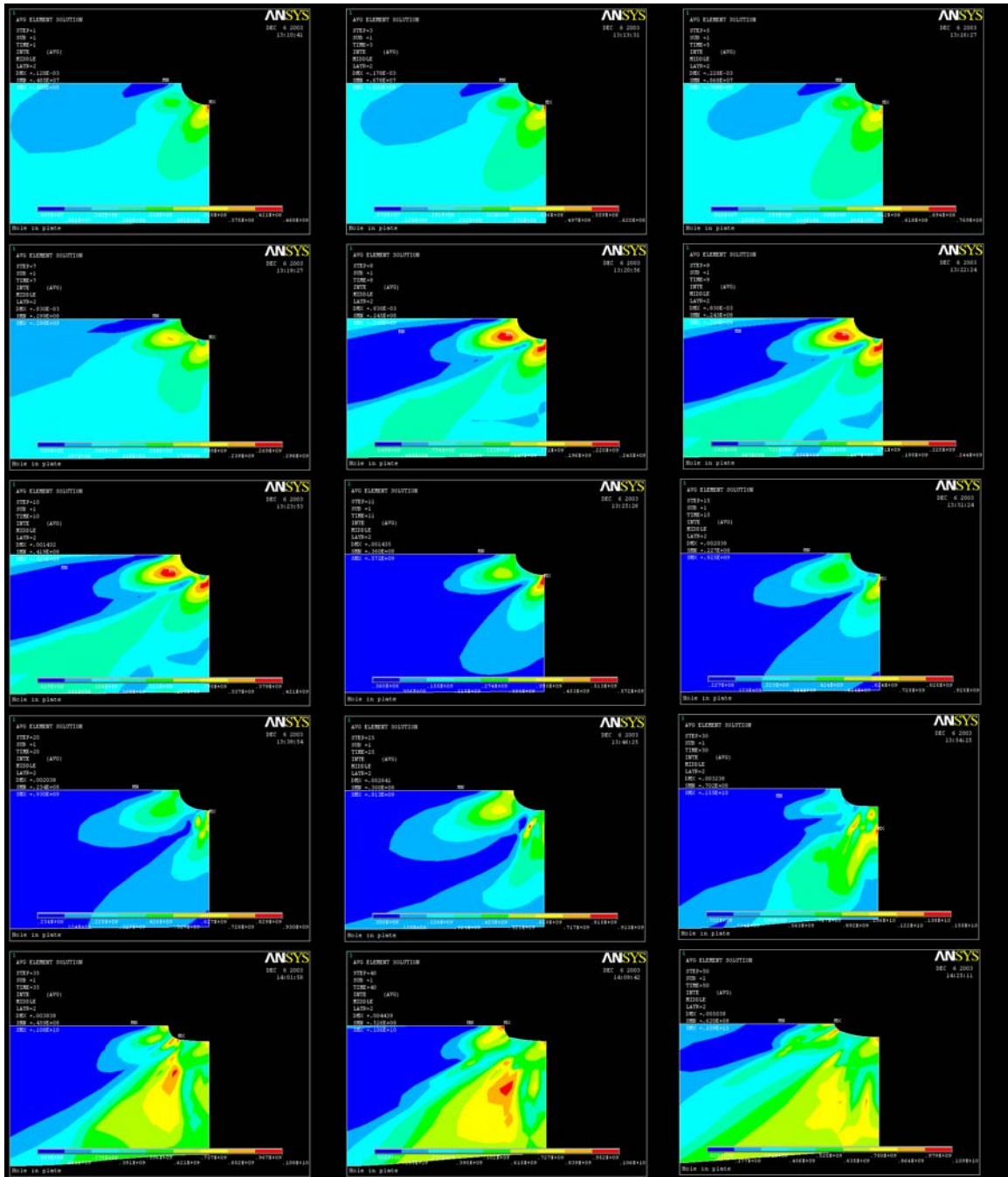


Figure 67: Ansys images showing stress intensity in the 45 degree layer during displacement step solution looping.

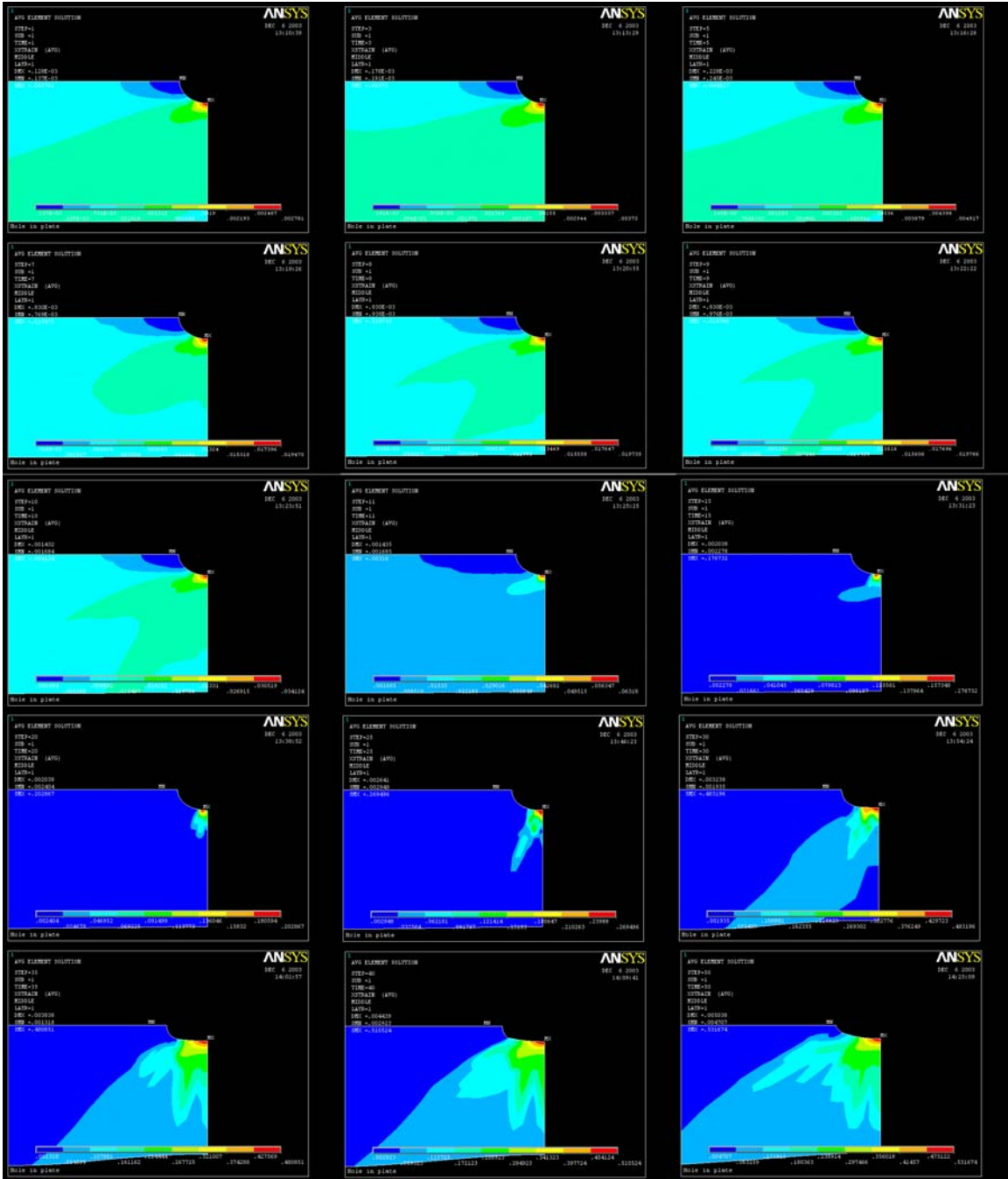


Figure 68: Ansys images showing x-direction strain in the zero degree layer during displacement step solution looping.

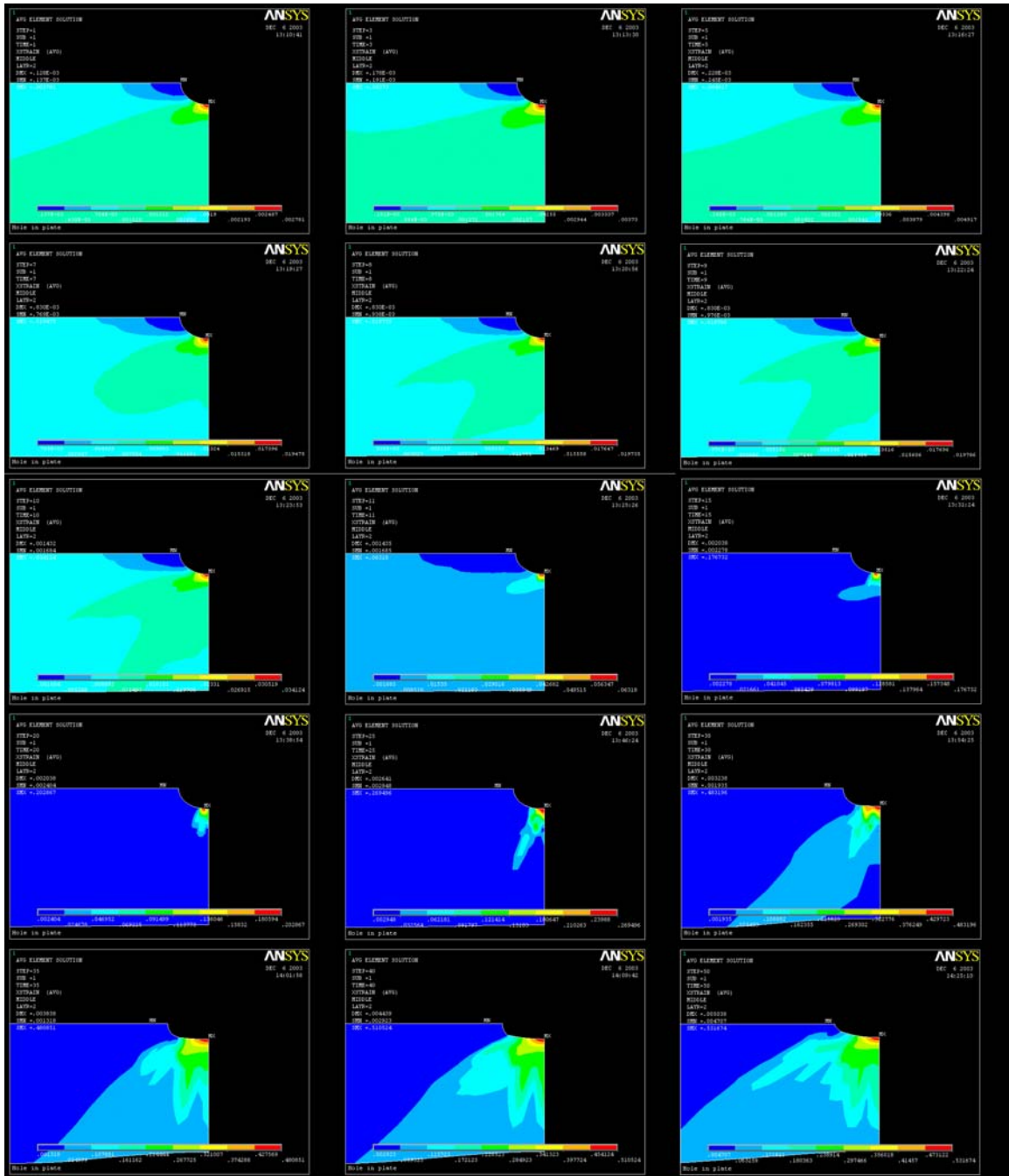


Figure 69: Ansys images showing x-direction strain in the 45 degree layer during displacement step solution looping.

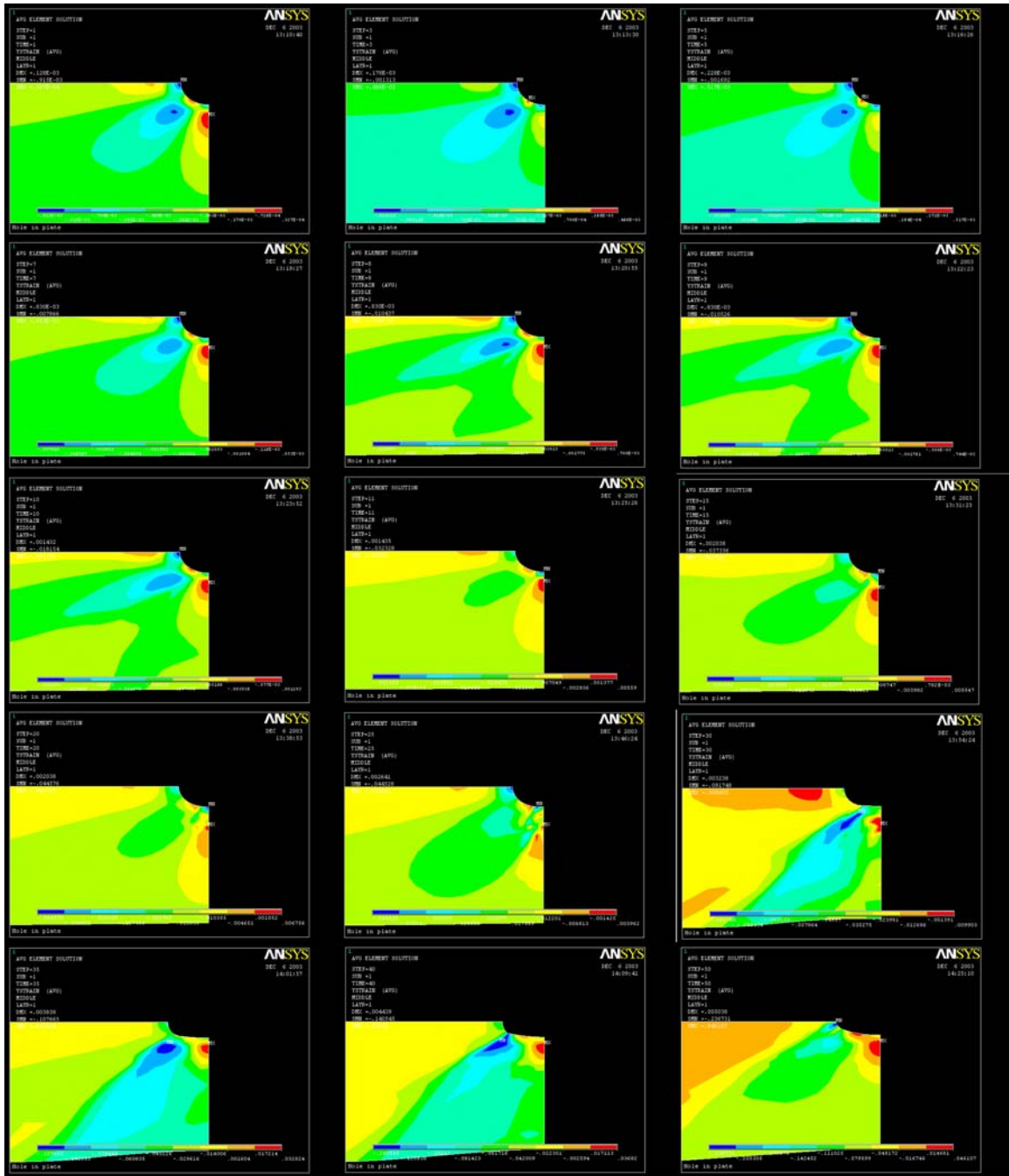


Figure 70: Ansys images showing y-direction strain in the zero degree layer during displacement step solution looping.

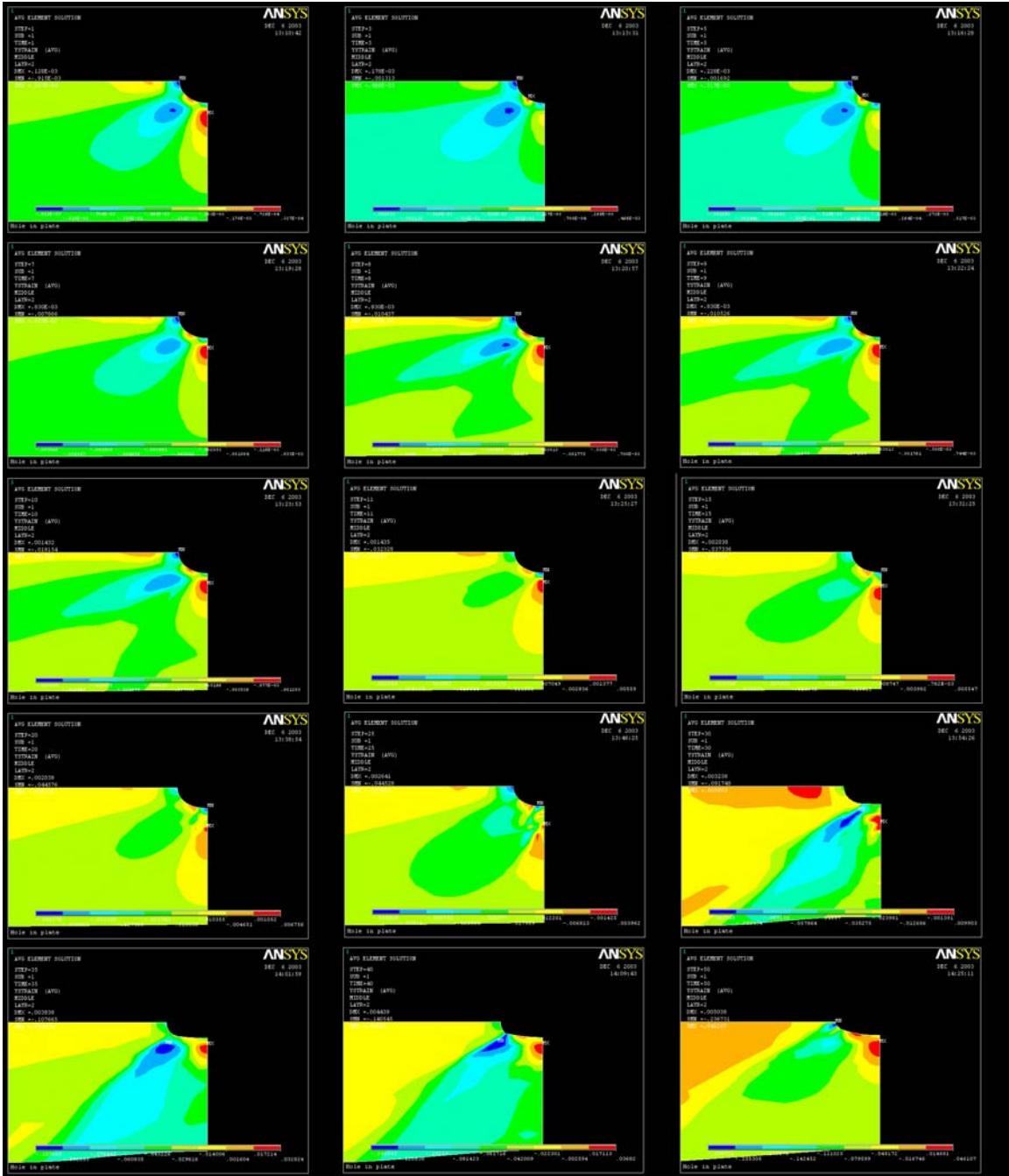


Figure 71: Ansys images showing y-direction strain in the 45 degree layer during displacement step solution looping.

Damage Mapping of Fiberglass.

A test fixture was designed and built to map the infrared transmittance of the chosen geometry, a plate with a hole in it. This fixture consisted of two stages for “x” and “y” movement, and an electrical circuit with an infrared LED and opposing phototransistor similar to the circuit described in the background section. The stages used were lead-screw type, and traveled 1.2 mm per screw revolution. For this test fixture, instead of using converted opto-interrupt sensor parts as was done for the hand-held device described previously (Figure 23), the components were purchased separately from Honeywell. Figure 72 shows the fixture that was built for these tests, and Table 11 details the electronic components used in the apparatus.

The resistance across the potentiometer used in this circuit was not measured, but it was not altered at any point during testing. It was set to a high resistance to allow for the highest resolution in output voltage and to reduce the current in the circuit. It was assumed that the lower current would reduce the possibility of component damage or thermal changes occurring in components as they dissipated energy generated by resistive heating.

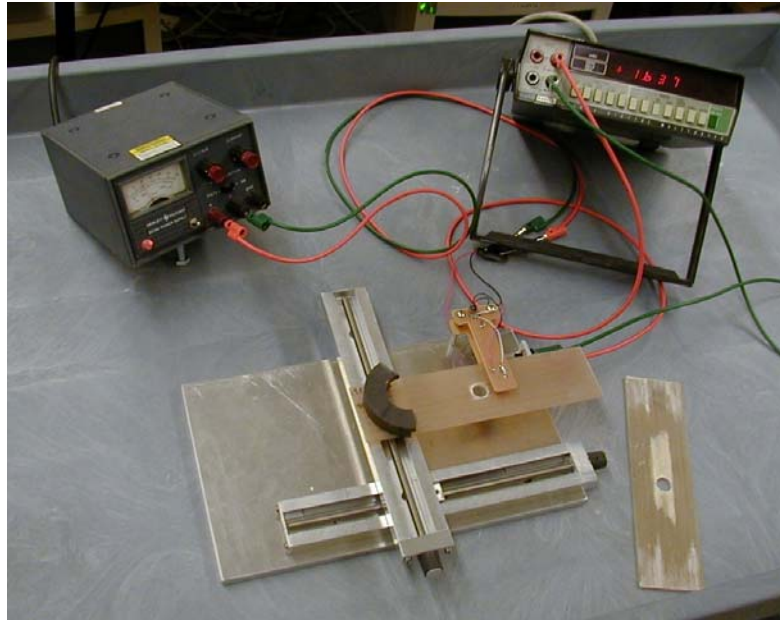


Figure 72: IR transmittance test fixture built for these tests.

Table 11: Components used in IR mapping fixture.

Label from Figure 24	Description	Supplier/Part number
DC power source	Power Supply	Rob
Voltage Output	Digital Multi-Meter	Beckman Industrial 310
R1	Standard resistor	680 Ω
R2	Potentiometer	High Ω
Infrared LED	Aluminum gallium arsenide infrared emitting diode	Honeywell SEP8706-003
Phototransistor	NPN silicon phototransistor	Honeywell SDP8406-003

Since the samples were intended to be fixtured, mapped, and removed several times, an indexing procedure was carefully developed to mount the samples into the fixture consistently. If the samples could not be re-indexed in subsequent repetitions to the same “zero” position, the resulting transmittance maps could not be reasonably compared. To test the consistency of indexing, before any loading was applied, the first sample was fixtured, and a linear transmittance curve was found by recording transmittance at several points along the “x” axis at an arbitrary “y” position (Figure 73). This process was repeated three times, measuring the transmittance at the same “x” locations and “y” position, and the results of this consistency test are shown in Figure 74. Since the transmittance curves of the three repetitions of this experiment reasonably agree, the fixturing and indexing procedure was assumed to be adequately consistent.

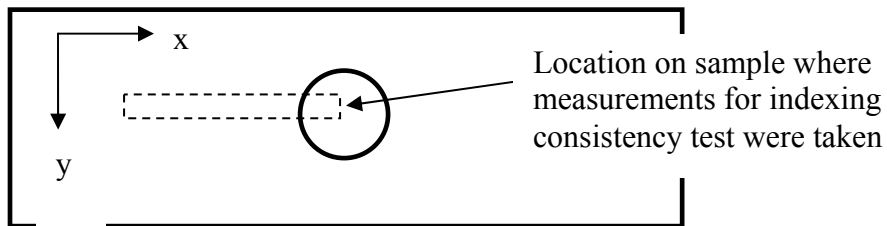


Figure 73: Sample mounting consistency test measurement area.

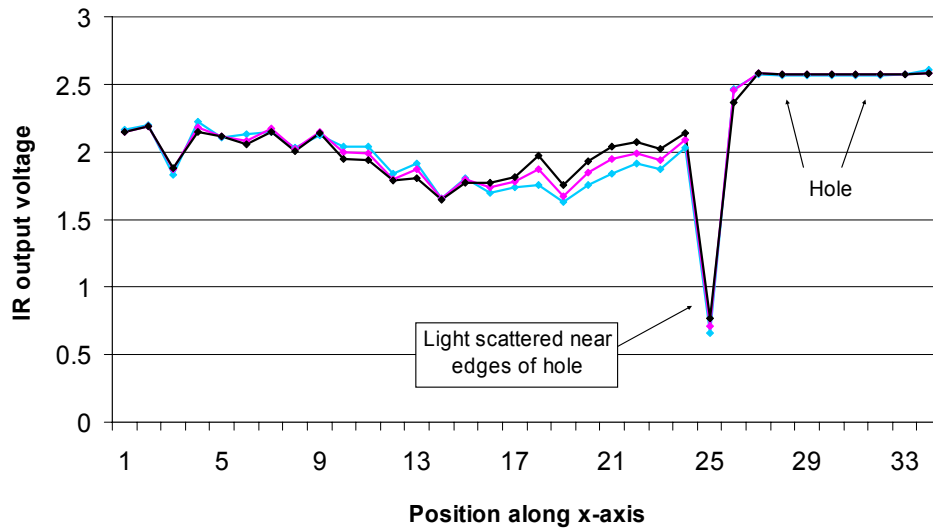


Figure 74: Sample indexing consistency test results.

The first sample tested was the pressure bag molded sample. Before any loading, the transmittance was measured to obtain the baseline, undamaged map. Before putting the sample in the test apparatus, the “open” IR response was recorded. The sample was fixtured according to the method tested above, and zeroed. The voltage response was manually recorded at the current point, and the x-axis lead screw was rotated one turn. This was repeated for the desired travel of the axis. The y-axis lead-screw was then rotated one turn, and the x-axis measurements were again manually recorded. There were 34 data points recorded in the x-direction (load direction) and 25 points recorded in the y-direction totaling 850 points per map. The sample was then removed from the IR device and loaded using the Instron until damage was first detected by the user. The sample was removed from the Instron and indexed in the transmittance fixture and

mapped. Quarter-symmetry was used for mapping. The general area of the sample that was mapped is shown in Figure 75. This entire process was repeated after successive loads that caused incremental damage. The loads at which the sample was mapped are shown in Table 12.

Table 12: Loading points where damage was mapped.

Load Cycle	Force, kN	Far-field Stress, MPa
0	0	0
1	36.7	312.9
2	40.0	341.3
3	42.3	360.3
4	46.7	398.2

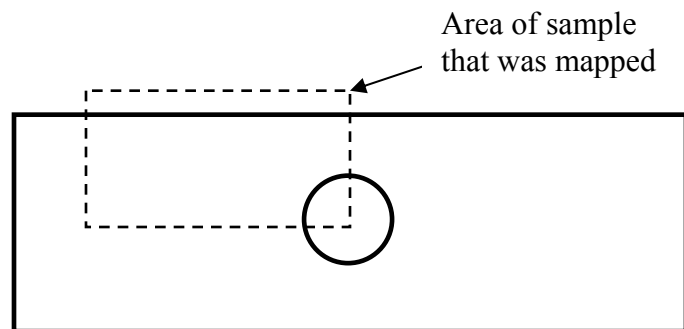


Figure 75: Quarter-symmetry used for transmittance mapping.

Damage Map Results. The raw voltage output values that were recorded during mapping were converted to percent of maximum. The maximum value used was the response voltage with no sample in the infrared beam. These values were arranged in a two dimensional grid and plotted. Early plots using Microsoft Excel were created, but these plots seemed to show fine detail beyond what the raw data should have been able to produce (Figure 76). Therefore, Matlab was used to create the majority of the transmittance plots presented in this thesis.

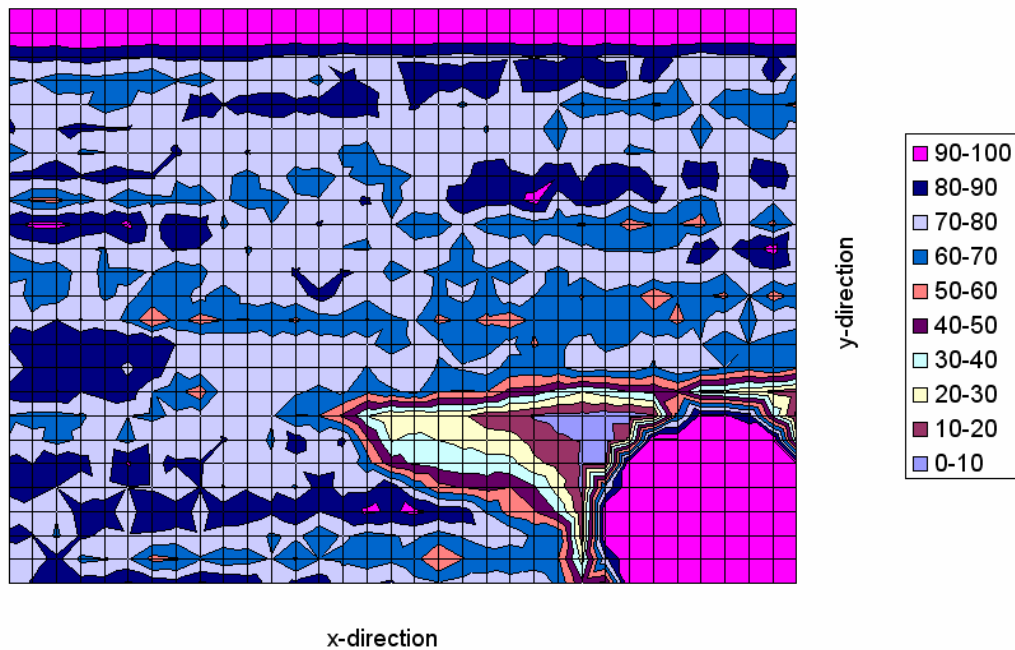


Figure 76: Excel surface plot of percent IR transmittance after 36.7kN load step.

The following figures are the contour plots of the percent transmittance generated by Matlab in the order of increasing load. The Matlab commands used to generate these plots are included in the Appendix.

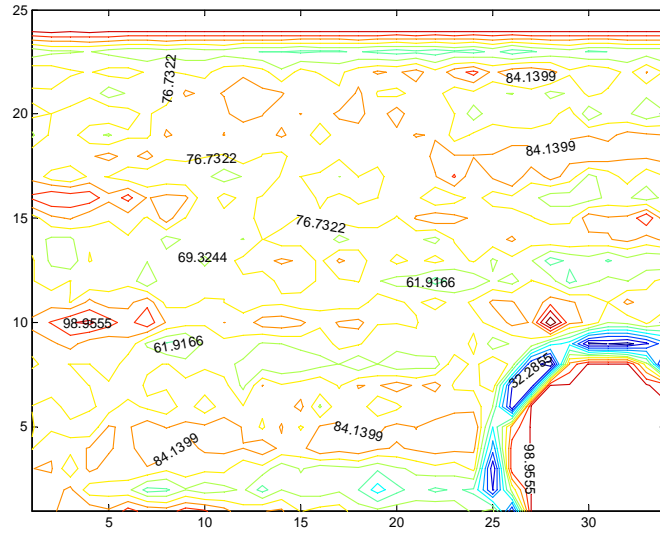


Figure 77: Baseline infrared transmittance map for fiberglass plate with a hole using quarter-symmetry.

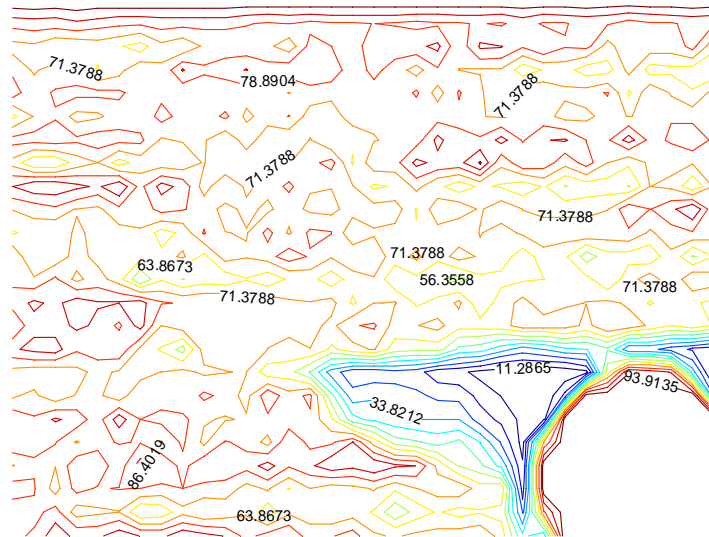


Figure 78: Infrared transmittance of plate with a hole after loading to 36.7 kN.

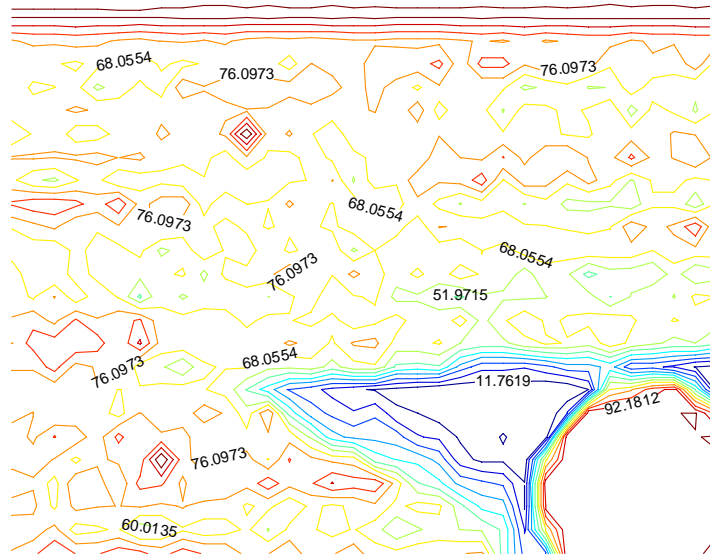


Figure 79: Infrared transmittance of plate with a hole after loading to 40 kN.

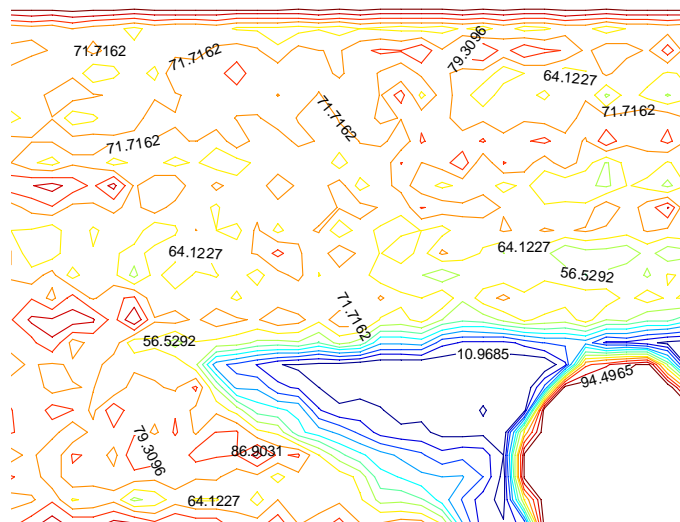


Figure 80: Infrared transmittance of plate with a hole after loading to 42.3 kN.

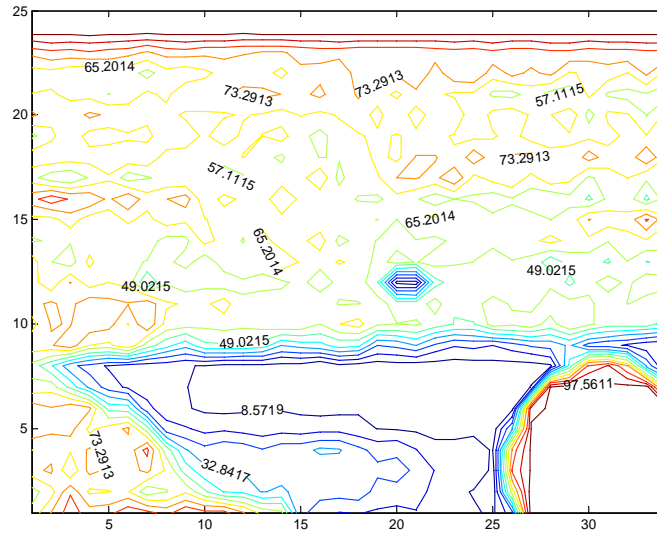


Figure 81: Infrared transmittance of plate with a hole after loading to 46.7 kN.

Some details that deserve mentioning that can be seen on the plots are:

- The hole is at the bottom right and shows the expected highest transmittance.
- The material closest to the edges of the hole shows low transmittance even for the baseline map. This was a result of local damage from the drilling operation causing IR light scattering.
- The large area of low transmittance that extends and grows horizontally from tangent to the hole is a large delamination of the surface zero degree layer.

From the IR mapping data, average values for IR transmittance were calculated.

Two sets of averages were found, one average of all values recorded, including the values recorded for the hole and for the major delamination area. A localized area was defined which excluded the hole and delamination areas. This local area consisted of 90 data

points. A set of averages was found for this local area also. The same geometric area of data points was used for this set of averages across all data sets. The approximate area chosen for the localized average is shown in Figure 82.

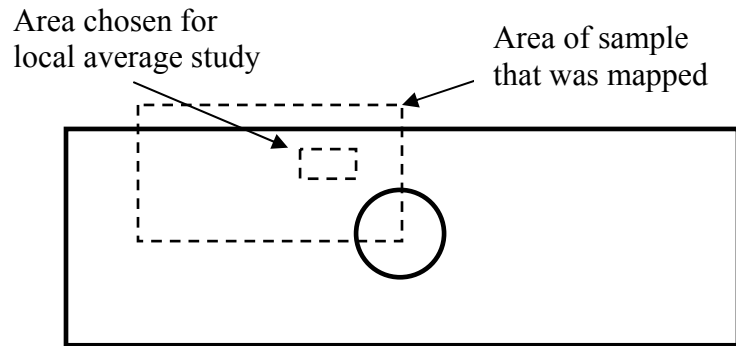


Figure 82: Ninety data point area used for local average IR transmittance study.

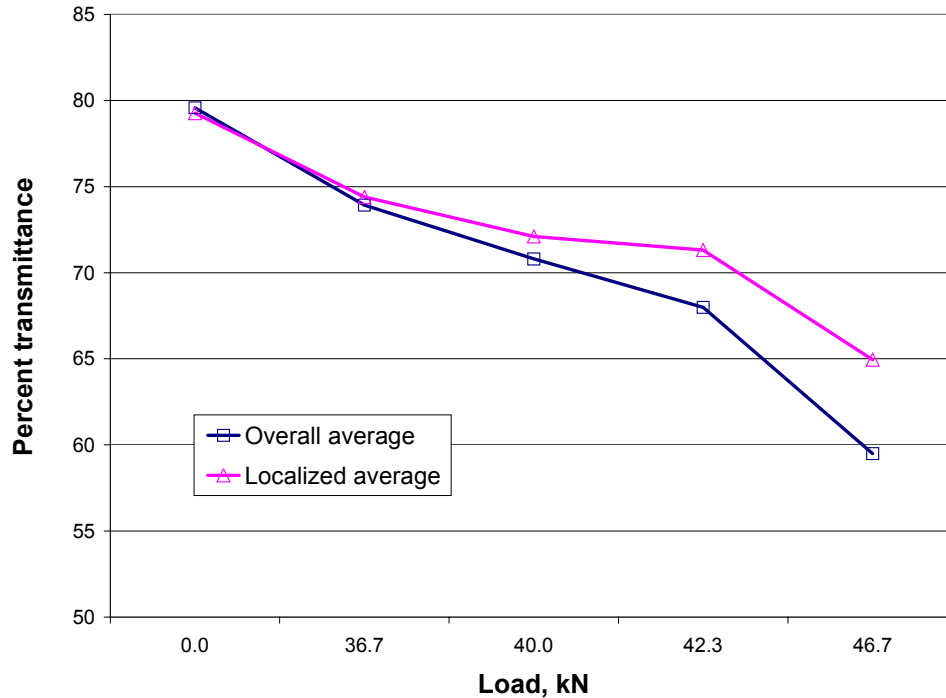


Figure 83: Overall and local percent transmittances for data sets measured during incremental loading of fiberglass plate with a hole.

Comparing Numerical Solution and Damage Maps.

Theoretically, the damage maps should resemble the Ansys prediction for damage progression. A visual comparison of the transmittance maps with the damage progression results obtained from Ansys (Figure 65), however, reveals that there is apparently little correlation. The statistical decline in transmittance revealed in Figure 83, however, does agree with the numeric solution prediction that matrix cracking would spread across the whole plate before significant fiber breakage would occur (middle images in Figure 65).

Another way of representing the resulting damage maps was to show not just the percent transmittance at a load point, but to show the difference in percent transmittance from the baseline map. When the data is presented in this manner, Microsoft Excel appears to be the better tool. Plotting the data arranged in this manner shows that there is a noticeable decline in transmittance in the area around the hole, and not just in the delaminated area. The data from the third load step presented in this manner is shown in Figure 84. The relatively larger concentration of yellow above the hole in this plot shows a noticeable decrease in transmittance. Nevertheless, this still doesn't show the damage pattern predicted by Ansys.

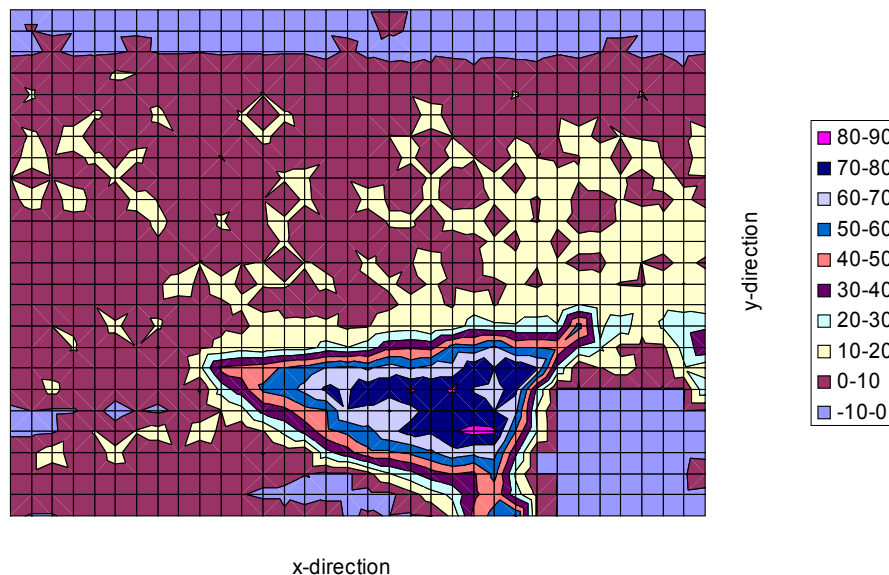


Figure 84: Difference in percent transmittance for sample after 42.3 kN load step compared to undamaged transmittance.

Reasons for Discrepancies. The numerical model was not able to predict the large delamination that occurred during mechanical testing. The failure criteria used simply

did not account for it. Modification could be done to the model to attempt to account for this. However, that was determined to be beyond the scope of this work, and is discussed in the “Future Work” section.

A closer look at the accuracy available from the design of the transmittance test was done. Recall that the data points were recorded with a spacing of 1.2 mm (one full lead-screw revolution). A follow-up test was done to determine if this spacing was small enough to adequately represent the transmittance properties of the samples. A specimen was mounted in the mapping device and data points were recorded for ten turns of the x-axis lead screw. For this test, instead of recording one data point per turn, six data points were recorded (at 60 degrees of screw revolution each). This data was plotted in two series, one series using every sixth point (one full turn of the lead-screw) representing the resolution of the mapping tests, and the second series including all of the data (six data points per turn). The results of this resolution test are shown in Figure 85. It can be seen in this chart that the 1.27 mm resolution is not nearly enough to accurately represent the transmittance properties.

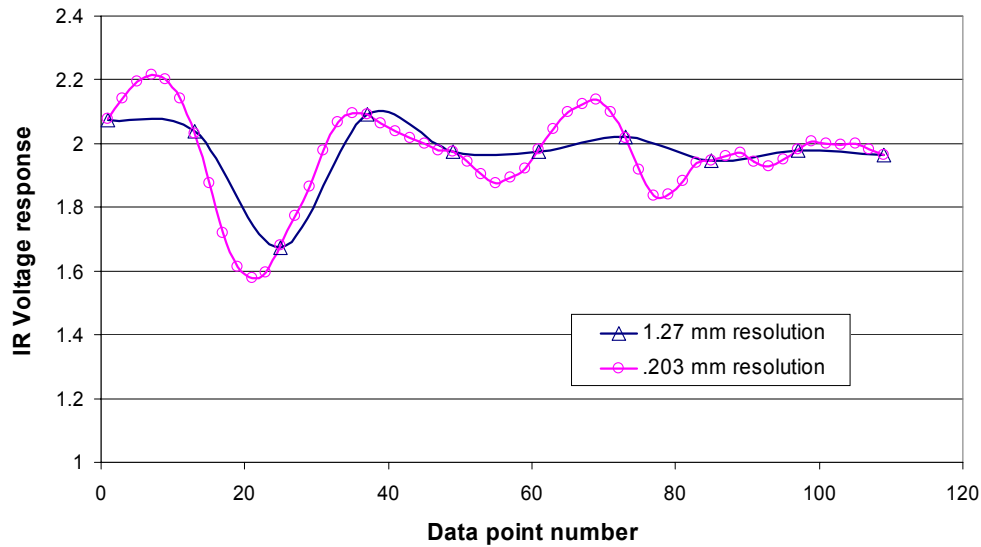


Figure 85: Resolution test results comparing the 1.27 mm resolution with .203 mm resolution.

Another step was taken to determine if the .203 mm resolution would be adequate to represent the transmittance properties. With the sample still mounted in the test apparatus, more data points were taken in the first 1.27 mm of travel that was shown in the previous test. The spacing of these points was reduced to 0.102 mm. As can be seen (Figure 86), there is no significant change in the shape of the resulting curves. Therefore, 0.203 mm resolution would probably have been adequate to accurately represent the transmittance properties. However, considering that the test device was designed for manual data recording, and that 850 points were recorded for each map using the 1.27 mm resolution, an increase in resolution to 0.203 mm would be require a prohibitive amount of time to map even a reduced area. Increasing the resolution of the mapping device is discussed in the “Future Work” section.

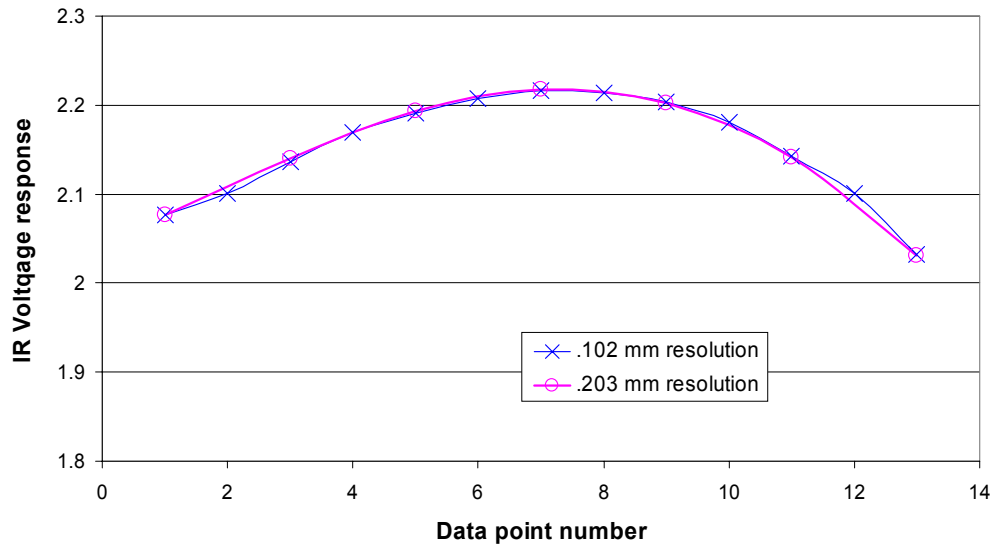
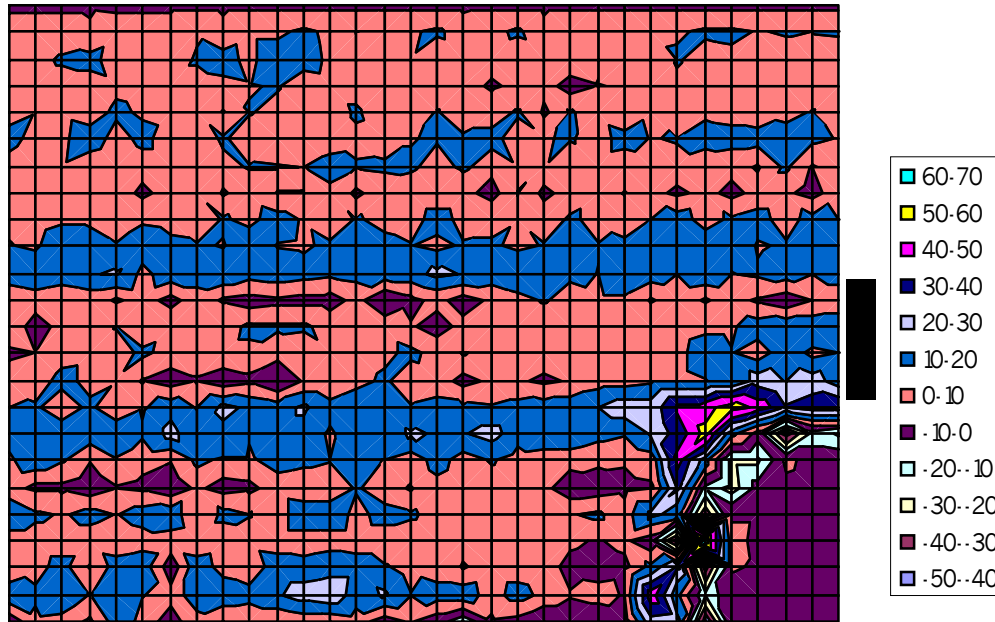


Figure 86: Resolution test results comparing 0.203 mm resolution with 0.102 mm resolution.

Comparing Transmittance Properties of RTM and Pressure Bag Molded Samples

This transmittance mapping test was intended to be designed to complement the pressure bag molding process qualification regime by comparing the damage progression properties of RTM samples and pressure bag molded samples. Since the resolution test of the transmittance device has revealed that the mapping does not show adequate detail to provide valid results, no accurate comparison of plates from different manufacturing processes can be made. Nevertheless, to continue with the design of the test, a plate with a hole in it manufactured by RTM was tested at the first loading point (36.7 kN in the previous test). Its transmittance map is compared with that of the pressure bag molded plate. The method of comparison used is the difference in transmittance from their undamaged data points, as in Figure 84.



X-direction

Figure 87: Difference in transmittance for RTM plate with a hole after loading to 36.7kN compared to undamaged transmittance.

In this plot, the horizontal bands may or may not be significant. They may be a result of a very slight alignment difference between the baseline data and the data after loading.

The blue area above the hole, however, is likely a result of damage causing a decline in transmittance. This transmittance map does show the start of a similar delamination as was seen in the pressure bag manufactured plate. To the extent that this test is able to compare these materials, there is no discernable difference in damage progression properties. However, because of the inadequate resolution, no real conclusions can be

drawn when comparing the damage progression properties of samples from these two manufacturing processes.

CHAPTER 6

CONCLUSIONS AND FUTURE WORK

Wind energy costs need to continue to decline to continue to become more competitive with traditional energy sources. One area that can help to accomplish this is improved manufacturing processes for wind turbine blades. An overview of the existing basic manufacturing processes used for low cost fiberglass materials was presented in this thesis along with a variation of these methods (pressure bag molding) that was developed for this work. As is standard with the implementation of any new manufacturing process, qualification work was done to verify that the products of the candidate process provide comparable performance to the currently used processes, or to understand differences in the products. In this work, standard destructive mechanical testing was complemented with a new nondestructive evaluation method used to compare the performances of products of the new manufacturing method with products of an established standard method (RTM). This nondestructive evaluation method may also show promise for several other applications not investigated in this work. In this section, conclusions are summarized for the major research topics investigated, and then suggestions are made for continued investigation in specific areas.

Pressure Bag Molding

The main focus of this work was the alternative manufacturing process “pressure bag molding”. As was stated previously, this process most closely resembles the FASTRAC process in flow mechanisms and products with a few differences which were

discussed. It was stated that because of the similarities, this work could be considered an independent evaluation of FASTRAC principles, or two-stage injection processes in general.

Pressure Bag Molding Conclusions

Low cost materials continue to be attractive for demanding applications. Manufacturing methods are therefore critical to yield products that meet the requirements of these applications. Various new developments in processing were discussed that are being developed and are currently used in industry. This work introduced a pressure bag molding process similar to FASTRAC. Several aspects of the process itself were evaluated, and mechanical properties of resulting products were compared with those of RTM. Some of the findings are as follows:

- The process that was developed in this work showed excellent potential for improved part quality and consistency.
- Pressure bag molding products showed a consistent ability to achieve relatively higher and more spatially consistent fiber volume percents compared with RTM.
- Pressure bag molding processes showed an ability to inject greater volumes per port in less time compared with RTM.
- Results from mechanical testing showed that pressure bag molded products performed comparably with products of RTM in tensile tests and short beam shear tests. Compression testing showed slightly reduced compression strengths and a greater variation in compressive strength values. A discussion of the compressive results is included in the next section.

Pressure Bag Molding Future Work

This work investigated some aspects of a two-stage infusion process. Many of the process variables were not altered during this work. To continue investigation of the behavior and results of pressure bag molding, the effect of varying several of these parameters needs to be investigated.

- The fabrics and lay-up were not altered in this work. Potential applications of higher performance processes such as this tend toward larger parts with thicker laminates. The abilities of this process to inject larger volumes per port in less time seem promising for these larger parts, but actual performance for these situations needs to be investigated.
- Resin type and viscosity were not altered. The surface properties of the resin and fabric are critical to injection processes. Different resin types may yield different results when used with this process.
- The vacuum used during injection was not significantly varied. In some high end injection processes, to use higher vacuums, resin is degassed prior to injection. This process removes materials that would otherwise boil out of the resin during injection. The effects of more or less vacuum during an injection could be investigated
- The various pressures used were not significantly varied. It is probably not desirable to use higher pressures, as that increases the mechanical loading requirements on the mold parts. In the (largely undocumented) experimentation

with this process, it was noted that higher pressures (in the 2 atmosphere range) during the second stage were actually detrimental. Results of varying second stage pressure from zero to two atmospheres need to be investigated.

- Varying the bagging material may have some effect on resulting products. In early investigations, a relatively thinner, more compliant film was used. It seemed that results were not as good using this material for bagging film. This aspect should be investigated.
- It was discussed that this pressure bag molding process is similar in mechanism and results to those of FASTRAC. Further investigation may be warranted to better understand similarities and differences.
- The reduction in compressive strengths observed for products of the pressure bag molding process (see Figure 46) needs further investigation. It is speculated that the hydrostatic pressure on one side of the laminate during injection is causing the layers of fabric nearest to the bag to become wavy, as they are pressed against the fabrics underneath. This waviness may be imposing a “pre-buckled” condition on the material nearest the surface, causing reduced compressive strength. If this is the case, it may be a significant finding, as the hydrostatic pressure on one side of the lay-up is a scenario that is common to not only this process, but FASTRAC, and SCRIMP, and therefore is frequently occurring in industry. It is also speculated that this phenomenon will be reduced as laminate thickness (and number of fabric layers) increases. Further testing is in order to gain a better understanding of the effect of manufacturing process (especially one-sided mold

processes such as pressure bag molding, SCRIMP, and FASTER) on compressive strengths.

Progressive Damage Model

Ansys was used in this work to model the failure characteristics of a fiberglass composite. A plate with a hole in it was modeled and analyzed for its damage accumulation behavior. Although this model was designed to assist in validating the products of the pressure bag molding process, there may be greater potential applications for the algorithm used.

Progressive Damage Model Results

The resulting predictions for damage seem to follow an intuitive scenario for what was observed during testing. However, the results of the damage model were compared with only one mechanical test. In this test, mixed results were seen:

- The Ansys progressive damage model performed as expected and seemed to be robust and stable. The predicted damage seemed intuitively reasonable.
- The model did not account for a major failure mode that occurred in the mechanical tests. Delamination began from the first loading step and grew with each successive load increment.
- The analysis tool used to quantify damage (the infrared mapping device) was shown to not be able to provide adequate resolution to confidently compare results from the damage model and mechanical testing.

- Some of the (albeit dubious) mechanical testing results obtained do suggest correlation with the damage model.

Progressive Damage Model Future Work

Several areas are available for further development of this tool. The first should be to find a way to accurately compare the predictions of Ansys with results from mechanical testing. This could be accomplished with an improved infrared mapping device (discussed later). Verification should be done to show some correlation with actual testing.

The progressive damage model that was developed in this work was constructed for this particular geometry and lay-up. The steps of failure progression were assumed prior to development of the solution algorithm. Evolution of the code such that these assumptions are not needed is critical if this progressive damage approach can be portable to other models and materials. To achieve that, a more complex approach to material property behavior definition is needed. The code used in this solution simply incremented the temperature dependent properties by 100 degrees whenever new failure was detected. That only worked because the failure steps were assumed to be known.

The failure model needs to be revised to account for delamination. There are several ways to do this in Ansys. Contact elements can be used, if the geometry of the delamination can be predicted and modeled accordingly. Since this is dependent on the failure being known prior to the solution being constructed, it introduces the same limitation as was discussed previously. Node coupling could be done on the whole model, or areas in the model where delamination is possible. This may be the method

most likely to give best results for performance and versatility. Another quick (but not very elegant) method may be to simply reduce the shear modulus to near zero as a possible failure mode. This may have undesirable side-effects though due to the resulting large displacements.

Infrared Transmittance

This work introduced a new non-destructive test method for fiberglass composites. The basic physics was briefly discussed, and some early exploratory experiments were documented. A device was built to facilitate two-dimensional mapping the infrared transmittance of fiberglass samples. Transmittance maps were compared with predicted damage progression from Ansys and were presented as a product qualification test.

Infrared Transmittance Results

Early exploratory tests with the hand-held IR device revealed several interesting aspects of this optical method.

- During a tensile test, IR transmittance is constant up to the point where matrix cracking starts. At that point, the transmittance begins to decrease approximately linearly until catastrophic fiber failure.
- When a fiberglass sample is subjected to a limited number of cycles of repeated loading and unloading, the IR transmittance decreases to a minimum at each maximum load. When the load is removed, the transmittance increases (probably

as a result of cracks closing), but not to the original value from before the load cycle. This behavior appears to be asymptotic (see Figure 30).

- IR transmittance has shown in this work to be able to quantify the quality of a fiberglass composite. Porosity and voids reduce the transmitted light as it is scattered as it crosses the boundaries of the voids.
- The presence of threads or weaving materials from a fabric interferes with transmittance, and makes the location of the transmittance beam an important consideration. Therefore pre-pregs and fabric architectures that have no weaving or stitching materials lend themselves better to this technique.

The device that was constructed to facilitate two-dimensional mapping of IR transmittance revealed several interesting aspects:

- The two-dimensional mapping technique showed promise for the capability of quantifying damage in a fiberglass composite plate.
- The resolution required to accurately represent the transmittance of samples (with the device constructed for this work) was shown in this work to be 0.203 mm for these materials and lay-up.
- When extended to a thicker laminate, results were predictable.
- Even though it was impractical to attempt to map a sample to the resolution given above, and a resolution of 1.2 mm was used, mapping data was recorded of a plate with a hole after damaging loads that showed the damage near the hole, where prediction and intuition indicated it would be found.

Infrared Transmittance Future Work

There are several potential applications of the IR technique described in this paper. There are two different general directions that research could proceed in: as a laboratory tool (such as in this work) or for built-in lifetime health monitoring.

Either path could benefit from a thorough spectrum response analysis of transmittance through commonly used composite materials including carbon fiber composites. The light frequency used for these experiments was in the infrared range. This is a safe frequency with minimal interference from ambient sources. However, this frequency does not transmit through carbon fiber composites. It has been shown that X-rays do penetrate carbon fiber composites. It is speculated that there may be a frequency (that does not introduce the health risks inherent with X-rays) that can provide the same performance for carbon fiber composites as infrared does for fiberglass. Research could be done to see if this frequency exists.

IR Transmittance as a Lab Tool. This technique may be employed as a research tool to possibly quantify any response that includes a change in opacity of a material. For fiberglass composites, that includes matrix cracking (mechanical testing), porosity, chemical responses, etc. A possible application would be to measure the property in the traditional method, and correlate these measurements with the associated IR transmittance. If the behavior is consistent and linear, the IR transmittance values can give the desired value without destructive testing or large time investment.

IR Transmittance for Lifetime Structural Health Monitoring. It may be possible to adapt the technique described in this work to provide structural integrity data. In other

words, it may be possible to laminate the LED-phototransistor into critical areas of parts such as wind turbine blades, and periodically query the devices to determine the IR transmittance. This could provide insight as to whether the part has endured a damaging strain event, and to what degree damage was sustained. Several areas of research would need to be conducted before this could be attempted:

- The LED and phototransistor components used for the hand-held device and for the x-y mapping device had a clear plastic overmold surrounding the component. This overmold has what is apparently a dome-shaped lens over the substrate area that may or may not be critical to the performance of the device. If these electronic devices are laminated into a structure, it will be desirable to remove or minimize this overmold feature to reduce the intrusiveness of the device. It needs to be determined whether or not this overmold is needed, and if the dome-shaped lens feature is needed.
- If the overmold can be removed, does the chemical environment of the uncured or cured resin affect the function of the components over time? Conversely, if the overmold is removed, does the operation of the LED affect matrix materials adjacent to the components? What other environmental conditions could affect performance?
- Other less intrusive configurations could be possible to achieve health monitoring. A reflective foil could be placed on one side of a laminate, and the LED and phototransistor could be placed next to each other outside of the laminate on the opposite side. The reflective foil could be placed between layers in the interior of

the laminate. The reflective foil may not be necessary at all for successful determination of damage.

REFERENCES CITED

1. "<http://www.vestas.com/>", Internet URL.
2. "<http://www.gewindenergy.com/>", Internet URL.
3. McKittrick, L. et al, "Design of a Composite Blade for the AOC 15/50 Wind Turbine Using a Finite Element Method," Sandia National Laboratories.
4. Rossell, Scott., "Fluid Flow Modeling of Resin Transfer Molding for Composite Material Wind Turbine Blade Structures", Masters Thesis, Chemical Engineering Department, Montana State University, 2000.
5. Skramstad, Jon D., "Evaluation of Hand Lay-up and Resin Transfer Molding in Composite Wind Turbine Blade Manufacturing", Masters Thesis, Mechanical Engineering Department, Montana State University, 2000.
6. Reinhart, T. J. et. al., "Engineered Materials Handbook, Volume 1", ASM International, 1987.
7. Barbero, Ever J., "Introduction to Composite Materials Design", Taylor and Francis, 1998.
8. Samborsky, Daniel D., "Fatigue of E-Glass Fiber Reinforced Composite Materials and Substructures", Masters Thesis, Civil Engineering Department, Montana State University.
9. "New International Version of the Bible".
10. "Journal of Composites Technology and Research", Volume 16, Issue 4, 1994.
11. "JOM", Volume 53, Issue 4, 2001.
12. Schwartz, Mel M., *Composite Materials*, Prentice-Hall, Inc., 1997.
13. "Material Safety Data Sheet (MSDS)", CAS #000100-42-5.
14. Published in January 1989, at 54 Fed. Reg. 2332, OSHA web site.
15. Kruckenberg, Teresa M., "Resin Transfer Moulding for Aerospace Structures", Kluwer Academic Publishers, 1998.
16. Humbert, Dell Raymond, "Modeling of Resin Transfer Molding of Composite Materials With Oriented Unidirectional Plies", Masters Thesis, Chemical Engineering Department, Montana State University, 1996.

17. N.R.L. Pearce, et al., "Improving the Resin Transfer Molding Process for Fabric-Reinforced Composites by Modification of the Fabric Architecture", *Composites, Part A* 31, pp 1433-1441, 2000.
18. "<http://www.matweb.com/>", Internet URL.
19. U.S. Patent and Trade Office, Patent #4902215.
20. Heider, Dirk, et al., "Experimental Validation and Optimization of the FASTRAC Process", 22nd International Conference and Tutorials, SAMPE Europe 2001.
21. Walsh, Shawn M., et al., "A Non-Contact Distribution Scheme for Promoting and Controlling Resin Flow for VARTM Processes", 32nd International SAMPE Technical Conference, SAMPE 2000.
22. Weisstein, Eric, "World of Science", <http://scienceworld.wolfram.com/>, Technical Internet Encyclopedia.
23. Larsen, Erik, et al., "Investigation of a Two-Stage Injection Process to Reduce the Effects of In-Plane Resin Flow", 2002 ASME Wind Energy Symposium, ASME/AIAA.
24. ASTM Standard D-2584.
25. Mandell, John F., et al., "Fatigue of Composite Materials and Substructures for Wind Turbine Blades", Sandia National Laboratories SAND2002-0771, 2002.
26. ASTM Standard D-2344.
27. Agastra, P., "Mixed Mode Delamination of Glass Fiber/Polymer Matrix Composite Materials", Masters Thesis, Chemical Engineering Department, Montana State University, 2003.
28. Hibbeler, R.C., "Mechanics of Materials", Prentice Hall, Inc., 2000.
29. Hull, D. and Clyne, T. W., "An Introduction to Composite Materials", Cambridge University Press, Great Britain, 1996.
30. Orozco, R., "Effects of Toughened Matrix Resins on Composite Materials for Wind Turbine Blades", Masters Thesis, Civil Engineering Department, Montana State University, 1999.
31. Knytex Corporation, "Fabric Handbook", 1994.
32. Ansys Release 7.0.

APPENDICES

APPENDIX A

Main Ansys fea macro file

MAIN ANSYS FEA MACRO FILE

```

!/BATCH
!/COM,ANSYS RELEASE 7.0

! ALL UNITS ARE METRIC: METERS, PASCALS

/TITLE,HOLE IN PLATE
/FILNAME,HOLE50,0

/PREP7

!BASE KEYPOINTS...
K,1,0,0,0
K,2,.11711,0,0
K,3,.125,0,0
K,4,.125,.01905,0
K,5,.125,.01905,1
K,6,.121825,.01905,0
K,7,.07901,.01905,0
K,8,0,.01905,0
K,9,.07901,0,0
K,10,.10595,0,0

!BASE LINES...
LSTR,1,9           !LINE 1
LSTR,9,10          !LINE 2
LSTR,10,2          !LINE 3
LSTR,2,3           !LINE 4
LSTR,6,7           !LINE 5
LSTR,7,8           !LINE 6
LSTR,8,1           !LINE 7
LSTR,7,9           !LINE 8

!ROTATE THE KEYPOINTS AT THE HOLE TO MAKE A LINE...
LROTAT,6,,,,,,,,4,5,22.5   !LINE 9 CREATES KEYPOINT 11...
LROTAT,11,,,,,,,,4,5,22.5  !LINE 10 CREATES KEYPOINT 12
LROTAT,12,,,,,,,,4,5,22.5  !LINE 11 CREATES KEYPOINT 13
LROTAT,13,,,,,,,,4,5,22.5  !LINE 12 CREATES KEYPOINT 14

!ADD THE LINES FOR THE NEW KEYPOINTS...
LSTR,14,3          !LINE 13
LSTR,13,2          !LINE 14
LSTR,12,10         !LINE 15
LSTR,11,9          !LINE 16

!DIVIDE THE RADIAL LINES...
LDIV,5,.2          !CREATES LINE17, KEYPOINT 15
LDIV,16,.2         !CREATES LINE18, KEYPOINT 16
LDIV,15,.25        !CREATES LINE19, KEYPOINT 17
LDIV,14,.25        !CREATES LINE20, KEYPOINT 18

```



```

LDIV,13,,25          !CREATES LINE21, KEYPOINT 19

!CREATE LINES FROM THE NEW KEYPOINTS AT LINE DIVISIONS...
LSTR,15,16           !CREATES LINE 22
LSTR,16,17           !CREATES LINE 23
LSTR,17,18           !CREATES LINE 24
LSTR,18,19           !CREATES LINE 25

!CREATE AREAS...
AL,6,7,1,8
AL,17,8,18,22
AL,18,2,19,23
AL,19,3,20,24
AL,20,4,21,25
AL,5,22,16,9
AL,16,23,15,10
AL,15,24,14,11
AL,14,25,13,12

!ELEMENT TYPE DEF...
ET,1,SHELL91,,1

KEYOPT,1,1,16        ! MAXIMUM NUMBER OF LAYERS (DEFAULT IS 16)
KEYOPT,1,2,1         ! DEFAULT
KEYOPT,1,4,0         ! NO USER SUBROUTINES TO DEFINE ELEMENT COORDINATE
SYSTEM
KEYOPT,1,5,2         ! OUTPUT AVERAGE RESULTS FOR TOP AND BOTTOM LAYER
KEYOPT,1,6,0         ! NO OUTPUT INTERLAMINAR SHEAR STRESSES
KEYOPT,1,8,1         ! STORE DATA FOR ALL LAYERS
KEYOPT,1,9,0         ! NO SANDWICH OPTION
KEYOPT,1,10,0        ! PRINT SUMMARY OF MAXIMUM OF ALL FAILURE CRITERION
KEYOPT,1,11,0        ! NODES LOCATED AT MIDDLE SURFACES AS OPPOSED TO BOTTOM
OR TOP

!*****!
! MATERIAL PROPERTY DEFS..
!*****!

!CONSTANTS:
E_L=3.836E10
E_T=9.966E9
G_LT=4.228E9
PR=.3

!FIRST MATERIAL (ZERO DEGREE MATERIALS)...
MPTEMP,,,,,,,,
MPTEMP,,0,100,200,300,400

MPDATA,EX,1,,E_L,E_L,E_L,.2*E_L,.1*E_L      !AT TEMPS 1,2,3,4,5

```

```

MPDATA,EY,1,,E_T,2*E_T,2*E_T,2*E_T,1*E_T
MPDATA,EZ,1,,E_T,2*E_T,2*E_T,2*E_T,1*E_T
MPDATA,PRXY,1,,PR,9*PR,7*PR,6*PR,1*PR
MPDATA,PRYZ,1,,PR,9*PR,7*PR,6*PR,1*PR
MPDATA,PRXZ,1,,PR,9*PR,7*PR,6*PR,1*PR
MPDATA,GXY,1,,G_LT,2*G_LT,2*G_LT,2*G_LT,1*G_LT
MPDATA,GYZ,1,,G_LT,2*G_LT,2*G_LT,2*G_LT,1*G_LT
MPDATA,GXZ,1,,G_LT,2*G_LT,2*G_LT,2*G_LT,1*G_LT

```

!SECOND MATERIAL (45 DEGREE MATERIALS)...

```

MPDATA,EX,2,,E_L,E_L,E_L,E_L,1*E_L!AT TEMPS 1,2,3,4,5
MPDATA,EY,2,,E_T,E_T,2*E_T,2*E_T,1*E_T
MPDATA,EZ,2,,E_T,E_T,2*E_T,2*E_T,1*E_T
MPDATA,PRXY,2,,PR,PR,7*PR,6*PR,1*PR
MPDATA,PRYZ,2,,PR,PR,7*PR,6*PR,1*PR
MPDATA,PRXZ,2,,PR,PR,7*PR,6*PR,1*PR
MPDATA,GXY,2,,G_LT,G_LT,2*G_LT,2*G_LT,1*G_LT
MPDATA,GYZ,2,,G_LT,G_LT,2*G_LT,2*G_LT,1*G_LT
MPDATA,GXZ,2,,G_LT,G_LT,2*G_LT,2*G_LT,1*G_LT

```

R,1

RMODIF,1,1,8,0.E+00, , , 0.E+00 ! 8 LAYERS, NO SYMMETRY

RMODIF,1,13,1,0,00044,0,0,0, ! STARTING AT POSITION 13, DEFINE MATERIAL,
! ORIENTATION ANGLE, THICKNESS

```

RMODIF,1,19,2,45,00022,0,0,0,
RMODIF,1,25,2,-45,0.00022,0,0,0,
RMODIF,1,31,1,0,00044,0,0,0,
RMODIF,1,37,1,0,00044,0,0,0,
RMODIF,1,43,2,-45,0.00022,0,0,0,
RMODIF,1,49,2,45,00022,0,0,0,
RMODIF,1,55,1,0,00044,0,0,0,

```

! SET UP LINES FOR AREA MESHING...

! THESE ARE THE "MESH DENSITY SETTINGS" REFERRED TO IN THESIS TEXT

MAINDIV = 7

SECONDARY = 4

```

*IF,MAINDIV,GT,6,THEN
  SECONDARY = 5
*ENDIF

```

```

*IF,MAINDIV,GT,8,THEN
  SECONDARY = 6
*ENDIF

```

```

*IF,MAINDIV,GT,9,THEN
  SECONDARY = 7
*ENDIF

```

```

*IF,MAINDIV,GT,10,THEN
  SECONDARY = 8

```

```
*ENDIF

*IF,MAINDIV,GT,12,THEN
  SECONDARY = 10
*ENDIF

*IF,MAINDIV,GT,13,THEN
  SECONDARY = 11
*ENDIF

LESIZE,1,,,SECONDARY
LESIZE,2,,,MAINDIV
LESIZE,3,,,MAINDIV
LESIZE,4,,,MAINDIV
LESIZE,5,,,MAINDIV
LESIZE,6,,,SECONDARY
LESIZE,7,,,MAINDIV
LESIZE,8,,,MAINDIV
LESIZE,9,,,MAINDIV
LESIZE,10,,,MAINDIV
LESIZE,11,,,MAINDIV
LESIZE,12,,,MAINDIV
LESIZE,13,,,MAINDIV
LESIZE,14,,,MAINDIV
LESIZE,15,,,MAINDIV
LESIZE,16,,,MAINDIV
LESIZE,17,,,SECONDARY
LESIZE,18,,,SECONDARY
LESIZE,19,,,SECONDARY
LESIZE,20,,,SECONDARY
LESIZE,21,,,SECONDARY
LESIZE,22,,,MAINDIV
LESIZE,23,,,MAINDIV
LESIZE,24,,,MAINDIV
LESIZE,25,,,MAINDIV

!FIX THE ELEMENTS' COORDINATE SYSTEMS TO ALIGN TO GLOBAL
ALLSEL,ALL
LOCAL,11,0
ESYS,11

! DEFINE COORDINATE SYSTEMS TO LATER USE ROTATING LAYER OUTPUT DATA
LOCAL,12,0,,,45
LOCAL,13,0,,, -45
LOCAL,14,0,,,0

!MESH THE AREAS...
AMESH,ALL

/SOLUTION
!APPLY BCS...
```

!ZERO DISPLACEMENT AT TOP SYMMETRY BOUNDARY...

DL,6,,UY,0

DL,17,,UY,0

DL,5,,UY,0

!ZERO DISPLACEMENT AT RIGHT SYMMETRY BOUNDARY...

DL,21,,UX,0

DL,13,,UX,0

!GRAB 3 POINTS TO CONSTRAIN IN Z DIRECTION...

DK,1,UZ,0

DK,15,UZ,0

DK,16,UZ,0

OUTRES,ALL !OUTPUTS EVERYTHING

BFE,ALL,TEMP,1,0

!*****!

!

!*****!

! SOLUTION LOOPING

!*****!

NUMLAYERS=8 !NUMBER OF LAYERS DEFINED FOR THIS SHELL91 ELEMENT

!*****FAILURE CRITERIA...*****

EP_YMAX = .002 ! .2% STRAIN MAX IN TRANSVERSE DIRECTION

EP_XMAX = .03 ! 3% STRAIN MAX IN LONGITUDINAL DIRECTION

ESEL,ALL

*GET,NUMELEM,ELEM,,COUNT !GETS THE NUMBER OF ELEMENTS...

SZSTART=-.000001 !1/1000TH OF A MILLIMETER

NSEL,ALL

!VARIABLE FOR REPEATING A DISPLACEMENT STEP OR NOT

REPEAT=0

!VARIABLE TO START AT A DISPLACEMENT JUST BEFORE FIRST OVERSTRAIN...

START=78

DISP=START*SZSTART

/AUTO, 1

/REP

/ZOOM,1,SCRN,1.236505,0.071698,1.388293,-0.170456 ! SETS THE VIEW FOR IMAGE SAVING...

*DO,DSTEP,1,50 !CHANGE MAX DISPLACEMENT STEP TO SUIT CURRENT NEEDS

!REPEAT WILL BE 1 IF NEW DAMAGE WAS DETECTED ON THE PREVIOUS DSTEP

```

!IF REPEAT IS ONE, WILL SOLVE LOAD STEP WITH NEW PROPS
*IF,REPEAT,GT,0,THEN
  REPEATING=1          !DEBUG VARIABLE
  STEPSZ=0
  REPEAT=0             !RESET THIS FLAG.
                       !IT WILL GET SET AGAIN IF MORE TEMPS ARE CHANGED
*ELSE
  REPEATING=0          !DEBUG VARIABLE
  *IF,DSTEP,GT,5,THEN !THIS CONTROLS THE DISPLACEMENT RAMP
    STEPSZ=-.0006
  *ELSE
    STEPSZ=-.00005
  *ENDIF
*ENDIF

DISP=DISP+STEPSZ  !DOESN'T CHANGE WHEN REPEATING

/SOLUTION
TIME,DSTEP

*IF,DSTEP,EQ,1,THEN
  ANTYPE,,NEW
*ELSE
  ANTYPE,,REST
*ENDIF

!APPLY DISPLACEMENT...

DL,7,,UX,DISP
SBCTRAN

SOLVE

/POST1

*DO,ELEMENT,1,NUMELEMS
  DAMAGE          ! THIS IS ESSENTIALLY A SUBROUTINE
                  ! IT DOES THE ETABLE SEARCH FOR DAMAGE
*ENDDO

/CONTOUR,ALL,9,0,,400
PLETAB,OLDTMP,AVG
/IMAGE,SAVE,%DSTEP%,TMP

ETABLE,INTE,S,INT

/CONTOUR,ALL
LAYER,1
ETABLE,ERASE
ETABLE,XSTRAIN,EPEL,X
ETABLE,YSTRAIN,EPEL,Y

```

```

ETABLE,INTE,S,INT
PLETAB,XSTRAIN,AVG          ! FOR THE ZERO DEGREE LAYERS...
/IMAGE,SAVE,%DSTEP%,XL1 ! CREATES IMAGE OF LONGITUDINAL STRAIN CONTOURS
PLETAB,INTE,AVG
/IMAGE,SAVE,%DSTEP%,SI1 ! CREATES IMAGE OF STRESS INTENSITY CONTOURS
PLETAB,YSTRAIN,AVG
/IMAGE,SAVE,%DSTEP%,YL1 ! CREATES IMAGE OF TRANSVERSE STRAIN CONTOURS

```

```

LAYER,2
ETABLE,ERASE
ETABLE,XSTRAIN,EPEL,X
ETABLE,YSTRAIN,EPEL,Y
ETABLE,INTE,S,INT
PLETAB,XSTRAIN,AVG          ! FOR THE 45 DEGREE LAYERS...
/IMAGE,SAVE,%DSTEP%,XL2 ! CREATES IMAGE OF LONGITUDINAL STRAIN CONTOURS
PLETAB,INTE,AVG
/IMAGE,SAVE,%DSTEP%,SI2 ! CREATES IMAGE OF STRESS INTENSITY CONTOURS
PLETAB,YSTRAIN,AVG
/IMAGE,SAVE,%DSTEP%,YL2 ! CREATES IMAGE OF TRANSVERSE STRAIN CONTOURS

```

```

LAYER,4
ETABLE,ERASE
ETABLE,XSTRAIN,EPEL,X
ETABLE,YSTRAIN,EPEL,Y
ETABLE,INTE,S,INT
PLETAB,XSTRAIN,AVG          ! THIS IS ESSENTIALLY REDUNDANT, BUT THERE MAY BE
/IMAGE,SAVE,%DSTEP%,XL4 ! SOME DIFFERENCES IN STRAIN IN INSIDE VS OUTSIDE
PLETAB,INTE,AVG          ! ZEROS DUE TO DIFFERENT ORIENTATION OF ADJACENT
/IMAGE,SAVE,%DSTEP%,SI4 ! LAYERS (IE, 45 OR -45).
PLETAB,YSTRAIN,AVG
/IMAGE,SAVE,%DSTEP%,YL4

```

```
*ENDDO
```

```
!/EOF
```

```
! THE FOLLOWING SECTION OF CODE WAS USED TO EXTRACT THE STRESS INTENSITY AT
! KEYPOINT 14 IN ALL LAYERS DURING THE MESH SENSITIVITY ANALYSES.
```

```

KSEL,,,14
NSLK,R
/PREP7
*GET,NODENUMBER,NODE,0,NUM,MAX
/POST1
/OUTPUT,SENS,TXT,,APPEND
LAYER,1
*GET,STRESSATNODE,NODE,NODENUMBER,S,INT
LAYER,2
*GET,STRESSATNODE,NODE,NODENUMBER,S,INT

```

```
/OUTPUT
```

```
/EOF
```

APPENDIX B

“Damage.mac” fea macro file

ANSYS FEA MACRO FILE FOR "DAMAGE" SUBROUTINE

```

! HAVE AN ELEMENT NUMBER AS "ELEMENT",
! NOW GO THROUGH LAYERS, AND LOOK FOR OVERSTRAIN...

NUMLAY=4    !SYMMETRY

/POST1

SHELL,MID          !GETS RESULTS FROM MIDDLE OF LAYER
SET,LAST          !READ THE LATEST DATA SET...

*DO,CURLAYER,1,NUMLAY    !CURRENTLAYER = 1 TO NUMLAYERS, USING SYMMETRY

!GET THE RIGHT COORDINATE SYSTEM FOR PROPER STRAIN READING...
*IF,CURLAYER,EQ,1,THEN
    RSYS,11
*ELSEIF,CURLAYER,EQ,2
    RSYS,12
*ELSEIF,CURLAYER,EQ,3
    RSYS,13
*ELSE
    RSYS,11
*ENDIF

!PRESOL,EPEL

LAYER,CURLAYER          !SETS THE LAYER FOR DATA READING
ETABLE,ERASE
ETABLE,XSTRAIN,EPEL,X
ETABLE,YSTRAIN,EPEL,Y
ETABLE,OLDTMP,BFE,TEMP

*GET,SRNX,ETABLE,1,ELEM,ELEMENT
*GET,SRNY,ETABLE,2,ELEM,ELEMENT
*GET,OLDTMP,ETABLE,3,ELEM,ELEMENT

EPXABS=ABS(SRNX/EP_XMAX)
EPYABS=ABS(SRNY/EP_YMAX)

NEWT=0

*IF,EPYABS,GE,1,THEN          !HAVE MATRIX FAILURE
    *IF,EPXABS,GE,1,THEN!HAVE FIBER FAILURE
        NEWT=300
    *ELSE
        NEWT=100          !ONLY MATRIX CRACKING. IS IT IN 0S OR 45S?
    *ENDIF
*ENDIF

!SET THE NEW TEMP SO IT CHANGES THE RIGHT MATERIAL PROPS...

```



```
*IF,NEWT,GT,0,THEN
  *IF,CURLAYER,EQ,2,THEN  !CHANGE MATERIAL #2 VALUES...
    NEWT = NEWT + 100
  *ELSEIF,CURLAYER,EQ,3
    NEWT = NEWT + 100
  *ENDIF
*ENDIF

!FIND OUT IF THIS ELEMENT HAS CHANGED TEMPS.
!IF IT HAS, REPEAT THE DISPLACEMENT STEP
*IF,NEWT,GT,OLDTMP,THEN !CHANGE PROPS AND REPEAT SOLUTION AT SAME DISP
  REPEAT=1
  /PREP7
  BFE,ELEMENT,TEMP,1,NEWT
  /POST1
*ELSE
  !REPEAT=0
  SETNEWT=0
*ENDIF

*ENDDO

/EOF
```

APPENDIX C

Matlab commands

MATLAB COMMANDS USED TO GENERATE INFRARED TRANSMITTANCE
CONTOUR PLOTS

With the data points arranged in the representative x-y grid and stored in a comma separated variable file (“*.csv”):

<code>x=1:34;</code>	(sets the x range)
<code>y=1:25;</code>	(sets the y-range)
<code>z=load('*.csv');</code>	(loads the transmittance data)
<code>[C,h] = contour(z,12);</code>	(creates the contour plot with 12 divisions)
<code>clabel(C,h,'manual');</code>	(allows user to click where labels are desired on the plot)